Volume 72C
Number 4
Oct.–Dec. 1968

Engineering and Instrumentation

U.S. DEPARTMENT OF COMMERCE

SECTION C

JOURNAL OF RESEARCH

NATIONAL BUREAU OF STANDARDS

Journal of Research
of the
National Bureau of Standards

C. Engineering and Instrumentation

Oct.–Dec. • 1968

VOLUME • 72C

NUMBER • 4

Editor: Martin Greenspan

Associate Editors: G. F. Montgomery, R. V. Smith, A. F. Schmidt

Publication dates:
Feb. 15, May 15, Aug. 15, Nov. 15, 1968

JOURNAL OF RESEARCH

The National Bureau of Standards Journal of Research reports research and development in the fields of activity shown at right. Also included from time to time are survey articles on topics closely related to the Bureau's scientific and technical program.

The Journal is published in three separate sections as follows:

A. Physics and Chemistry

Contains papers of interest primarily to scientists working in these fields. Issued six times a year. Annual subscription: domestic, $6.00; foreign, $7.25. Single copy, $1.00.

B. Mathematical Sciences

Presents studies and compilations designed mainly for the mathematician and the theoretical physicist. Issued quarterly. Annual subscription: domestic, $2.25; foreign, $2.75. Single copy, 75¢.

C. Engineering and Instrumentation

Reports research and development results of interest chiefly to the engineer and the applied scientist. Issued quarterly. Annual subscription: domestic, $2.75; foreign, $3.50. Single copy, 75¢.

The National Bureau of Standards[1] was established by an act of Congress March 3, 1901. Today, in addition to serving as the Nation's central measurement laboratory, the Bureau is a principal focal point in the Federal Government for assuring maximum application of the physical and engineering sciences to the advancement of technology in industry and commerce. To this end the Bureau conducts research and provides central national services in three broad program areas and provides central national services in a fourth. These are: (1) basic measurements and standards, (2) materials measurements and standards, (3) technological measurements and standards, and (4) transfer of technology.

The Bureau comprises the Institute for Basic Standards, the Institute for Materials Research, the Institute for Applied Technology, and the Center for Radiation Research.

THE INSTITUTE FOR BASIC STANDARDS provides the central basis within the United States of a complete and consistent system of physical measurement, coordinates that system with the measurement systems of other nations, and furnishes essential services leading to accurate and uniform physical measurements throughout the Nation's scientific community, industry, and commerce. The Institute consists of an Office of Standard Reference Data and a group of divisions organized by the following areas of science and engineering:

Applied Mathematics—Electricity—Metrology—Mechanics—Heat—Atomic Physics—Cryogenics[2]—Radio Physics[2]—Radio Engineering[2]—Astrophysics[3]—Time and Frequency.[3]

THE INSTITUTE FOR MATERIALS RESEARCH conducts materials research leading to methods, standards of measurement, and data needed by industry, commerce, educational institutions, and government. The Institute also provides advisory and research services to other government agencies. The Institute consists of an Office of Standard Reference Materials and a group of divisions organized by the following areas of materials research:

Analytical Chemistry—Polymers—Metallurgy—Inorganic Materials—Physical Chemistry.

THE INSTITUTE FOR APPLIED TECHNOLOGY provides for the creation of appropriate opportunities for the use and application of technology within the Federal Government and within the civilian sector of American industry. The primary functions of the Institute may be broadly classified as programs relating to technological measurements and standards and techniques for the transfer of technology. The Institute consists of a Clearinghouse for Scientific and Technical Information,[3] a Center for Computer Sciences and Technology, and a group of technical divisions and offices organized by the following fields of technology:

Building Research—Electronic Instrumentation—Technical Analysis—Product Evaluation—Invention and Innovation—Weights and Measures—Engineering Standards—Vehicle Systems Research.

THE CENTER FOR RADIATION RESEARCH engages in research, measurement, and application of radiation to the solution of Bureau mission problems and the problems of other agencies and institutions. The Center for Radiation Research consists of the following divisions:

Reactor Radiation—Linac Radiation—Applied Radiation—Nuclear Radiation.

[1] Headquarters and Laboratories at Gaithersburg, Maryland, unless otherwise noted; mailing address Washington, D.C. 20234.
[2] Located at Boulder, Colorado 80302.
[3] Located at 5285 Port Royal Road, Springfield, Virginia 22151.

U.S. DEPARTMENT OF COMMERCE
C. R. Smith, Secretary
NATIONAL BUREAU OF STANDARDS
A. V. Astin, Director

Order all publications from the Superintendent of Documents
U.S. Government Printing Office, Washington, D.C. 20402.

Use of funds for printing this publication approved by the Director of the Bureau of the Budget (June 22, 1966).

JOURNAL OF RESEARCH of the National Bureau of Standards—C. Engineering and Instrumentation
Vol. 72C, No. 4, October–December 1968

Theoretical and Experimental Study on Longitudinal Impact of Tapered Rods

L. R. Hettche*

Institute for Basic Standards, National Bureau of Standards, Washington, D.C. 20234

(July 1, 1968)

To examine the adequacy of the one-dimensional, rate-independent theory of plastic-wave propagation for annealed, commerically pure aluminum, experimental results from the longitudinal impact of uniform and tapered rods are compared to a theoretical analysis. The theoretical description is a numerical solution which utilizes the characteristic properties of the governing equations to construct difference relations for a constant mesh spacing. Numerical evidence of convergence and stability of the solution is presented. A constant-velocity boundary condition is defined by the axial collision of identical specimens, 6 inches (152 mm) in length and tapered slope varying between ± 0.03, using a $^3/_4$-inch (19 mm) bore gas gun. Strain-time profiles are measured at cross-section distances of 1, 2, and 4 inches (25, 51, and 102 mm) from the impact face with resistance gages. Quantitative agreement between theoretical prediction and experimental data, e.g., dispersive features and unloading patterns of the strain wave, show the theory and method of solution to be a reasonably accurate model of the deformation. The selection of the specimen geometry as the experimentally controllable parameter in the longitudinal impact experiment is found to be a useful testing method in investigating the dynamic response of materials.

Key Words: Aluminum; experiments; longitudinal impact; numerical solution; one-dimensional; plastic-wave propagation; rate-independent theory; tapered rods.

1. Introduction

The one-dimensional, rate-independent theory of plastic-wave propagation in thin, uniform rods has been extensively studied and the object of experimental verification since its inception in the independent works of von Kármán [1][1], Taylor [2], and Rakhmatulin [3]. Assuming that the motion and stress state are uniaxial and that the stress-strain curve is not only strain-rate independent but also concave toward the strain axis, this theory predicts the following results: A strain of ϵ propagates along the bar with a speed $\lambda = [f'(\epsilon)/\rho]^{1/2}$ where $f'(\epsilon)$ is the slope of the stress-strain curve at the strain ϵ, and ρ is the mass density; the relationship between impact velocity v and strain is given by $v = \int_0^\epsilon \lambda d\epsilon$. Experimental investigations have centered, for the most part, on verifying the above results and the strain-rate independent assumption of the stress-strain curve.

Conventionally, strain-rate independence of mechanical response is taken to imply that a material is characterized by an invariant stress-strain relation for increasing or constant values of strain (loading) and another stress-strain relation, usually linear, for decreasing values of strain (unloading). The separation of material response into loading and unloading is suggested by the well-known yielding phenomenon and elastic-plastic response of a uniaxial tension/compression specimen. When abrupt yielding or unloading occurs under dynamic conditions, the discontinuous behavior of f' causes an elastic-plastic boundary to propagate in the solution field. This boundary not only separates regions of elastic and plastic response but also defines a locus of discontinuities in particle acceleration and propagation speed λ. Such a boundary is called a weak discontinuity in contrast to a strong discontinuity (shock) where stress and particle velocity are discontinuous. The location of the elastic-plastic boundaries is a domonant feature of the dynamic analysis and often necessitates a hybrid solution where analytic, graphical, and numerical techniques are employed. The analysis by Lee [4] involving the constant-velocity impact of a uniform rod of finite length is a notable example. In many cases, idealization of boundary conditions and stress-strain behavior are made to facilitate the identification of the elastic and plastic regions

*Present address: Naval Research Laboratory, Washington, D.C. 20390.
[1] Figures in brackets indicate the literature references on page 239.

in the x, t-plane.

The degree to which the rate of strain influences the stress-strain curve has remained an active concern, as well as a point of controversy, among investigators. As emphasized by Bell [5], the governing stress-strain curve need not be the static relationship to classify a material response as strain-rate independent. Indeed, from his finite-amplitude; plastic-wave measurements Bell [6] has correlated the governing stress-strain curve for annealed, commerically pure aluminum with a rate-independent, parabolic law. This relationship is applicable between strain rates of 10 sec^{-1} to 10^3 sec^{-1} and diverges from the static curve for strains above 0.02. Contrary to the results of Bell, however, dynamic stress-strain curves of 0-tempered, commercially pure aluminum published by several authors [7, 8] show a strong dependence of mechanical response to rate of loading. These data are obtained for a range of strain rates, 10^{-3} sec^{-1} to 10^3 sec^{-1}, using several loading techniques (e.g., pressurized gas loaders, and split Hopkinson bar). In each case, loads and displacements of adjacent loading heads are simultaneously recorded under near constant strain rates. Implicit in such a measurement and a limitation to maximum loading rates obtainable in such devices is the assumption that a uniaxial strain is uniformly distributed throughout the specimen.

Within the general context of the above discussion and with the anticipation of developing a useful testing technique, the longitudinal impact of rods of nonuniform cross-sectional areas are examined in this study. The objective here is to define a constant and physically realizable loading (boundary) condition in the longitudinal impact problem, and through specimen geometry alter both the dispersive characteristics and unloading pattern of the deformation. In this way, experimental observations are readily made to test various aspects of theory and method of solution. Results are reported for three specimen geometries of annealed, commercially pure aluminum (1100–0). In each case, the boundary condition corresponds to a constant-velocity impact except that the step in velocity has a finite rise time.

The theoretical analysis is a numerical solution of the one-dimensional, rate-independent equations of plastic-wave propagation. The characteristic properties of the governing equations are utilized to construct difference relations for a constant mesh spacing. Boundaries separating regions of elastic and plastic response are located in the x, t-plane by an iterative scheme where the solution at each point is compared to its previous strain history. Shock-type motion is not encountered since only stress-strain curves concave toward the strain axis are considered. Numerical evidence of convergence and stability of the method is examined by several test problems.

A constant-velocity loading of 800 in per second (20 meters per second) is achieved by the axial collision of identical specimens. Strain-time profiles are measured on the stationary specimens at cross-section distances of 1, 2, and 4 in (25, 51, and 102 mm) from the impact face with resistance gages. In each test, the responses at two positions are recorded from a dual-beam oscilloscope, and at least three tests are made for each of the three specimen geometries considered.

2. Numerical Solution

The integration of hyperbolic differential equations in two independent variables by finite difference methods is a well developed area of applied mathematics. Chapter 2 of the text by Forsythe and Wasow [9] gives important theoretical results and surveys existing methods. The selection or development of any one scheme usually is influenced if not dictated by the problem in question. For the class of elastic-plastic problems considered in this study, the governing equations are first transformed into the normal form (see appendix for derivation)

$$\left(\frac{\partial\sigma}{\partial t}\pm\lambda\frac{\partial\sigma}{\partial x}\right)\pm\lambda\rho\left(\frac{\partial v}{\partial t}\pm\lambda\frac{\partial v}{\partial x}\right)\pm\lambda\frac{\partial A}{\partial x}\frac{\sigma}{A}=0 \qquad (1)$$

where σ is the nominal stress, v is the particle velocity, ρ the mass density, and A the cross-sectional area. The coefficient $\lambda=(f'/\rho)^{1/2}$ is identified as the characteristic wave speed and f', the slope of the stress-strain diagram, satisfies the following relations:

$$f'=E \text{ when } \epsilon<\epsilon_y \text{ or } \dot{\epsilon}^p=0$$

$$E>f'>0, \textit{ and } f''<0 \text{ when } \dot{\epsilon}^p\neq 0 \qquad (2)$$

where E is Young's modulus, ϵ_y is the strain at the proportional limit, and $\dot{\epsilon}^p$ is plastic-strain rate. In the above formulation compressive stresses and strains are positive, and the stress-strain behavior is restricted to linear elastic response on stress reversal.

A desirable property of hyperbolic equations transformed to the normal form is that the dependent variables are differentiated in a common direction. That is, σ and v are differentiated along the so-called characteristic curve $x=x(t)$ for which $dx/dt=\pm\lambda$. This form of the governing equations is amenable to finite difference approximation. The approach here is to write eq (1) as

$$d\sigma+\lambda\rho dv+\lambda\frac{\partial A}{\partial x}\frac{\sigma}{A}dt=0;\ \frac{dx}{dt}=\lambda \qquad (3)$$

$$d\sigma-\lambda\rho dv-\lambda\frac{\partial A}{\partial x}\frac{\sigma}{A}dt=0;\ \frac{dx}{dt}=-\lambda \qquad (4)$$

where $d\sigma$ and dv in eqs (3) and (4) are differentials along the $+$ and $-$ characteristic curves respectively.

To construct a difference equation problem to the above equations consider a rectangular mesh in the x,t-plane of constant spacing, Δx and Δt, as shown in figure 1. At the points P, Q, and R along a constant time line t, the solution is considered known. The solution is sought at point S at a later time $t+\Delta t$. Equations (3) and (4) can be integrated along the, as

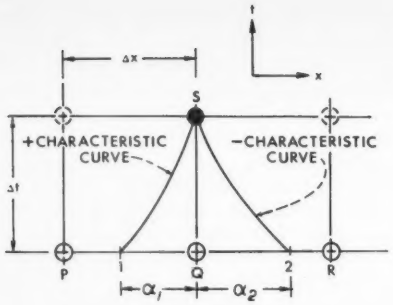

FIGURE 1. *Characteristic curves at a typical mesh point.*

yet unknown, + and − characteristic curves from their intersection with the line t, point 1 and 2 respectively, to point S. Thus, along the + characteristic curve

$$\sigma(S)/\lambda(S)-\sigma(1)/\lambda(1)+\rho[v(S)-v(1)] -\int_1^s \sigma d\lambda^{-1}+\int_1^s \frac{\partial A}{\partial x}\frac{\sigma}{A}\,dt=0 \tag{5}$$

and along the − characteristic curve

$$\sigma(S)/\lambda(S)-\sigma(2)/\lambda(2)-\rho[v(0)-v(2)] -\int_2^s \sigma d\lambda^{-1}-\int_2^s \frac{\partial A}{\partial x}\frac{\sigma}{A}\,dt=0 \tag{6}$$

where the numbers in parentheses and limits of integration denote the value of the variables at the correspondingly numbered points in figure 1.

Thus far, the solution of the quasi-linear, elastic-plastic equations has been reduced to the evalation of the integrals in eqs (4) and (5), the location of the intersection of characteristic curves with the line t (i.e., points 1 and 2), and obtaining the values of stress and velocity at the latter points. To ensure that the characteristic curves intersect between adjacent mesh points and to satisfy the important convergence requirement that the interval of dependence for the difference equations is greater than or equal to the one for the differential equations, the incremental distance Δx to the incremental time Δt ratio is taken as the elastic-propagation velocity. That is

$$\frac{\Delta x}{\Delta t}=(E/\rho)^{1/2}. \tag{7}$$

This result follows from the definition of the characteristic curves and relationships (2).

The distance α_i, locating points 1 and 2 in figure 1, is given by the line integral

$$\alpha_i=\int_i^s \lambda dt; \qquad i=1,2 \tag{8}$$

along the respective curves. When λ is a constant in the region of interest (the characteristic curves are linear), the integration of eq (8) is elementary and the first integrals in eqs (5) and (6) are seen to vanish. In the more general case, α_i is obtained from the difference approximation

$$\alpha_i=\int \lambda dt=\bar{\lambda}_i\Delta t+0(h^2), \qquad i=1,2 \tag{9}$$

where, for example,

$$\bar{\lambda}_2=\lambda(S)/2+[\lambda(R)\alpha_2+\lambda(Q)(\Delta x-\alpha_2)]/2\Delta x. \tag{10}$$

Consistent with the approximation made in eq (9), the value of the dependent variables at points 1 and 2 are determined by linear interpolation between adjacent points, for example,

$$\sigma(2)=\sigma(Q)+\frac{[\sigma(Q)-\sigma(R)]\alpha_2}{\Delta x}. \tag{11}$$

To complete the difference approximations, the integrals of eqs (5) and (6) are approximated by the following relations:

$$\int_i^s \sigma d\lambda^{-1}=[\sigma(S)+\sigma(i)]\,\frac{\lambda(i)-\lambda(S)}{2\lambda(i)\lambda(S)}+0(h^2) \tag{12}$$

$$\int_i^s \frac{\partial A}{\partial x}\frac{\sigma}{A}\,dt=\left(\frac{\partial A}{\partial x}\frac{\sigma}{A}\bigg|_s+\frac{\partial A}{\partial x}\bigg|_i\right)\frac{\Delta t}{2}+0(h^2). \tag{13}$$

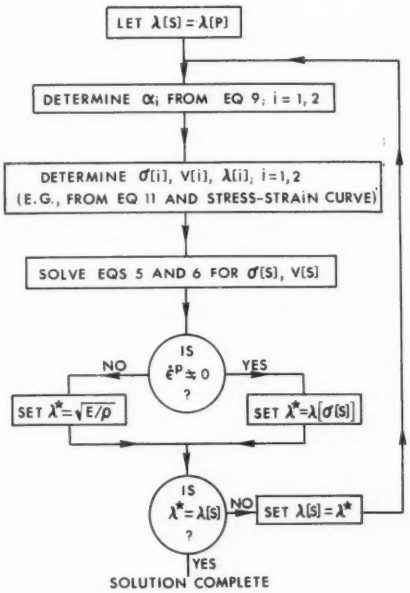

FIGURE 2. *Flow diagram of numerical solution.*

The $0(h^2)$ approximation in the above relations hold if the integrands satisfy a Lipschitz condition.

With the given difference approximations, eqs (9) through (13), a noniterative solution of eqs (5), (6), and (8) can be obtained by approximating $\lambda(s)$ [e.g., $\lambda(s)=\lambda(Q)$]. This simplification however, proved unsatisfactory for the problems considered in this paper, and an iterative scheme was formulated. This solution for a typical mesh point, see figure 1, is conveniently illustrated in the flow diagram of figure 2. When adjacent points span an elastic-plastic boundary, the location of the boundary is taken at the midpoint of the mesh spacing. For example, if point P is unloaded and $\alpha_1 \geqq 0.5\Delta x$, $\lambda(1)=(E/\rho)^{1/2}$. Otherwise, $\lambda(1)=\lambda[\sigma(1)]$. Thus, the unloading boundary is located to within a mesh spacing in the numerical output and estimated in the calculation to within one-half of a mesh spacing.

3. Example of Numerical Solution

To illustrate the behavior of the numerical solution, the plastic-wave motion in an infinite, uniform rod subject to a stress-pulse loading at the end is examined. This problem was chosen for illustration since it contains the general features of the unloading phenomena in elastic-plastic analyses and a sufficiently accurate graphical solution is available for comparison. The boundary condition is given by

$$\sigma(0, t)=8\sigma_y \frac{t}{T}(1-t/T) \tag{14}$$

where σ_y is the yield stress, $\sigma(0, t)$ is the stress at $x=0$, t again denotes time, and T is the pulse duration. The stress at the end of the rod, $x=0$, is seen to obtain a maximum value of $2\sigma_y$ at $t=0.5T$. The stress-strain curve is a bilinear relationship with an elastic modulus to plastic-tangent modulus ratio (E/E') of 16. The elastic-wave speed is, therefore, 4 times the plastic-wave speed $(\lambda=4\lambda')$.

An overall picture of the deformation is contained in the dimensionless $x/\lambda' T-t/T$ plane of figure 3. The initial elastic response, region I, is bounded by the parallel elastic-characteristic curves $x=\lambda t$. On yielding, $\sigma(0, t)=\sigma_y$, the diverging elastic-characteristic and plastic-characteristic curves define a constant state solution in region II. For t greater than $0.5T$, the stress boundary condition decreases in absolute value and an unloading boundary propagates into the solution field. The area between the unloading boundary and the initial plastic disturbance, region III, defines the zone of plastic deformation. Above the unloading boundary the response is elastic. The graphical solution of this problem can be found in the book by Rakhmatulin and Den' Yanov [10] and was originally published by Shapiro [11].

Dimensionless stress-time and velocity-time relationships of the graphical solution at positions $x=0$, $0.5\lambda' T$, $1.0\lambda' T$, $1.5\lambda' T$ are shown in figures 3 and 4. Superimposed on this description are the numerical calculations for mesh spacings of $\Delta t=0.05T$, $0.0125T$, and $0.00625T$, and $\Delta x=\lambda\Delta t$. The numerical description is seen to converge to the more accurate graphical relationships as the mesh size is decreased. The symbols used to designate the numerical solution are made open and dark at alternate positions for clarity in the 3-dimensional plot of figure 3. Only during the plastic deformation at $x=1.0\lambda' T$ does the convergence of the numerical solution appear

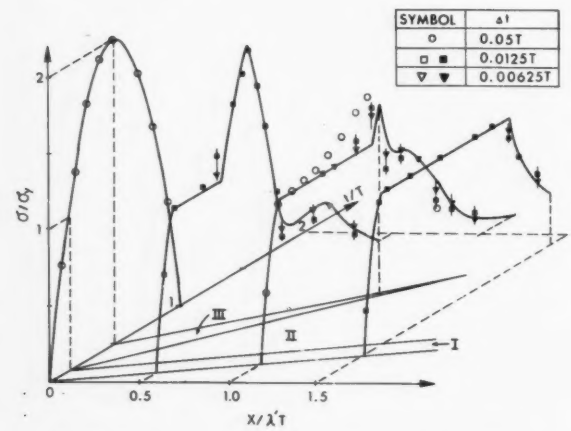

FIGURE 3. *Graphical and numerical solution of stress pulse problem (dimensionless stress-time-x plot).*

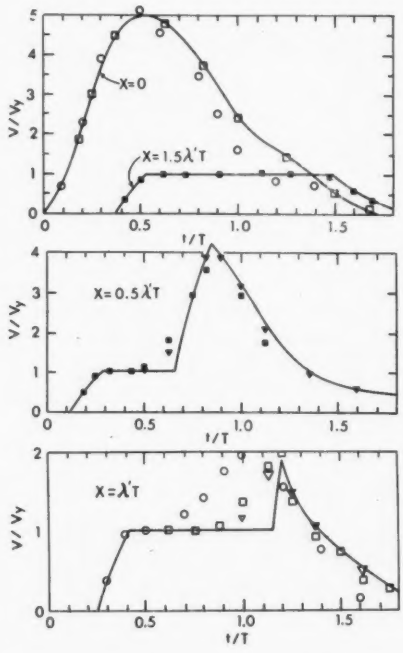

FIGURE 4. *Graphical and numerical solution of stress pulse problem (dimensionless velocity-time plot).*

objectionably slow. Examination of the $x/\lambda' T - t/T$ plane of figure 3 shows the width of the plastic zone, region III, at this point is the same order of magnitude as the smallest Δx mesh spacing. Thus, the mesh size must be decreased severalfold to obtain a more accurate solution in this region. The location of the elastic-plastic boundaries exhibit similar behavior. That is, the numerical solution is reliable in locating the elastic-plastic boundaries of figure 3 to within the accuracy of the mesh size and the precision of the calculations.

An important observation is that the numerical calculations show no evidence of instability. This hypothesis is supported by the agreement between the graphical and numerical solutions in the region of constant state, on the unloading portion of the stress-wave, and the totally elastic response at $x = 1.5\lambda' T$. For the above and similar test problems, a theoretical energy balance of kinetic, elastic, and plastic energy to work input was found to be a measure of the overall accuracy of the numerical solution. This result is used in estimating the error in the numerical description of the following section where alternate methods of solution are not available.

4. Constant-Velocity Impact of Tapered Rods

Unlike the stress pulse problem of the previous section, the last integral term of eqs (5) and (6) is nonzero for a rod of nonuniform cross-sectional area. The additional terms cause no change in the numerical scheme illustrated in the flow diagram of figure 2. Furthermore, since the difference relations of eqs (12) and (13) are consistent—that is, of the same degree of approximation—no complication in the observed behavior of the numerical solution is anticipated. Indeed, convergence of the numerical solution in this case was found to be similar if not faster than the results shown in figure 3 and other test problems. For example, the calculations presented in the following discussion for tapered rods are, for the most part, convergent to 3 significant figures for Δt equal 0.254 and 0.127 μs. A test problem of a uniform, semi-infinite rod subjected to the same boundary conditions, stress-strain relationship, grid size, and total time of calculations also exhibited convergence to 3 significant figures, and at no time was the difference between the numerical and exact solutions greater than 4 percent. The theoretical energy balance also indicated that the accuracy of the solutions presented in this section is within this range. Although analytic or so-called closed form solutions of plastic-wave propagation in rods of nonuniform cross-sectional areas have received attention in the literature (see E. Wlodarczyk [12, 13] for a notable contribution and a list of important publications), the idealizations required in this approach are too restrictive for the interests of this investigation. In fact, while such descriptions employ a variety of analytical methods, the term closed-form is sometimes misleading in that solutions often require numerical procedures and evaluation of implicit functions. Thus, more direct evaluation of the numerical method in this case was not attempted.

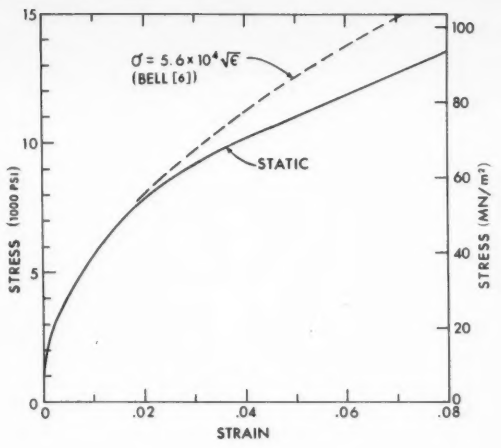

FIGURE 5. *Stress-strain curves for commercially pure aluminum annealed 2 hr at 1100 °F (593 °C) and furnace cooled.*

The material selected for investigation is commercially pure aluminum (1100–0) which has been annealed for 2 hr at 1100 °F (593 °C) and furnace cooled. The stress-strain curve shown in figure 5 is obtained from the average data of 8 static tests, and is closely approximated by 20 linear segments for use in the computer code. Three specimen geometries presented for discussion and subsequently compared to experiments are a rod of uniform cross-sectional area and rods with a ± 0.03 tapered slope. In each case, the rods are initially unstressed and 6 in (152 mm) in length; the boundary condition at the impact face corresponds to a constant-velocity impact except that the step in velocity has a finite rise-time. This phenomenon of longitudinal impact testing is caused by the physical limitation of achieving a plane impact of flat surfaces and is also influenced by the two-dimensional wave structure of the deformation near the impact face. For an impact velocity of 800 in/s (20 m/s), the loading condition was approximated by

$$V = 800 \sin \frac{\pi t}{80} \quad \text{for } 0 \leqq t \leqq 40 \ \mu\text{s}$$

and (15)

$$V = 800 \qquad \text{for } t > 40 \ \mu\text{s}$$

The 40 μs rise-time in the above relations was estimated from strain-time observations in the impact of uniform rods and agrees with similar data published by Bell [14]. From symmetry conditions of the longitudinal impact of two identical specimens, the constant-velocity loading, equal to one-half the speed of the projectile, can be shown to hold until the axial stress at the impact boundary is reduced to zero.

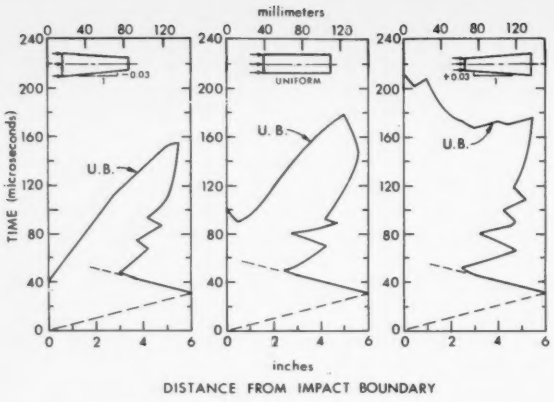

FIGURE 6. *Theoretical location of unloading boundary (U. B.) in x,t-plane.*

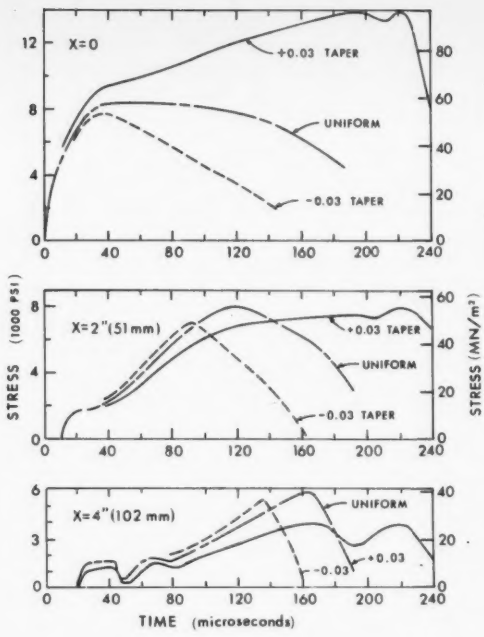

FIGURE 7. *Theoretical stress-time relationships.*

It was hypothesized that the rise-time would be relatively constant for the uniform and tapered rods for the same impact velocity. At the free end of the rods, the stress is zero for all times.

The theoretical locations of the unloading boundaries in the x,t-plane for the above defined problems are shown in figure 6. In all cases, unloading is initiated at the free end, $x = 6.0$ in (152 mm), and travels at the elastic speed into the solution field. Due to the interaction with the incident compressive wave, however, these disturbances are contained near the free end producing a sawtooth appearance. For the cross-sectional area decreasing in the direction of motion, -0.03 tapered rod, unloading also takes place at the impact face ($x = 0$) immediately after the velocity obtains a constant value (t greater than 40 μs). This boundary is seen to propagate at a near constant velocity of 0.188 times the elastic speed and produces a stress-pulse wave form. In the case of the uniform bar, a similar unloading pattern develops at a later time of 90 μs and is attributed to the influence of the free end. For the cross-sectional area increasing in the direction of motion, $+0.03$ tapered rod, the eventual unloading along the bar starts near its center at a time of 160 μs.

The attenuation and amplification of the stress wave as a function of position along the bar and specimen geometry are shown in the diagrams of figure 7. Influencing the wave shape, in any one case, are the combined and interrelated effects of changes in mass along the bar and the occurrence of unloading. For example, while the cross-sectional area decreasing in the direction of motion tends to raise the transient stress level, the relatively rapid unloading of the specimen in this case limits maximum stress values to levels below the corresponding values in the uniform bar.

As indicated in the relationships of figure 7, the stress can be expected to change from compression to tension. A tension stress can not obviously be maintained at the impact faces, and the boundary condition at the moment when the stress changes sign should be changed from constant velocity to stress free. The solutions presented for discussion were terminated sometime after the specimen had unloaded along its entire length. During this time, compression stresses were maintained at the impact face and the maximum tension stress in the bar only slightly exceeded 1200 psi (8.27 MN/m²), the virgin compression-yield stress of the material. Nonetheless, this behavior points to the need of incorporating the response of the material on stress reversal, e.g., a Bauschinger effect, into the dynamic analysis. Also, there is no guarantee that plastic deformation cannot reappear at a later time. The relative importance of these uncertainties in the present problems will be determined from experimental observations.

5. Experimental Observations

A constant-velocity loading is achieved by the axial collision of identical specimens using a ¾-in (19 mm) bore gas gun. A schematic view of the experimental setup is shown in figure 8. Fibrous washers are used to make the tapered projectiles concentric with the barrel. Impact velocities are measured by a light screen and photomultiplier tube system whose signals alternately start and stop a timer on passage of the projectile. The instrumented specimens are axially alined with the barrel and rest on point supports.

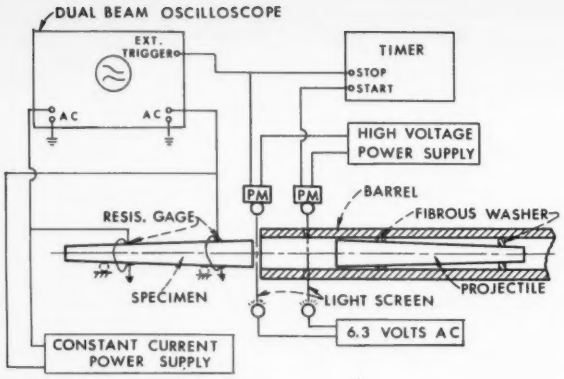

FIGURE 8. *Schematic diagram of experimental apparatus and instrumentation.*

Except for the small constraint of the fibrous washers, the projectile and specimen are in free flight during collision.

Strain-time profiles are measured at cross-sectional distances of 1, 2, and 4 in (25, 51, and 102 mm) from the impact face with epoxy back, 0.063-in (1.6 mm) gage length, constantan, resistance gages. For each measurement, two gages are mounted diametrically opposite one another with either RTC epoxy or Eastman 910 cements; the gages are wired in series and connected to a constant current power supply of 25 mA. Before each test, the circuit is calibrated by shunting a series of resistors across the gages. Outputs from two sets of gages are fed to a-c coupled, vertical amplifiers of a dual beam oscilloscope. The horizontal sweep of the oscilloscope beams is triggered by the signal from the photomultiplier tube just before impact. The writing speed is 20 μs/cm, and the vertical sensitivity is between 20 and 100 mV/cm depending on the maximum strain level. The response of the oscilloscope for the latter operating condition, better than 1 μs rise-time, is more than adequate for the observed transient signals. The signals are recorded by an open shutter camera.

Both the experimental and theoretical strain-time profiles for the three problems are shown in figures 9, 10, and 11. The designated points on the experimental traces correspond to calibration levels. Asterisks denote interpolations between calibration points. The reproducibility of the data is considered good. Two important considerations in obtaining representative data are (1) to minimize bending deformation caused by unsymmetrical and skew impact of specimen and projectile, and (2) to accommodate the one-dimensional approximation to the motion by making measurements in that section of the specimen where radial inertia effects are negligible. To investigate these factors in the present experiments, tests were made in which two sets of gages are mounted 90° apart at the same cross-sectional distance. One set of gages is mounted in the standard way to measure the axial strain; the other set of gages, 0.25 in (6.4 mm) length by 0.032 in (0.8 mm) width, is mounted so as to measure circumferential strain. Typical data is shown in figure 10, test No. 14 for the uniform rod at the one inch position. The axial strain is seen to equal twice the circumferential strain. These results are in agreement with the incompressible behavior of plastic flow for a uniaxial stress state; and therefore, indicate that effects of bending and radial motion are small.

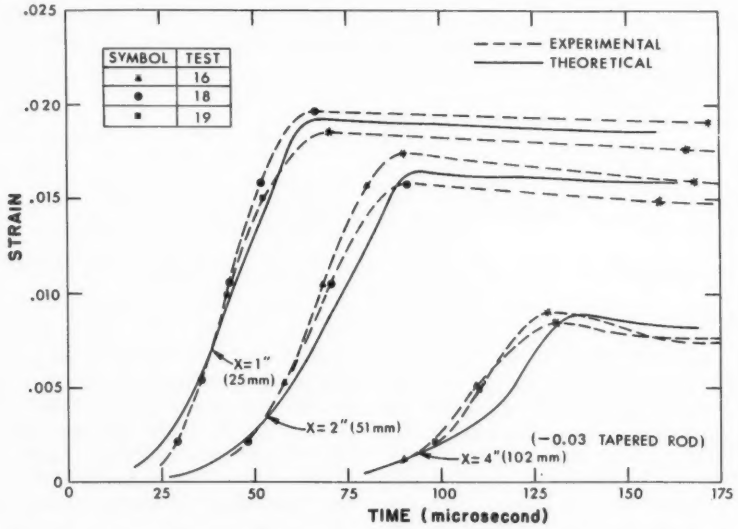

FIGURE 9. *Experimental and theoretical, axial strain-time profiles (−0.03 tapered rod).*

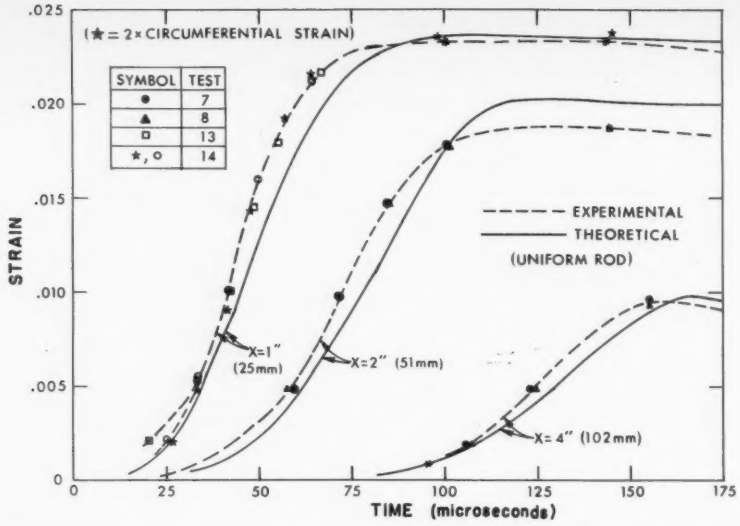

FIGURE 10. *Experimental and theoretical, axial strain-time profiles (uniform rod).*

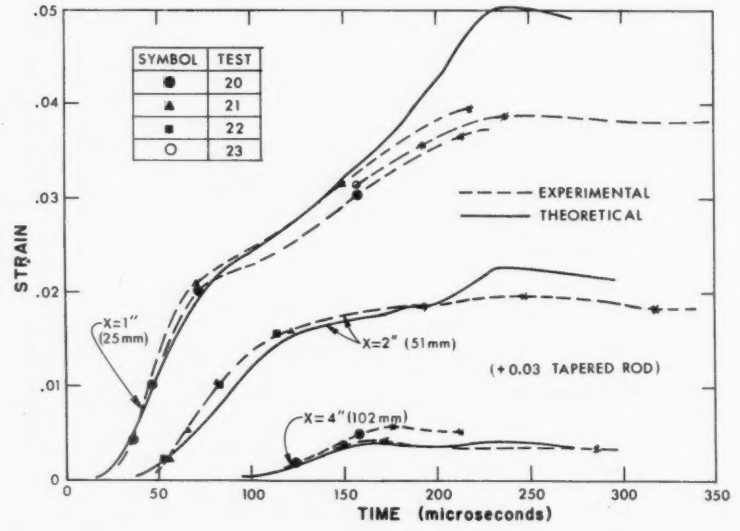

FIGURE 11. *Experimental and theoretical, axial strain-time profiles (+0.03 tapered rod).*

Considering the approximation of the boundary condition defined in eq (15), comparison of the theoretical and experimental strain-time profiles show the theory and method of solution to be an accurate model of the deformation. That is, the general features of the strain waves predicted by the numerical solution are, for the most part, in quantitative agreement with the observed behavior. Of particular note is the development of the unloading boundary in the −0.03 tapered rod which is well defined by the peak levels of the strain-time traces. This boundary is seen not only to initiate near the impact face but its propagation speed is within 10 percent of the theoretical value.

At 1 in from the impact end, each of the three specimens experienced a near constant strain-rate of 40/s. For the uniform and −0.03 tapered rods, the calculated maximum strain levels of 0.024 and 0.019, respectively, are in close agreement with experimental values. In the case of +0.03 tapered rod, however, the measured maximum strain is

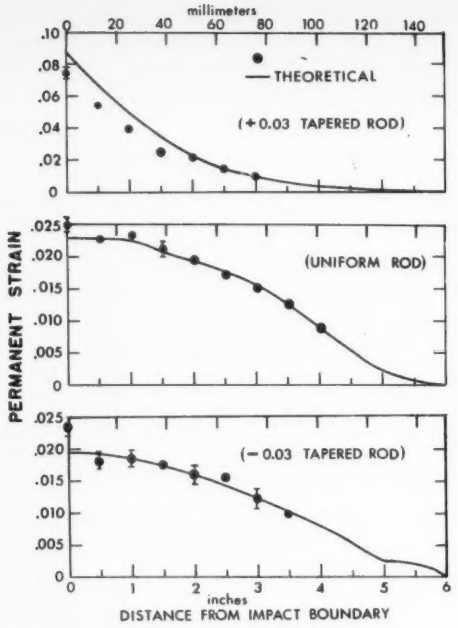

FIGURE 12. *Experimental (2 × diametral strain) and theoretical, axial, permanent-strain distribution.*

significantly less than the predicted value. While this difference suggests a strain-rate dependence of material response, the above results can also be rationalized in light of the dynamic stress-strain curve of this material reported by Bell [6]. As shown in figure 5, Bell's dynamic curve diverges from the static relationship for strains above 0.02. Furthermore, at a stress level of 11 ksi (75.8 MN/m²), the difference in strain between the dynamic and static curve is the same order of magnitude observed in figure 11.

Post-mortem examinations of the specimens and projectiles are made by measuring the diametral deformation with micrometers of 0.0001 in resolution. As shown in figure 12, twice the diametral strain is found nearly equal to theoretical prediction of the permanent, axial-strain distribution except for higher values of strain noted above. These results also satisfy the incompressible behavior of plastic flow, and resolve an earlier contention that plastic deformation of the longitudinal impact problems is confined to the time periods described in figures 9, 10 and 11. Thus, the restriction of the stress-strain curve to linear-elastic response on stress reversal is of little consequence in this study. It is noted that this restriction on the stress-strain curve is caused by the absence of a unique formulation of plastic flow on cyclic loading, and is not due to any limitation in the method of solution. Comparison of data in figures 11 and 12 also shows the resistance gages are reliable in measuring the maximum strain of these magnitudes at the 1-in (25-mm) position.

The adequacy of the rate-independent theory to describe the dynamic deformation of annealed aluminum reported above is in general concordance with the recent studies of Bodner and Clifton [15] on the stress-pulse propagation in uniform rods at room temperature; and of Schultz, Tuschak, and Vicario [16] on the transverse wire impact measurements. It would seem unlikely that close correlation between theory and experiment would be obtained for such diverse studies if the governing stress-strain curve were rate-dependent to the degree reported in references 7 and 8. In the latter references, the rate-dependent behavior of 0-tempered, commercially pure aluminum is determined by a split Hopkinson bar for a strain rate of 40/s. These data show a marked increase in flow stress above the static curve for strains between yield point and 0.10. Since the theoretical-experimental comparisons cited above do not measure simultaneously stress and strain at a material point these results are a necessary but not a sufficient measure of materials' rate-independent behavior. Nonetheless, results of the split Hopkinson bar suffers from similar limitations in assuming the stress state is quasi-static and uniaxial; and therefore, the seemingly contradictory results are noteworthy.

6. Conclusion

An iterative-explicit, numerical solution has been formulated to a large class of problems in the one-dimensional, rate-independent theory of plastic-wave propagation. Convergence and stability behavior of the method are found sufficient for machine computation. For example, solutions presented in this study with $\Delta t = 0.254$ μs required approximately 5 min/1000 time steps on a Univac 1108 computer. The solution has been used to design experiments in the longitudinal impact of uniform and tapered rods of annealed aluminum. Close correlation between theory and measured response has been obtained for strain-rates and strains as high as 40/s and 0.024. The one-dimensional theory is, however, of questionable value near the impact face, within one-half diameter, where the wave structure is two-dimensional. Also consistent with the uniaxial approximation is the requirement that the change in cross-sectional area be kept to some minimum, nominal value.

7. References

[1] von Kármán, Th., On the Propagation of Plastic Deformation in Solids, NDRC Report No. A-29, OSRD No. 365 (1942).

[2] Taylor, G. I., The Plastic Wave in a Wire Extended by an Impact Load, The Scientific Papers of G. I. Taylor (Edited by G. K. Batchelor, University Press, Cambridge) 467–479 (1958).

[3] Rakhmatulin, Kh. A., The Propagation of unloading waves, Prikladnaya Matematika i Mekhanika **9,** 1 (1945).

[4] Lee, E. H., A boundary value problem in the theory of plastic wave propagation. Quarterly of Applied Mathematics **10,** 335–346 (1952).

[5] Bell, J. F., The Dynamic Plasticity of Metals of High Strain Rates, Behavior of Materials Under Dynamic Loading (Ed. N. J. Huffinton, ASME, N.Y.) 19–41 (1965).

[6] Bell, J. F., Experimental study of the interrelation between the theory of dislocations in polycrystalline media and finite wave propagation in solids, J. Applied Physics **32**, 10, 1982–1993 (Oct. 1961).
[7] Holt, D. L., Babcock, S. G., Green, S. L., and Maiden, C. J., The strain-rate dependence of the flow stress in some aluminum alloys, Trans. American Society for Metals **60**, 2, 152–160 (June 1967).
[8] Lindholm, U. S., and Yeakley, L. M., High strain-rate testing: tension and compression, Experimental Mechanics **8**, 1–9 (Jan. 1968).
[9] Forsythe, G. E., and Wasow, W. R., Finite-Difference Methods for Partial Differential Equations, ch. 2 (John Wiley & Sons, New York, N. Y. (1960).
[10] Rakhmatulin, Kh. A., and Den' Yanov, Yu. A., Strength Under High Transient Loads, Israel Program for Scientific Translations, Jerusaleum (Daniel Davey and Co., Inc., New York, N.Y.) 31–33 (1966).
[11] Shapiro, G. S., Prodol' nye kolebaniya sterzhnei (Longitudinal vibrations of bars), Prikladnaya Matematika i Mekhanika **10**, 5 and 6 (1946).
[12] Wlodarczyk, E., Propagation of elastic-plastic and shock waves in a bar of finite length and monotone decreasing cross-sectional area, Proceeding of Vibration Problems, Warsaw **2**, 7, 135–153 (1966).
[13] Wlodarczyk, E., Propagation of a loading and unloading wave in a bar with monotone increasing cross-sectional area and curvelinear (σ-E) relation, Bulletin De L'Academie, Polonaise Des Sciences, Serie de science techniques **14**, 3, 185–252 (1966).
[14] Bell, J. F., Study of Initial Conditions in Constant Velocity Impact, J. Applied Physics **31**, 12, 2188–2195 (Dec. 1960).
[15] Bodner, S. R., and Clifton, R. J., An experimental investigation of elastic-plastic pulse propagation in aluminum rods, J. Applied Mechanics **34**, 1 (Mar. 1967).
[16] Schultz, A. B., Tuschak, P. A., and Vicario, A. A., Jr., Experimental evaluation of material behavior in a wire under transverse impact, J. Applied Mechanics **34**, 2 (June 1967).

8. Appendix: Transformation of Governing Equations into Normal Form

Adopting a Lagrangian description of the deformation, let $u(x, t)$ denote the particle displacement from its initial position x in an unstrained rod of nonuniform cross-sectional area. Hence, the nominal strain, change in length per unit initial length, is $\epsilon = \dfrac{\partial u}{\partial x}$, and the particle velocity is $v = \dfrac{\partial u}{\partial t}$. The kinematic identity follows

$$\frac{\partial \epsilon}{\partial t} = \frac{\partial v}{\partial x} \tag{1a}$$

and the equation of motion is

$$\frac{\partial \sigma}{\partial x} + \rho \frac{\partial v}{\partial t} + \frac{\partial A}{\partial x}\frac{\sigma}{A} = 0 \tag{2a}$$

where σ denotes the nominal stress, force per unit area, ρ is the mass density, and A is the cross-sectional area. A determinate system of equations is obtained by introducing the stress-strain relation, $\sigma = f(\epsilon)$, of the material in the form

$$\frac{\partial \sigma}{\partial t} - f' \frac{\partial \epsilon}{\partial t} = 0 \tag{3a}$$

where $f' = d\sigma/d\epsilon$. In the above formulation compressive stresses and strains are positive, and conservation of mass is implicitly satisfied.

The three governing equations can be written in the matrix form

$$L[\bar{w}] = A\bar{w}_x + B\bar{w}_t + d\bar{w} = 0 \tag{4a}$$

where $\bar{w} = (v, \sigma, \epsilon)$ and

$$A = \begin{bmatrix} 0 & 1 & 0 \\ 1 & 0 & 0 \\ 0 & 0 & 0 \end{bmatrix}; \quad B = \begin{bmatrix} \rho & 0 & 0 \\ 0 & 0 & 1 \\ 0 & 1 & -f' \end{bmatrix}; \quad d = \begin{bmatrix} 0 & \dfrac{\partial A}{\partial x}\dfrac{1}{A} & 0 \\ 0 & 0 & 0 \\ 0 & 0 & 0 \end{bmatrix}$$

The characteristic roots λ of the above equations are obtained by setting the determinate of the characteristic matrix Λ to zero, that is,

$$\det \Lambda = \det (A - \lambda B) = 0 \tag{5a}$$

and are found to be

$$\lambda = \pm (f'(\epsilon)/\rho)^{1/2};\ 0. \tag{6a}$$

The nonzero roots are recognized as the wave speed corresponding to a strain ϵ.

Associated with the characteristic matrix and each root is a null vector $\bar{l}$ which satisfies

$$\Lambda \bar{l} = 0. \tag{7a}$$

For eqs (4a), the null vectors are to an arbitrary scale factor

$$\begin{aligned} \bar{l}_+ &= (\lambda, \lambda^2\rho, 1) \qquad \text{when } \lambda = +(f'/\rho)^{1/2} \\ \bar{l}_- &= (\lambda, -\lambda^2\rho, -1) \qquad \text{when } \lambda = -(f'/\rho)^{1/2} \\ \bar{l}_0 &= (0, 0, 1) \qquad \text{when } \lambda = 0. \end{aligned} \tag{8a}$$

The normal form of eq (4a) is obtained by their scalar product with the null vector, that is

$$\bar{l} \cdot L[\bar{w}] = 0. \tag{9a}$$

Performing the above operation one obtains

$$\lambda\left(\frac{\partial \sigma}{\partial x} + \rho\frac{\partial v}{\partial t} + \frac{\partial A}{\partial x}\frac{\sigma}{A}\right) + \lambda^2\rho\left(\frac{\partial \epsilon}{\partial t} + \frac{\partial v}{\partial x}\right) + \left(\frac{\partial \sigma}{\partial t} - f'\frac{\partial \epsilon}{\partial t}\right) = 0$$

$$\lambda\left(\frac{\partial \sigma}{\partial x} + \rho\frac{\partial v}{\partial t} + \frac{\partial A}{\partial x}\frac{\sigma}{A}\right) - \lambda^2\rho\left(\frac{\partial \epsilon}{\partial t} + \frac{\partial v}{\partial x}\right) - \left(\frac{\partial \sigma}{\partial t} - f'\frac{\partial \epsilon}{\partial t}\right) = 0$$

$$\left(\frac{\partial \sigma}{\partial t} - f'\frac{\partial \epsilon}{\partial t}\right) = 0. \tag{10a}$$

Substituting eq (3) and the last of the above equations into the first two and rearranging terms, the normal form is

$$\left(\frac{\partial \sigma}{\partial t}+\lambda \frac{\partial \sigma}{\partial x}\right)+\lambda \rho\left(\frac{\partial v}{\partial t}+\lambda \frac{\partial v}{\partial x}\right)+\lambda \frac{\partial A}{\partial x} \frac{\sigma}{A}=0$$

$$\left(\frac{\partial \sigma}{\partial t}-\lambda \frac{\partial \sigma}{\partial x}\right)-\lambda \rho\left(\frac{\partial v}{\partial t}-\lambda \frac{\partial v}{\partial x}\right)-\lambda \frac{\partial A}{\partial x} \frac{\sigma}{A}=0. \quad \text{(11a)}$$

(Paper 72C4–260)

JOURNAL OF RESEARCH of the National Bureau of Standards—C. Engineering and Instrumentation
Vol. 72C, No. 4, October–December 1968

Analytical Studies of Probe Conduction Errors in Ground Temperature Measurements

B. A. Peavy

Institute for Applied Technology, National Bureau of Standards, Washington, D.C. 20234

(August 27, 1968)

Vertical probes with temperature sensing elements placed at fixed positions along their length are commonly used for measuring earth temperature variations with time. Mainly for structural reasons, the probes are comprised of materials whose thermal properties are not the same as those of the surrounding earth, so that the temperatures as measured at a given time by the probe are not the same as that for the undisturbed earth. A mathematical analysis for steady periodic, two-dimensional heat flow in a two body composite has been made to determine the probe conduction errors in ground temperature measurements. Several examples are given to show the relative magnitude of probe conduction errors.

Key Words: Earth temperature; probe conduction errors; steady periodic heat flow.

1. Introduction

The diurnal and annual variation of the temperatures in earth or soil at varying depths beneath the ground surface has a considerable significance in a wide variety of applications. These include the determination of thermal properties of undisturbed soils from temperature measurements, the depth at which water and sewer pipes have to be buried to prevent damage by freezing, the effect of temperature variations on heat losses from buried utility pipes and the design of house foundations, and the need to know the temperature as a function of time and depth adjacent to unoccupied underground cavities in order to evaluate heat transfer in the earth from time of occupancy.

The accurate measurement of temperature variations demands that some attention be given to the method of measurement. Some of the considerations necessary for the method are that the earth be relatively undisturbed by the insertion of temperature sensing elements (usually thermocouples, resistance thermometers or thermistors), and that the depth of the element below the surface of the earth be known quite accurately. These considerations are usually met by attaching thermocouples securely at fixed positions along the length of a rigid probe (pipe or tube) before inserting the probe into the earth. The positions or depths below the surface of the thermocouples are then known quite accurately. Other considerations for the accurate measurement of temperature are the protection of the temperature sensing elements from corrosion and stray electric fields.

The probe which is inserted into the undisturbed earth must be sufficiently strong and rigid that it not be deformed or broken upon insertion. This structural requirement may not be compatible with the requirement that the thermal properties of the probe material be similar to the thermal properties of the surrounding earth. Under the influence of temperature variations at the surface of the earth, appreciable differences in thermal properties will lead to errors in the measured variation of temperature.

The purpose of this paper is to show the effect on temperature variations at depths below the surface by placing a vertical probe in the earth.

2. Mathematical Analysis

This analysis of steady, periodic, two-dimensional heat flow assumes a simple model such as shown in figure 1, where a sine-wave temperature variation is applied to the surface, $z=0$, and at a sufficient depth, $z=l$, below the surface, the temperature is invariant with time. Region 1 comprises the earth with a thermal conductivity λ_1 and thermal diffusivity α_1. Region 2 is comprised of the probe material with a thermal conductivity λ_2 and thermal diffusivity α_2, and is in perfect thermal contact with region 1. Other more complex models and boundary conditions can be assumed using a similar analysis.

For a cylindrical geometry with the axis of the system at the center of region 2 (fig. 1), the partial differential equation for heat conduction in two regions is

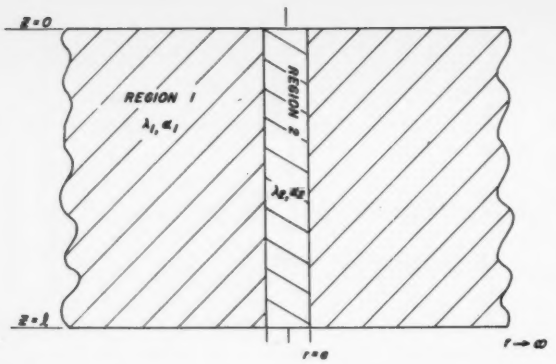

FIGURE 1. *Model for steady periodic heat flow in earth (region 1) shown with probe (region 2) of radius,* r = a.

At surface $z=0$ temperature varies sinusoidally and at $z=l$ the temperature is invariant with time.

$$\frac{\partial^2 v_i}{\partial r^2}+\frac{1}{r}\frac{\partial v_i}{\partial r}+\frac{\partial^2 v_i}{\partial z^2}=\frac{1}{\alpha_i}\frac{\partial v_i}{\partial t} \tag{1}$$

where v is the temperature potential measured from the temperature at $z=l$, α is the thermal diffusivity and subscript i denotes either region 1 or 2. There are several methods by which this problem may be solved and the author has found it convenient to use the Laplace transform method. The Laplace transform of (1) is

$$\frac{\partial^2 \bar{v}_i}{\partial r^2}+\frac{1}{r}\frac{\partial \bar{v}_i}{\partial r}+\frac{\partial^2 \bar{v}_i}{\partial z^2}=q_i^2\bar{v}_i \tag{2}$$

where $q_i^2=p/\alpha_i$ and p is the parameter of the Laplace transform.

For region 1, the radial temperature gradient is assumed to approach zero for very large values of the radius, r. The boundary conditions and continuity conditions at the interface of the two regions (fig. 1) with their respective Laplace transforms are as follows:

Surface		Condition	Transform	
$z=0$	$0\le r<\infty$	$v_1=v_2=\sin\omega t$	$\bar{v}_1=\bar{v}_2=\frac{\omega}{p^2+\omega^2}$	(3)
$z=l$	$0\le r<\infty$	$v_1=v_2=0$	$\bar{v}_1=\bar{v}_2$	(4)
$r=a$	$0\le z\le l$	$v_1=v_2$	$\bar{v}_1=\bar{v}_2$	(5)
$r=a$	$0\le z\le l$	$\lambda_1\frac{dv_1}{dr}=\lambda_2\frac{dv_2}{dr}$	$\lambda_1\frac{d\bar{v}_1}{dr}=\lambda_2\frac{d\bar{v}_2}{dr}$	(6)

where $\omega=2\pi/T$. and T is the period of a cycle. Solutions of (2) that satisfy (3) and (4) for the two regions are

$$\bar{v}_1=\frac{\omega}{p^2+\omega^2}\frac{\sinh q_1(l-z)}{\sinh q_1 l}+\sum_{n=1}^{\infty}\frac{A_nK_0(\gamma_n r)}{K_0(\gamma_n a)}\sin\frac{n\pi z}{l} \tag{7}$$

$$\bar{v}_2=\frac{\omega}{p^2+\omega^2}\frac{\sinh q_2(l-z)}{\sinh q_2 l}+\sum_{n=1}^{\infty}\frac{B_nI_0(\beta_n r)}{I_0(\beta_n a)}\sin\frac{n\pi z}{l} \tag{8}$$

where $\gamma_n^2=q_1^2+(n\pi/l)^2$, $\beta_n^2=q_2^2+(n\pi/l)^2$, I_0 and K_0 are zero order modified Bessel functions of the first and second kind respectively, and A_n and B_n are constants to be determined from (5) and (6). Substitution of (7) and (8) at $r=a$ in (5), yields

$$\sum_{n=1}^{\infty}(A_n-B_n)\sin\frac{n\pi z}{l}=\frac{\omega}{p^2+\omega^2}\left[\frac{\sinh q_2(l-z)}{\sinh q_2 l}-\frac{\sinh q_1(l-z)}{\sinh q_1 l}\right].$$

Multiplying both sides by $\sin\frac{k\pi z}{l}$ ($k=1,2\ldots$) and integrating from $z=0$ to l, gives

$$A_n-B_n=\frac{2\omega n\pi(q_1^2-q_2^2)}{l^2(p^2+\omega^2)\gamma_n^2\beta_n^2}=\frac{2\omega l^2 p\left[\frac{1}{\alpha_1}-\frac{1}{\alpha_2}\right]}{n^3\pi^3(p^2+\omega^2)(1+pd)(1+pc)} \tag{9}$$

where $d=l^2/\alpha_2 n^2\pi^2$ and $c=l^2/\alpha_1 n^2\pi^2$. Differentiation of (7) and (8) with respect to r and substitution in (6) yields

$$B_n=-\frac{A_n\lambda_1\gamma_n K_1(\gamma_n a)I_0(\beta_n a)}{\lambda_2\beta_n K_0(\gamma_n a)I_1(\beta_n a)}. \tag{10}$$

Substitution of (10) in (9) gives A_n, which when substituted in (7) gives at the interface, $r=a$,

$$\bar{v}_1(a)=\frac{\omega}{p^2+\omega^2}\frac{\sinh q_1(l-z)}{\sinh q_1 l}+\frac{2\omega l^2 p\left[\frac{1}{\alpha_1}-\frac{1}{\alpha_2}\right]}{p^2+\omega^2}\sum_{n=1}^{\infty}\frac{\sin n_\pi z/l}{n^3\pi^3 W(p)} \tag{11}$$

where

$$W(p)=(1+pc)(1+pd)\left\{1+\frac{\lambda_1(1+pc)^{1/2}I_0(L)K_1(J)}{\lambda_2(1+pd)^{1/2}I_1(L)K_0(J)}\right\}$$

$$L=\frac{n\pi a}{l}(1+pd)^{1/2}$$

$$J=\frac{n\pi a}{l}(1+pc)^{1/2}.$$

To obtain v_1 from $\bar{v}_1$, the Inversion Theorem for the Laplace transformation is used, where for determining the steady periodic portion only the simple poles at $p=\pm i\omega$ need be considered. The residues at the poles yield

$$v_1(a)=[(XR+YS)\sin\omega t+(XS-RY)\cos\omega t]/(X^2Y^2)$$

$$+2\omega l^2\left[1-\frac{\alpha_1}{\alpha_2}\right]\sum_{n=1}^{\infty}\frac{(P\cos\omega t+Q\sin\omega t)\sin n\pi z/l}{n^3\pi^3(P^2+Q^2)} \quad (12)$$

where $\psi=\sqrt{\pi/(\alpha_1 T/l^2)}$

$$X=\sinh\psi\cos\psi$$

$$Y=\sin\psi\cosh\psi$$

$$R=\sinh\psi\,(1-z/l)\cos\psi\,(1-z/l)$$

$$S=\sin\psi\,(1-z/l)\cosh\psi\,(1-z/l)$$

$$W(\pm i\omega)=P\pm iQ$$

The real and imaginary parts of W are determined using complex arithmetic where the real and imaginary parts of the Bessel functions of complex argument are given by

$$I_n(\rho e^{i\varphi})=M_n(\rho,\varphi)+iN_n(\rho,\varphi)$$

$$K_n(\rho e^{i\varphi})=G_n(\rho,\varphi)+iH_n(\rho,\varphi).$$

A computer subroutine has been programmed to give values for M_n, N_n, G_n, and H_n for $n=0$ and 1. Numerical values for the temperature potential at the interface between the probe and the earth have been calculated from (12) using a Univac 1108 digital computer.

3. Numerical Solutions

If the thermal diffusivities of the earth and the probe material are equal, the last term on the right side of (12) goes to zero and temperature variations with time and depth from the surface will be the same at corresponding depths anywhere in the earth.

For numerical solutions, there are numerous possible variations of the parameters. For this reason, only the effects of variations in the thermal properties of the probe material (region 2) will be studied while the other parameters will be held constant. For a diurnal temperature variation, let

$T=24$ hr (86400 s)

$l=5$ ft (1.524 m)

$a=0.05$ ft (0.01524 m)

$\lambda_1=0.21$ BTU hr^{-1} ft^{-1} (deg F)$^{-1}$ (0.3633 w m^{-1} K^{-1})

$\alpha_1=0.01$ ft^2 hr^{-1} (2.58×10^{-7} m^{2}s^{-1}).

Because the probe may not be comprised of a homogeneous material and in most cases will be a filled tube, its thermal properties are difficult to specify. For this reason, four sets of "effective" thermal properties were investigated characterizing undisturbed earth and low, medium and high thermal conductivity probe materials. The thermal properties for case 2 may approximate those for wood or bakelite, for case 3, stone or masonry and for case 4, stainless steel.

Numerical solutions of v_1 against time (12) for the four cases are shown in figure 2. Curves are shown for the 2 in (0.0508 m), 6 in (0.1524 m) and 12 in (0.3048 m) depths and for only a 12 hr portion of the 24 hr cycle. Since the amplitude of the temperature potential was assumed to be unity (3), the actual temperature $\theta(a, z, t)$ at the radius $r=a$ as a function of time and position may be found from the ratio

$$v_1(a, z, t)=\frac{\theta(a, z, t)-\theta_1}{\theta_2}$$

where θ_1 is the temperature at $z=l$ and θ_2 is the amplitude of the temperature variation at $z=0$.

In case 1, the probe material has the same properties as the surrounding earth and therefore the temperature variation is the same as that for undisturbed earth under the boundary conditions cited. Temperature variations for cases 2 and 3 give negligibly small deviation from the undisturbed earth temperature at the 12 in depth. Case 4 representing a highly conductive probe shows large deviations from the undisturbed earth temperature at these depths. With this probe there is a considerable phase angle deviation which increases with increase in depth below the surface.

Figures 3a, 3b, and 3c show the temperature differences between the temperature potential at $r=a$ and that for the undisturbed earth for case 2, 3, and 4 as a function of time and position below the surface $z=0$. Letting Δ be the temperature difference as described above, then the actual temperature difference between the temperature of the probe at $r=a$ and that for the undisturbed earth is

	λ_2		α_2	
	BTU hr^{-1}ft^{-1} (deg F)$^{-1}$	wm^{-1}K^{-1}	ft^{2}hr^{-1}	m^{2}s^{-1}
Case 1 (Undisturbed earth)	0.21	0.3633	0.01	2.58×10^{-7}
Case 2 ("Low" conductivity)	0.08	.1384	.0044	1.135×10^{-7}
Case 3 ("Medium" conductivity)	0.8	1.384	.03	7.742×10^{-7}
Case 4 ("High" conductivity)	10.	17.3	.4	1.032×10^{-5}

$$\Delta_a = \theta_2 \Delta.$$

Assuming a 10 °F amplitude for the diurnal variation, then for case 4 at $t = 6$ hr the actual temperature difference is 2.26 °F for the 2 in depth, 3.06 °F for the 4 in depth, 2.66 °F for the 6 in depth and 0.45 °F for 12 in depth.

4. Discussion

The mathematical development given in a previous section considers a pure sine-wave temperature variation at the surface of the earth, whereas in nature the actual surface temperature variation for a weather cycle is given by the trigonometric series

$$v = \sum_{m=1}^{\kappa} B_m \sin(\omega_m t - \varphi_m)$$

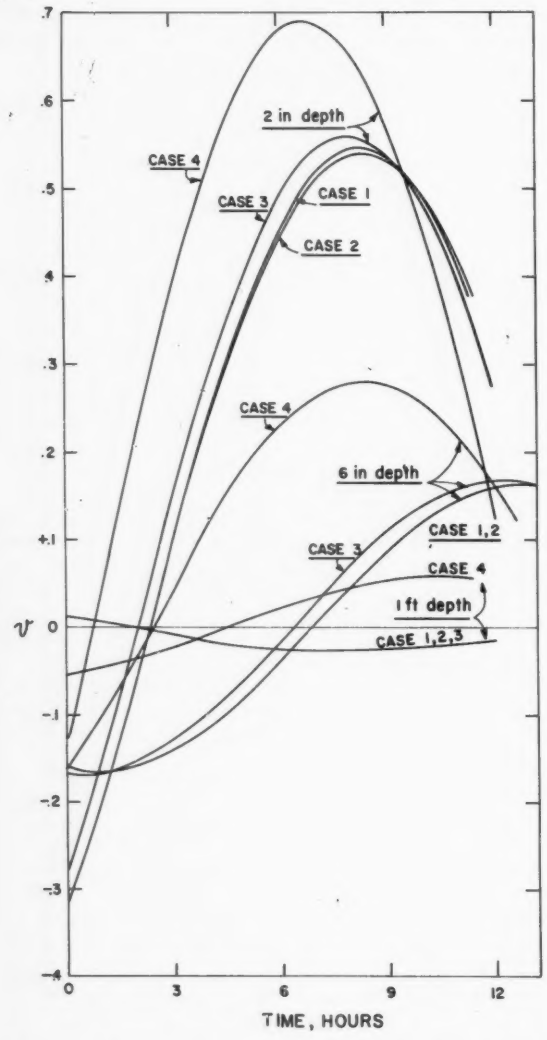

FIGURE 2. *Temperature variation with time and depth below the surface at the radius* r = a *(fig. 1) for the four cases, assuming unit amplitude in the temperature variation at the depth* z = 0.

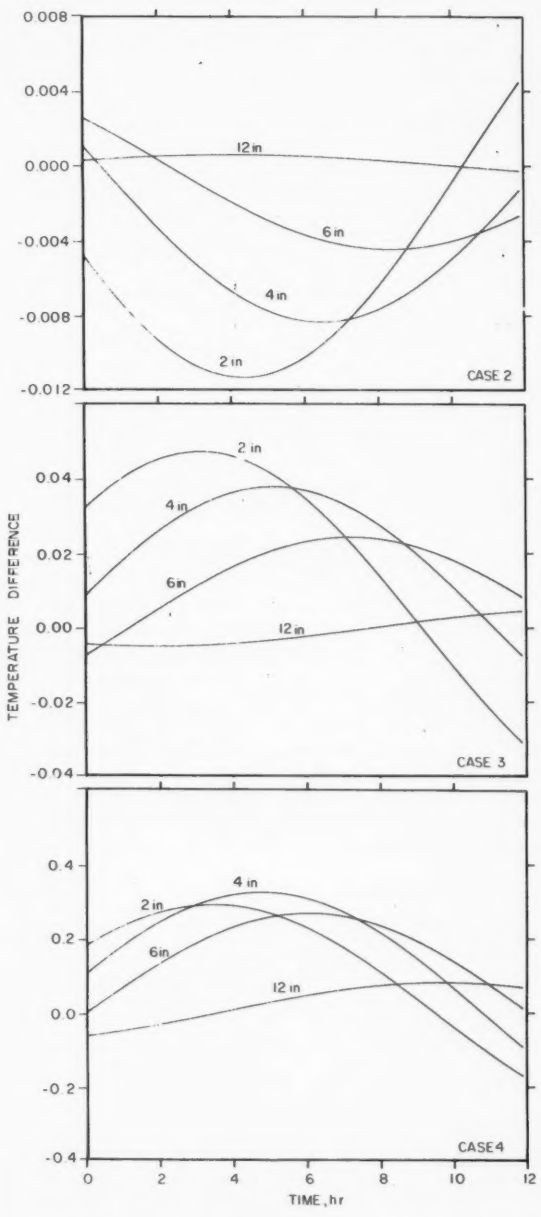

FIGURE 3. *Temperature difference between temperature at* r = a *and that for undisturbed earth for (a) case 2, (b) case 3 and (c) case 4 as a function of time and position below the surface* z = 0.

where κ can be considered to be a finite number. This relationship can also be satisfied in the mathematical development by its substitution for (3). This was not considered necessary for the purpose of this paper, which is to present an analytical method and to show by numerical results the relative magnitude of probe conduction errors on a diurnal basis. If an annual cycle is to be considered, the depth l, at which the temperature is assumed to be invariant with time should be much greater than the 5 ft used for the diurnal cycle.

A study of the transient case was made by Brown.[1] He performed tests which produced a monotonically increasing temperature change with time at the various depths below the surface. For the usual periodic weather cycle (diurnal and annual), the present analysis permits estimation of the magnitude of the harmonically varying probe conduction errors represented by the differences in temperature when employing probes of different thermal properties (cases 2, 3, and 4) compared to that of undisturbed earth (case 1).

The impetus for this paper is the determination of the thermal properties of undisturbed soils or earth from ground temperature measurements. This work is currently sponsored by the Office of Civil Defense, Department of the Army, and consists of this analysis, laboratory tests of probe configurations under time-varying temperature conditions, and actual field measurements now underway.

(Paper 72C4–281)

[1] W. G. Brown, Thermal model tests for probe conduction errors in ground temperature measurement (Res. Paper 194, Division of Building Research, National Research Council, Canada, Sept. 1963).

319-617 O - 68 - 2

JOURNAL OF RESEARCH of the National Bureau of Standards—C. Engineering and Instrumentation
Vol. 72C, No. 4, October–December 1968

Nonlinear Constrained Optimization by a Nonrandom Complex Method

R. A. Mitchell and J. L. Kaplan [1]

Institute for Basic Standards, National Bureau of Standards, Washington, D.C. 20234

(September 4, 1968)

A nonrandom complex method is described for application to optimization problems characterized by nonlinear objective and constraint functions involving continuous and/or discrete optimization variables. The method is a mutation of the "complex" method (involving a pseudo-random process) developed by M. J. Box. Application of the method is demonstrated by two minimum weight structural analysis problems: (1) an n-degree elliptical elastic ring with sinusoidally varying cross section dimensions; and (2) a rib-stiffened, simply supported elastic plate. The ring problem has six continuous independent variables, and the plate problem has four independent variables, two of which are discrete.

Key Words: Curved bar analysis; discrete variables; elastic; force transducer; minimum weight; n-degree elliptical ring; nonlinear programming; nonrandom complex method; optimization; rib-stiffened plate; structural analysis.

1. Introduction

There are many engineering problems which have an unlimited number of adequate solutions, but which have an optimum solution with regard to some criterion such as weight or cost. This paper describes a nonrandom complex method for seeking the optimum solution for a class of such problems characterized by nonlinear objective and constraint functions of continuous and/or discrete variables. The nonrandom complex method is a mutation of the "complex" method of Box [1].[2] Both the nonrandom method and the Box method have an important advantage over many other methods for nonlinear optimization in that they do not require computation of partial derivatives of the functions.

The nonrandom method and the Box method begin a search by generating a configuration of points (an initial complex) whose coordinates are values of the independent optimization variables. At least one point of the initial complex (the initial point) must be known, in advance, to fall inside all constraint bounds of the problem. All other points of the complex are computed to fall inside or on the constraint bounds.

In the Box method, the points of an initial complex are generated by a pseudo-random process. Numerical results by Hilleary [2], using the Box method, demonstrate that the rate of convergence to a solution is dependent on the character of the initial complex, and that a poor initial complex may result in failure of the method to converge.

In the nonrandom complex method reported here, the character of the initial complex is influenced by the initial point to a much greater degree than in the Box method. Thus, a good initial point leads to a relatively good initial complex. This characteristic is used to advantage by generating a new initial complex about a new initial point if the convergence of a search sequence becomes excessively slow or stops. The same characteristic also facilitates a more efficient discrete variable optimization than would be expected from the Box method. The nonrandom method imposes a lower bound on initial complex size by selecting initial complex points in such a way that at least one-half the constraint bounded range of each independent variable (in the one-dimensional subspace containing the initial point) is included within the complex span.

The nonrandom complex method has been used successfully for the following two minimum weight structural analysis problems:

1. An n-degree elliptical elastic ring with sinusoidally varying cross-section dimensions, loaded by two forces acting in opposite directions along a diameter; and
2. A rib-stiffened simply supported plate, loaded by in-plane compressive forces.

The ring problem has six continuous independent variables, and the plate problem has four independent variables, two of which are discrete. Both problems have nonlinear objective and constraint functions. A large class of optimization problems fall within the range of mathematical complexity represented by these two problems.

[1] Present address: Mathematics Department, University of Maryland, College Park, Maryland.
[2] Figures in brackets indicate the literature references at the end of this paper.

List of Symbols

x_k independent variable of the optimization problem,
g_i implicit constraint function,
h_i implicit constraint lower bound,
k_i implicit constraint upper bound,
E^m m-dimensional Euclidean space,
P_j a point of the optimization complex,
a_k lower explicit bound on x_k,
b_k upper explicit bound on x_k,
α reflection factor of complex optimization method,
m the number of independent variables of the optimization problem,
p the number of independent discrete variables of the optimization problem,
L total force applied to ring,
P $=L/2$, force applied to one quadrant of ring,
δ curved bar deflection, one-half ring deflection,
r, θ polar coordinates of ellipse,
n degree of ellipse,
a, b semimajor and semiminor axes of ellipse,
h ring cross-section width,
t ring cross-section thickness normal to tangent of ellipse,
c average of maximum and minimum ring width,
d average of maximum and minimum ring thickness,
e dimensionless parameter of ring width variation,
f dimensionless parameter of ring thickness variation,
s arc length variable measured along ellipse,
M moment,
N normal force,
V shearing force,
k curvature of ellipse,
g integral defined in equations (7) and (8),
ν Poisson's ratio,
E modulus of elasticity,
σ normal stress,
S design maximum stress,
λ scale factor,
W weight,
γ material density,
N_l normal force per unit width of plate,
l, w length and width of rib-stiffened plate,
t_p flat plate thickness,
t_r rib thickness,
b_p rib spacing,
b_r rib width,
H $=t_p+b_r$, total thickness of rib-stiffened plate.

2. The Nonrandom Complex Method

The following paragraphs describe the nonrandom complex method as it is applied to a continuous variable problem. Adaptation of the method for discrete variable optimization is described later.

The nonrandom complex method searches for a set of values of the independent continuous variables $x_1, x_2, \ldots, x_m$ which gives a minimum value of an arbitrary objective function $f(x_1, x_2, \ldots, x_m)$, subject to explicit constraints on the variables, and subject to implicit constraint bounds on arbitrary functions of the variables. The implicit constraint functions $g_i(x_1, x_2, \ldots, x_m)$ are subject to inequalities of the form $h_i \leq g_i \leq k_i$, where the bounds h_i and k_i represent arbitrary limits and either one or both may appear.

To begin the method it is required that a point $(x_1', x_2', \ldots, x_m')$, in m-dimensional Euclidean space, E^m, be known which is feasible (i.e., does not violate any constraint) and which does not lie on any constraint bound. Using this initial point, a set of $2m+1$ points in E^m is then generated by the following procedure:

1. Denote the jth point in the set of $2m+1$ points by P_j. Let $P_1 = (x_1', x_2', \ldots, x_m')$.

2. Denote the explicit constraints on the independent variables by $a_k \leq x_k \leq b_k$ for $k = 1, 2, \ldots, m$. Set $k = 1$.

3. Let $P_{2k} = (x_1', x_2', \ldots, x_{k-1}', b_k, x_{k+1}', \ldots, x_m')$. This point is the same as the initial point P_1 except in the kth coordinate, where x_k' has been replaced by its explicit upper bound b_k.

4. Evaluate all implicit constraint functions at P_{2k}. If all are satisfied, move on to step 5. If any implicit constraint is violated, set

$$P_{2k} = \left(x_1', x_2', \ldots, x_{k-1}', \frac{b_k + x_k'}{2}, x_{k+1}', \ldots, x_m'\right).$$

This moves P_{2k} one-half the distance toward the initial point P_1. Once again, evaluate the implicit constraint functions at P_{2k}, go to step 5 if they are satisfied, or move P_{2k} one-half the remaining distance to P_1 otherwise. Repeat the process until P_{2k} is feasible.

5. Let $P_{2k+1} = (x_1', x_2', \ldots, x_{k-1}', a_k, x_{k+1}', \ldots, x_m')$. This point is the same as the initial point P_1 except in the kth coordinate, where x_k' has been replaced by its explicit lower bound a_k.

6. Proceed with point P_{2k+1} as in step 4, moving P_{2k+1} one-half the distance to the initial point P_1 until P_{2k+1} is feasible.

7. Reiterate steps 3 through 6 for $k = 2, 3, \ldots, m$. This gives a collection of $2m+1$ points $\{P_1, P_2, \ldots, P_{2m+1}\}$ which is the initial complex.

The method proceeds to search for an optimum by repeatedly altering the complex, one point at a time, as follows. The objective function $f(x_1, x_2, \ldots, x_m)$ is evaluated at each complex point P_j. The complex point with the worst (greatest) objective function value is selected, and the centroid of the remaining $2m$ points is computed. The worst complex point is then discarded and replaced by a new point, with the exception that the second worst point is discarded if the worst point is also the newest complex point. That is, a given complex point is not permitted to be changed in consecutive iteration cycles. A provisional replacement point is computed which is:

1. Collinear with the discarded (worst or second worst) point and the centroid of the $2m$ complex points excluding the worst point;

2. On the side of the centroid opposite the discarded point; and

3. Located α times as far from the centroid as was the discarded point, where α is a constant parameter called the reflection factor.

If the provisional replacement point violates an explicit constraint on any variable, the corresponding coordinate is set equal to the violated constraint bound. If the new provisional point then violates an implicit constraint, it is repeatedly replaced by a new point, located one-half the distance to the centroid of the $2m$ points, until a feasible new complex point is found. The new centroid of all $2m+1$ complex points is then determined, and the objective function at that centroidal point is evaluated and used as an index of convergence. This completes one cycle of the iterative search process.

During a search, a series of cycles may yield an oscillating value of the centroidal objective function with little or no net convergence. If a preassigned number of consecutive oscillating cycles yield no net improvement in the centroidal objective function value, a new initial complex is generated, using the best centroid yet computed as the initial point.

A search is stopped if a preassigned number of consecutive cycles yield no change in the value of the centroidal objective function greater than a preassigned small amount. This condition may indicate that an approximation of the global optimum has been found. But, the same condition could indicate that a relative (nonglobal) optimum has been found, or that the complex has collapsed to a small size due to the reflection factor being too small or due to some other characteristic of the particular problem. Cycle count and elapsed time stops are also used to prevent excessive computer time.

A search may also be stopped if the centroid of the $2m$ nonworst complex points lies on or outside a constraint bound. This can be caused by a nonconvex constraint surface or, if the complex is small, it can be caused by numerical rounding errors.

If a search is stopped before a satisfactory approximate optimum is found, it can be restarted by generating a new initial complex, using one of the better complex centroids already computed as the initial point. A centroid somewhat offset inside all constraint bounds, and not necessarily the centroid with the lowest objective function value, is used for this purpose.

3. Discrete Variable Optimization

If variables x_1 through x_p of the m optimization variables, where $p \leq m$, are limited to known sets of discrete values, the following adaptation of the nonrandom complex procedure is applicable. All m optimization variables are temporarily assumed to be continuous and an optimum continuous variable solution $\bar{x}=(\bar{x}_1, \bar{x}_2, \ldots, \bar{x}_m)$ is found by the nonrandom complex method. A set of 4^p neighboring discrete value points is then generated by the following procedure:

1. Select the two discrete values of the kth discrete variable, where $k \leq p$, that are greater than $\bar{x}_k$ and that most nearly approximate $\bar{x}_k$.

2. Select the two discrete values of x_k that are less than or equal to $\bar{x}_k$ and that most nearly approximate $\bar{x}_k$.

3. Reiterate steps 1 and 2 for $k=1, 2, \ldots, p$. This gives 4 discrete approximate values for each $\bar{x}_k$, $k \leq p$.

4. Generate the 4^p distinct combinations of the discrete values obtained by step 3. Each combination is a set of the discrete coordinates for a discrete approximation to the continuous variable solution point $\bar{x}=(\bar{x}_1, \bar{x}_2, \ldots, \bar{x}_m)$. The remaining coordinates for the 4^p discrete points that surround and approximate $\bar{x}$ are the continuous variable coordinates $\bar{x}_k$, where $k > p$.

The objective and constraint functions are then evaluated at each of the 4^p discrete value points, and the best (lowest objective function value) and second best feasible points are selected. These two points are used as the initial points for two nonrandom complex optimization searches. For each search, the discrete variables are held constant and the continuous variables are optimized within the subspace defined by the discrete coordinates. The two resulting solutions are then compared. If the better of the two solutions results from the better initial point, that solution is assumed to be the optimum solution to the problem. If the better solution results from the second best initial point, the next (third) best feasible point of the 4^p discrete points is used as the initial point for a third continuous variable optimization within the discrete coordinate subspace containing the point. The process is repeated similarly until a solution results that is worse than a previous solution.

If the number of independent discrete variables is such that 4^p discrete value points would be an excessively large number to evaluate, an alternative procedure is advisable. A reasonable compromise would be to generate and evaluate the 2^p adjacent discrete value points that bound the continuous variable solution $\bar{x}$.

4. Elastic Ring Problem

An earlier paper [3] reported a minimum weight structural analysis of an n-degree elliptical elastic ring, with sinusoidally varying cross section dimensions, by a sequential grid method. The same elastic ring optimization problem is here used to demonstrate application of the nonrandom complex method to a difficult continuous variable problem.

The objective of the optimization problem is to find the dimensions of the minimum weight ring that would satisfy the arbitrary force capacity, deflection, and dimensional requirements of the load supporting element of a force transducer. The force capacity requirement is satisfied by a scaling procedure. Ring deflection

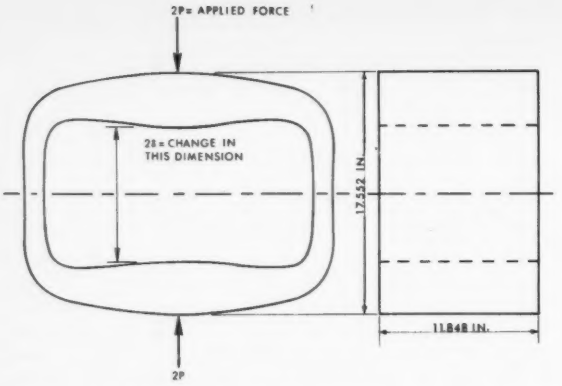

FIGURE 1. *A 1,000,000 lb capacity n-degree elliptical ring with sinusoidally varying thickness.*

and critical ring dimensions are expressed as implicit constraint functions.

An elastic ring force transducer is loaded by two forces acting in opposite directions along a diameter, as shown in figure 1. Corresponding ring deflections 2δ are measured and related to applied forces $2P$ by a calibration factor. A structural analysis (and FORTRAN computer program) for the elastic ring was given in the earlier paper [3]. The ring was analyzed as a thick curved bar, assuming small deflections, plane strain, Winkler-Bach bending stress distribution, uniform normal stress distribution, and parabolic shear stress distribution. The following paragraphs summarize the structural analysis and give the equations required for the nonrandom complex optimization.

For a ring of the shape shown in figures 1 and 2, the locus of centroids of ring cross sections is an n-degree ellipse defined by the equation

$$r = ab(b^n \cos^n \theta + a^n \sin^n \theta)^{-1/n}, \; n \geq 2. \tag{1}$$

Ring rectangular cross-section width h and thickness t are given by

$$h = c(1 - e \cos 2\theta), \tag{2}$$

and

$$t = d(1 - f \cos 2\theta), \tag{3}$$

in which c and d are positive parameters and e and f are parameters of absolute value less than unity.

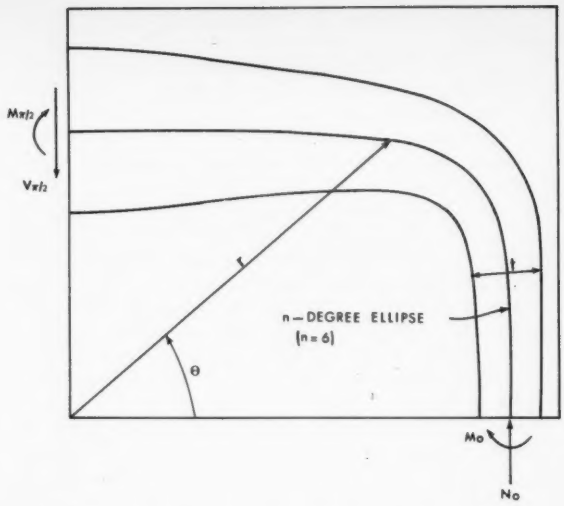

FIGURE 2. *Loads acting on one quadrant of a ring.*

Using these equations, the shape of a ring within this geometric class can be specified by the seven parameters a, b, c, d, e, f, and n. If $a = b$, $n = 2$, and $e = f = 0$, the ring shape is circular with uniform rectangular cross section.

Figure 2 shows the loads acting on one quadrant of the ring. The resultant moment and forces acting on a typical normal cross section are

$$M = M_{\pi/2} - Pr \cos \theta = PM', \tag{4}$$

$$N = P\left(\sin \theta \frac{dr}{ds} + r \cos \theta \frac{d\theta}{ds}\right) = PN', \tag{5}$$

and

$$V = P\left(r \sin \theta \frac{d\theta}{ds} - \cos \theta \frac{dr}{ds}\right) = PV', \tag{6}$$

in which ds is the increment of arc length of the n-degree ellipse. With the assumed stress distributions, the strain energy of the ring quadrant is obtained by integrating over the quadrant volume. Castigliano's strain energy theorem is used to determine the moment and deflection at the point of load application to be

$$M_{\pi/2} = P\left[\frac{\int_0^{\pi/2} \frac{(1-\nu^2)gr \cos \theta}{h} ds - \int_0^{\pi/2} \frac{k \sin \theta}{ht} dr - \int_0^{\pi/2} \frac{kr \cos \theta}{ht} d\theta}{\int_0^{\pi/2} \frac{(1-\nu^2)g}{h} ds}\right], \tag{7}$$

and

$$\delta_{\pi/2} = \frac{P}{E} \int_0^{\pi/2} \frac{1}{ht}\left[N'^2 + \frac{12}{5}(1+\nu)V'^2 - (1-\nu^2)gtr \cos \theta M' + kM'N' - kr \cos \theta N'\right] ds, \tag{8}$$

in which

$$k=\frac{r^2+2\left(\frac{dr}{d\theta}\right)^2-r\frac{d^2r}{d\theta^2}}{\left[r^2+\left(\frac{dr}{d\theta}\right)^2\right]^{3/2}},$$

$$g=\int_t\left[\frac{k}{t}+\frac{y}{(1+ky)\int_t\frac{y^2}{(1+ky)}\,dy}\right]^2 dy,$$

ν = Poisson's ratio,
E = modulus of elasticity,
and y is the distance from a cross-section centroid to a point in the cross section, positive in the outward direction. The stress in the ds direction on the inner surface of the ring is given by

$$\sigma_T=P\left[\frac{M'k}{ht}-\frac{M't}{h(2-kt)\int_t\frac{y^2}{(1+ky)}\,dy}+\frac{N'}{ht}\right]. \tag{9}$$

For the optimization analysis, it is assumed that the force resisting capacity of the ring is limited by the maximum value of σ_T for all θ. The possibility of capacity being limited by some other component of stress or combined stress should be checked in any final design analysis.

To make each numerical solution have the required force capacity, all length dimensions in the r-θ plane are scaled by a factor λ that will make the maximum value of σ_T, for the entire ring, equal a prescribed maximum design stress S. Cross-section width h is not scaled. The scale factor is

$$\lambda=\frac{L_\lambda}{2S}\left[\frac{M'k}{ht}-\frac{M't}{h(2-kt)\int_t\frac{y^2}{(1+ky)}\,dy}+\frac{N'}{ht}\right]_{\max.}, \tag{10}$$

in which S = design maximum stress,
L_λ = required force capacity,
and the maximum value of the bracketed function for all θ is used.

In the optimization analysis the above equations are first solved for a ring of unit value of mean radius, that is

$$\frac{a+b}{2}=1. \tag{11}$$

Since a and b are functionally dependent, the ring shape can be specified by the six independent shape parameters a, c, d, e, f, and n. After the structural equations are solved for the unit size ring (using Simpson numerical integration), the results are scaled to full size using the scale factor λ. The width parameter c is not scaled during the entire analysis, and the shape parameters e, f, and n are nondimensional and are not scaled.

The six shape parameters a, c, d, e, f, and n are the six independent variables $x_1, x_2, \ldots, x_6$, respectively, of the constrained optimization problem. The objective function $f(x_1, x_2, \ldots, x_6)$ is the scaled ring weight

$$W=4\gamma\lambda^2\int_0^{\pi/2} ht\,ds, \tag{12}$$

in which γ is the material density. The following six implicit constraint functions g_i are applied:

$$g_1=2\lambda\delta_{\pi/2}=\text{total ring deflection}, \tag{13}$$

$$g_2=\lambda d(1+|f|)=\text{maximum thickness of ring cross section}, \tag{14}$$

$$g_3=\lambda(2a+d+df)=\text{outside width of ring}, \tag{15}$$

$$g_4=\lambda(4-2a+d+df)=\text{outside height of ring}, \tag{16}$$

$$g_5=c(1+|e|)=\text{maximum width of ring cross section}, \tag{17}$$

and

$$g_6=\lambda(4-2a-d-df)=\text{inside clear height of ring}. \tag{18}$$

Implicit lower bounds h_i and/or upper bounds k_i are imposed on the functions g_i to limit ring deflection and dimensions.

The scaling procedure used here could have been avoided by expressing force capacity as an implicit constraint function with a lower bound. It is not known whether such a procedure would be more efficient than the scaling procedure used.

Numerical solutions were obtained for seven different minimum weight elastic ring problems. Tables 1 and 2 give the initial points, the constraint bounds and the solutions obtained. The material properties were: $S=150{,}000$ lb/in^2, $E=30{,}000{,}000$ lb/in^2, $\nu=0.3$, and $\gamma=0.29$ lb/in^3. The computations were coded in FORTRAN V and run on a UNIVAC 1108 computer. Time required for a solution ranged from 4 min to 18 min with a mean of 9 min. The number of initial complex regenerations required for a solution ranged from 2 to 21 with a mean of 9. A reflection factor of 1.5 was used for all seven solutions.

For each of the two 1,000,000 lb capacity n-degree elliptical rings, the best solution reported in the earlier paper [3] (weight = 539.08 lb) was used as the initial point. For the other five problems, the initial feasible points were obtained by using the relatively simple equations for a thin circular ring of uniform cross section. The thin circular ring equations, although they may be in error by several percent, give a good enough approximation of ring characteristics for beginning an optimization search. The coordinates obtained by the thin ring equations were offset slightly inside their explicit bounds, where that was necessary, to comply with the requirements of the optimization method. To hold a particular parameter constant, the upper and lower explicit bounds were set equal to the initial point coordinate value.

TABLE 1. *Initial points and constraint bounds for elastic ring problems*

Force capacity	Problem dimension	Initial point coordinates and explicit bounds																	Implicit bounds						
		a_1	a	b_1	a_2	c	b_2	a_3	d	b_3	a_4	e	b_4	a_5	f	b_5	a_6	n	b_6	h_1	k_1	k_2	k_3	k_4	k_5	h_6
Lb		*Inch*	*Inch*	*Inch*	*Inch*	*Inch*	*Inch*	*Inch*	*Inch*	*Inch*										*Inch*	*Inch*	*Inch*	*Inch*	*Inch*	*Inch*	*Inch*
100,000	5	1.0	1.01	1.3	3.0	5.0	6.0	0.05	0.151	0.3	0.0	0.0	0.0	−0.9	0.0	0.9	2.0	2.1	20.0	0.25	0.55	4.0	40.0	40.0	6.0	9.0
300,000	5	1.0	1.01	1.3	4.0	8.0	10.0	.1	.188	.4	0.0	0.0	0.0	−0.9	0.0	0.9	2.0	2.1	20.0	.25	.55	4.0	40.0	40.0	10.0	9.0
1,000,000	2	1.0	1.00	1.0	6.0	12.0	14.0	.1	.250	.5	0.0	0.0	0.0	0.0	0.0	0.0	2.0	2.0	2.0	.25	.55	7.0	50.0	50.0	18.0	9.0
1,000,000	5	1.0	1.21	1.3	6.0	13.3	14.0	.1	.305	.5	0.0	0.0	0.0	−0.9	0.5	0.9	2.0	6.0	20.0	.25	.55	7.0	50.0	50.0	18.0	9.0
1,000,000	6	1.0	1.21	1.3	6.0	13.3	14.0	.1	.305	.5	0.9	0.0	0.9	−0.9	0.5	0.9	2.0	6.0	20.0	.25	.55	7.0	50.0	50.0	18.0	9.0
3,000,000	5	1.0	1.01	1.3	14.0	18.0	20.0	.25	.311	.5	0.0	0.0	0.0	−0.9	0.0	0.9	2.0	2.1	20.0	.25	.55	9.0	60.0	60.0	20.0	9.0
9,000,000	5	1.0	1.01	1.3	20.0	28.0	32.0	.3	.387	.5	0.0	0.0	0.0	−0.9	0.0	0.9	2.0	2.1	20.0	.25	.55	15.0	85.0	85.0	32.0	9.0

TABLE 2. *Solutions for elastic ring problems*

Force capacity	Problem dimension	Ring shape parameters of unit size ring						Implicit constraint function values						Scale factor	Ring weight	Cycles
		a	c	d	e	f	n	g_1	g_2	g_3	g_4	g_5	g_6			
Lb		*Inch*	*Inch*	*Inch*				*Inch*	*Inch*	*Inch*	*Inch*	*Inch*	*Inch*		*Lb*	
100,000	5	1.07509	5.35807	0.14689	0.00000	0.79775	5.36445	0.2502	1.5078	12.4472	12.0703	5.3581	9.0546	5.710	52.40	210
300,000	5	1.09246	8.40706	.19659	.00000	.67392	4.52213	.2503	2.3088	15.7788	15.0431	8.4071	10.4256	7.016	163.17	201
1,000,000	2	1.00000	12.32346	.27146	.00000	.00000	2.00000	.2501	4.1548	34.7653	34.7653	12.3235	26.4558	15.305	1427.90	190
1,000,000	5	1.19033	11.87379	.31110	.00000	.56132	9.39859	.2509	3.8990	20.2053	16.8975	11.8738	9.0996	8.027	492.49	179
1,000,000	6	1.19717	11.77591	.31561	−.02669	.56049	8.15270	.2512	3.9900	20.5215	16.9984	12.0902	9.0184	8.102	497.78	263
3,000,000	5	1.02028	16.12696	.33864	.00000	.62951	5.93016	.2504	6.6805	26.2232	30.4025	16.1270	17.0414	12.107	1686.69	522
9,000,000	5	1.02117	25.64302	.45811	.00000	.51622	5.69466	.2503	9.7050	31.6321	37.0573	25.6430	17.6474	13.972	4819.54	414

For the five n-degree elliptical rings with uniform cross section width, the ratio of weight to force capacity ranges from 4.92×10^{-4} to 5.62×10^{-4}. At least a rough proportionality between weight and force capacity might be expected for structures of this geometric class. Thin ring equations would predict a constant ratio of weight to force capacity for uniform cross section, circular rings having the same deflection at capacity load.

In each of the seven solutions, ring deflection, g_1, is near its lower bound, $h_1=0.25$ in. In three of the solutions, inside clear height, g_6, is near its lower bound, $h_6=9.0$ in. Exact minimum weight solutions would apparently lie exactly on at least one of the bounds. Continued iteration would have resulted in closer approximations to exact solutions. But the searches were stopped because of the relatively large computer costs involved and because the convergence rate decreases as an optimum is approached.

The seven solutions include three 1,000,000 lb capacity rings of different geometric complexity. One ring is circular with uniform cross section; one is n-degree elliptical with constant cross-section width and sinusoidally varying thickness; and one is n-degree elliptical with sinusoidally varying width and thickness. The three cases are respectively two-dimensional, five-dimensional, and six-dimensional optimization problems. All three cases have the same implicit constraint bounds. Both n-degree elliptical rings have a weight of about 35 percent of the weight of the circular ring, and the outside dimensions of the more complex rings are significantly less than those of the circular ring. Since the five-dimensional problem is a special case of the six-dimensional problem, an exact solution to the six-dimensional problem would have a weight equal to or less than any solution to the five-dimensional problem. Although both elliptical rings have about the same weight, the ring with nonuniform cross-section width would probably cost more to manufacture than would the other elliptical ring.

5. Rib-Stiffened Plate Problem

The minimum weight analysis of a rib-stiffened elastic plate is presented here to demonstrate the application of the nonrandom complex method to a discrete variable problem. It is assumed that the rib-stiffened plate is built-up from flat plates that are available in only a limited number of thicknesses.

Figure 3 gives a schematic drawing of a rib-stiffened plate of the type studied. The flat plate is reinforced by a rectangular grid system of ribs having the same dimensions and spacing in both directions. The rib-stiffened plate is simply supported along all four edges and loaded only with a compressive load N_l in the plane of the plate.

Schmit, Kicher, and Morrow [4] have studied the application of gradient optimization methods to a more general class of rib-stiffened plates, subjected to combinations of both shear and biaxial normal loads. They considered three possible elastic buckling modes to be applicable to their problem. The following specialized forms of the buckling equations used in their study are assumed to apply to the present problem:

1. Critical load for gross buckling of the simply supported, rib-stiffened plate,

$$N_{cr}=\frac{\pi^2}{w^2}\left[D_1\left(\frac{w^2}{l^2}+\frac{l^2}{w^2}\right)+2D_3\right], \tag{19}$$

in which

$$D_1=\frac{EH^3}{4}\left\{\frac{1}{3(1-\nu^2)}\left(\frac{t_p}{H}\right)^3+\frac{1}{3}\left(1-\frac{t_p}{H}\right)^3\left(\frac{t_r}{b_p}\right)+\frac{\nu}{2(1-\nu^2)}\left(1-\frac{t_p}{H}\right)\left(\frac{t_p}{H}\right)\left(\frac{t_r}{b_p}\right)\times\left[\frac{1+\nu}{\left(\frac{\nu}{1-\nu}\right)\left(\frac{t_p}{H}\right)+\nu\left(1-\frac{t_p}{H}\right)\left(\frac{t_r}{b_p}\right)}+\frac{1-\nu}{\left(\frac{\nu}{1+\nu}\right)\left(\frac{t_p}{H}\right)+\nu\left(1-\frac{t_p}{H}\right)\left(\frac{t_r}{b_p}\right)}\right]\right\},$$

$$D_3=\frac{EH^3}{4}\left\{\frac{1}{3(1-\nu^2)}\left(\frac{t_p}{H}\right)^3+\frac{\left(\frac{\nu}{1-\nu^2}\right)\left(\frac{t_p}{H}\right)\left(1-\frac{t_p}{H}\right)^2\left(\frac{t_r}{b_p}\right)^2}{\left[\left(\frac{1}{1-\nu^2}\right)\left(\frac{t_p}{H}\right)+\left(1-\frac{t_p}{H}\right)\left(\frac{t_r}{b_p}\right)\right]^2-\left(\frac{1}{1-\nu^2}\right)^2\left(\frac{t_p}{H}\right)^2}\right\},$$

$E=$ modulus of elasticity,
$\nu=$ Poisson's ratio,

and the length dimensions are those indicated in figure 3.

2. Critical load for local buckling of a stiffening rib as a flat plate, simply supported along three edges and free along the fourth edge,

$$\bar{N}_{cr}=\frac{\pi^2E}{12(1-\nu^2)}\left(\frac{t_r}{b_r}\right)^2\left[\frac{b_pt_p+b_rt_r}{b_p}\right]\left[\left(\frac{b_r}{b_p-t_r}\right)^2+0.425\right]. \tag{20}$$

3. Critical load for local buckling of a square panel as a flat plate, spanning between two pairs of ribs and simply supported along all four edges,

$$\bar{N}_{cr}=\frac{\pi^2Et_p^2}{3(1-\nu^2)(b_p-t_r)^2}\left[\frac{b_pt_p+b_rt_r}{b_p}\right]. \tag{21}$$

The critical material stress in the rib-stiffened plate is assumed to be equal to the applied load divided by the gross cross-sectional area of the flat plate and

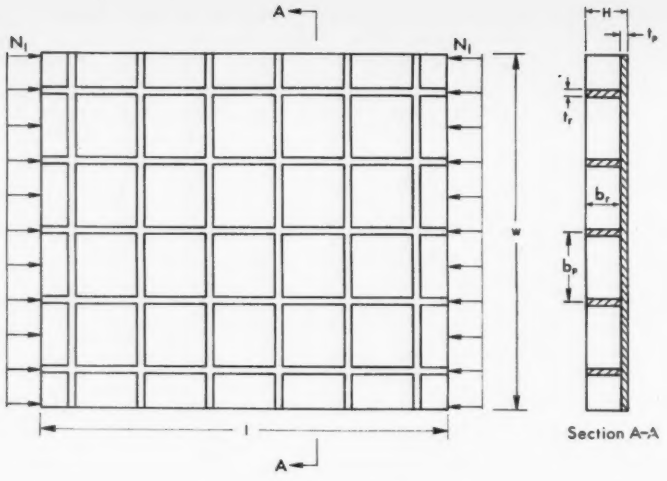

FIGURE 3. *Rib-stiffened plate.*

ribs. That is,

$$\sigma_l = \frac{N_l}{t_p + b_r\left(\frac{t_r}{b_p}\right)}. \tag{22}$$

The gross weight of the rib-stiffened plate is given approximately by

$$W = \gamma l w t_p \left[1 + \frac{b_r t_r}{b_p t_p}\left(2 - \frac{t_r}{b_p}\right)\right], \tag{23}$$

in which γ is the material density. Equation (23) does not include the net weight resulting from the fastening of the stiffening ribs to the larger flat plate or to each other.

For the particular numerical problem presented here, plate length and width, l and w, are held constant and the four plate dimensions t_p, t_r, b_p, and b_r are the variable parameters of the optimization search. The plate thicknesses, t_p and t_r, are discrete variables. The objective function is the gross weight of the plate, W. The following implicit constraint functions are applied:

$$g_1 = N_{cr} = \text{gross buckling load}, \tag{24}$$

$$g_2 = \bar{N}_{cr} = \text{rib buckling load}, \tag{25}$$

$$g_3 = \tilde{N}_{cr} = \text{panel buckling load}, \tag{26}$$

$$g_4 = \sigma_l = \text{critical stress}, \tag{27}$$

and $$g_5 = t_p + b_r = \text{total stiffened plate thickness}. \tag{28}$$

The applied load that the plate is required to support is a lower bound on g_1, g_2, and g_3. The design stress, S, is an upper bound on g_4.

A numerical solution was obtained for a rib-stiffened plate 30 in wide by 40 in long with an applied compressive load $N_l = 350$ lb/in. Lower and upper bounds of 0.5 in and 0.7 in, respectively, were imposed on total stiffened plate thickness, g_5. Explicit constraint bounds on the variable optimization parameters were as follows (in inches):

$$0.005 \leq t_p \leq 0.500$$

$$0.005 \leq t_r \leq 0.500$$

$$2.000 \leq b_p \leq 6.000$$

$$0.100 \leq b_r \leq 0.700.$$

The material properties were: $S = 20{,}000$ lb/in^2, $E = 10{,}500{,}000$ lb/in^2, $\nu = 0.32$, and $\gamma = 0.101$ lb/in^3. Forty-four discrete plate thicknesses from 0.0040 in to 0.5800 in were assumed to be available. The computations were coded in FORTRAN V and run on a UNIVAC 1108 computer. Total computer time required for the solution was 55 s. A reflection factor of 1.6 was used.

It was determined by direct computation that a 0.2043 in thick plate was the thinnest available plate that would support the applied load as a flat plate, without stiffening ribs. Such a plate would weigh about 24.76 lb. The 0.2043 in flat plate thickness combined with a reasonable set of rib dimensions were used as the initial point coordinates for the first continuous variable search.

Table 3 gives the initial points and results for the series of five optimization searches employed in finding a discrete variable solution. The result of the first continuous variable search was a solution point near

TABLE 3. *Initial points and results for rib-stiffened plate problem*

Optimization search	Variable parameters				Implicit constraint function values					Gross weight	Cycles
	t_p	t_r	b_p	b_r	N_{cr}	$\bar{N}_{cr}$	$\bar{N}_{cr}$	σ_1	H		
	Inch	*Inch*	*Inch*	*Inch*	*Lb/Inch*	*Lb/Inch*	*Lb/Inch*	*Lb/Inch²*	*Inch*	*Lb*	
First continuous	0.20430 (Initial point)	0.20430	4.00000	0.30000						28.3805	
	.04541 (Result)	.04526	3.44039	.64625	350.00	945.27	371.19	6492.0	0.69166	7.5510	246
Second continuous	.04767 (Initial point)	.05041	3.72198	.63748	350.10	1242.35	365.24	6216.3	.68515	7.8563	
	.03068 (Result)	.02961	2.00111	.64446	350.10	350.00	374.79	8703.1	.67514	6.0128	215
Third continuous	.03068 (Initial point)	.02961	2.00110	.64444	350.10	350.10	374.91	8702.2	.67512	6.0133	
	.02989 (Result)	.02988	2.00000	.64409	350.15	350.51	350.00	8858.2	.67398	5.9375	111
First discrete	.03200 (Initial point)	.03200	2.00000	.64409	376.95	430.72	430.46	8273.2	.67609	6.3565	
	.03200 (Result)	.03200	2.19138	.64465	350.00	406.67	350.00	8451.3	.67665	6.1436	91
Second discrete	.03590 (Initial point)	.02850	2.00000	.64409	351.38	363.79	575.24	7764.3	.67999	6.5600	
	.03590 (Result)	.02850	2.08008	.65105	350.01	350.00	528.17	7809.0	.68695	6.4985	114

the gross buckling constraint and not far from both the panel buckling constraint and a total plate thickness constraint. The continuous variable search was restarted, in a second computer run, using a complex centroid somewhat offset inside all constraints as the initial point. The result of the second continuous variable search was a solution point near a rib spacing constraint, near the gross buckling constraint, near the rib buckling constraint, and not far from the panel buckling constraint. The continuous variable search was again restarted, in a third computer run, and the resulting solution point was near a rib spacing constraint and all three buckling constraints. As a continuation of the third computer run, the two best discrete solution points near the continuous variable solution were selected and used as initial points for two searches within the subspaces defined by the discrete coordinates. The better of the two discrete solutions resulted from the better discrete initial point. Therefore, no additional discrete subspace searches were executed. The gross weight for the discrete solution is about 25 percent of the weight of the thinnest available flat plate that would support the applied load without stiffening ribs. Initial complex regeneration, to overcome excessively slow convergence, was not required during any of the five optimization searches.

6. Discussion

Unfortunately, a general method is not available for determining whether or not a solution found by the nonrandom complex method is (approximately) the true optimum. But a careful study of the search record can yield a basis for judgment. The study should include not only the final values (centroidal) of the variables and functions, but also the variation of these values for the entire search. The entire complex, at regular cycle intervals, should also be examined.

Multiple searches along different paths can be used to test apparent optimum solutions. The search path depends on the objective and constraint functions, the constraint bounds, the initial point, the reflection factor, the complex regeneration criterion, and numerical errors. A change in one or more of these factors can cause a search to progress along a different path. Of course the rate of convergence is, in general, different for different search paths.

Discrete variables can occur in practical problems in several different forms. The rib-stiffened plate problem involves two discrete variables with tabular noninteger values. That problem could have been written to include an integer optimization variable by expressing rib spacing as a function of the number of equally spaced longitudinal ribs. Schmit and Mallett [5] have discussed the optimization of material selection by initially treating one material property as an independent variable, with other material properties expressed as continuous functions of the independent material property. With such a procedure, material selection could be treated as a discrete optimization variable in a nonrandom complex search. Similarly, the selection of commercially available elements, such as metal beams and columns, could be optimized by initially expressing element geometric properties as continuous functions of a single independent variable, for example weight per unit length.

Numerous other optimization methods applicable to problems with nonlinear objective and constraint functions have been discussed in the literature, for example by Box [1], Hilleary [2], Schmit, Kicher, and Morrow [4], Schmit and Mallett [5], and Wilde and Beightler [6]. The limited computational experience reported in the present paper is insufficient to warrant a definitive claim of superiority of the nonrandom complex method over other available methods.

7. Conclusion

A nonrandom complex method has been developed for application to optimization problems characterized by nonlinear objective and constraint functions involving continuous and/or discrete optimization variables. The nonrandom method appears to offer significant advantages over the Box [1] method which involves a pseudo-random process. The method was successful in finding approximate minimum weight solutions to:

1. Seven elastic ring structural problems involving from two to six independent variables each; and
2. A rib-stiffened elastic plate structural problem involving four independent variables, two of which are discrete.

These results, for problems of this complexity, suggest that the method is applicable to a large class of optimization problems.

The subroutines for solving the structural equations of the elastic ring problem were coded in FORTRAN V by R. M. Slesser while he was an employee of the National Bureau of Standards Center for Computer Sciences and Technology.

8. References

[1] Box, M. J., A new method of constrained optimization and a comparison with other methods, The Computer Journal **8,** 42–52 (Apr. 1965).

[2] Hilleary, R. R., The tangent search method of constrained minimization, U.S. Naval Postgraduate School Tech. Rep./Res. Paper No. 59 (Mar. 1966).

[3] Mitchell, R. A., Analysis of *n*-degree elliptical elastic rings of nonuniform cross section, J. Res. NBS **72C** (Engr. and Instr.). No. 2, 139–160 (1968).

[4] Schmit, L. A., Jr., Kicher, T. P., and Morrow, W. M., Structural synthesis capability for integrally stiffened waffle plates, J. AIAA **1,** No. 12 (Dec. 1963).

[5] Schmit, L. A., Jr., and Mallett, R. H., Structural synthesis and design parameter hierarchy, J. Struct. Div. ASCE **89,** No. ST4, (Aug. 1963).

[6] Wilde, D. J., and Beightler, C. S., Foundations of Optimization (Prentice-Hall, Inc., 1967).

(Paper 72C4–282)

JOURNAL OF RESEARCH of the National Bureau of Standards—C. Engineering and Instrumentation
Vol. 72C, No. 4, October–December 1968

Publications of the National Bureau of Standards*

Selected Abstracts

Pope, C. I., **Blemish formation in processed microfilm,** *J. Res. NBS* **72A** (*Phys. and Chem.*), *No. 3, 251–259 (May–June 1968).*
Oxidizing and reducing agents by paper cartons during storage may react with the image silver to form blemishes. The type of fixing bath, concentration of chlorine in the wash water, washing time and composition of the storage cartons can be factors that accelerate or retard the attack of the peroxide on the image silver. Microfilm washed after fixation in distilled water or chlorine-free tap water formed blemishes when exposed to peroxide paper. A trace of silver chloride in the image silver of processed microfilm augmented the formation of the natural type blemishes when exposed to peroxide paper, but high concentrations of residual silver chloride inhibited blemish formation. During storage, some storage cartons evolved formaldehyde, formic acid, and ammonia which created a chemical environment favorable for blemish formation in microfilm in the presence of peroxide. A correlation was found between the incidence of blemishes and the brand of paper storage cartons. A procedure was developed for testing processed microfilm to determine its susceptibility to blemish formation. According to the present theory, peroxide reacts with the silver in the image, forming colloidal silver which imparts a yellowish or reddish color to the blemishes.

Key Words: Archival record film; blemishes due to aging; colloidal silver; microfilm; microfilm storage cartons; permanent record film; peroxides.

Catanzaro, E. J., Murphy, T. J., Shields, W. R., Garner, E. L., **Absolute isotopic abundance ratios of common, equal-atom, and radiogenic lead isotopic standards,** *J. Res. NBS* **72A** (*Phys. and Chem.*), *No. 3, 261–267 (May–June 1968).*
Absolute values have been obtained for the isotopic abundance ratios of common, equal-atom, and radiogenic lead isotopic standards using solid-sample mass spectrometry. Samples of known $^{208}Pb/^{206}Pb$ ratio, prepared from nearly pure separated ^{206}Pb and ^{208}Pb solutions, were used to calibrate the mass spectrometers.

Key Words: Absolute ratios; abundance; isotopic standards; lead.

Yakowitz, H., Jenkins, W. D., Hahn, H., **Role of nickel in Al-10 percent Si composites containing nickel-coated sapphire whiskers,** *J. Res. NBS* **72A** (*Phys. and Chem.*), *No. 3, 269–272 (May–June 1968).*
The role of nickel in regard to whisker-matrix bonding in a composite of nickel-coated sapphire whiskers inserted into a matrix of aluminum-10 percent silicon alloy by means of liquid phase hot-pressing was investigated. The study was carried out with the aid of optical and electron microscopy, electron probe microanalysis, and microhardness measurements. Results show that most of the nickel is distributed within the matrix alloy; it does not remain on the whiskers. Some of the nickel apparently interacts with the matrix and forms $NiAl_3$. The presence of $NiAl_3$ in this form increases the average hardness of the composite but apparently does not contribute significantly to strengthening of the alloy. Occasionally, clusters or clumps or nickel-rich material which also contains aluminum are found at or very near whisker-matrix interfaces. It is concluded that if any bonding of the nickel to the sapphire occurred, it was in these regions. Finally, a heat treatment to improve nickel to sapphire bonding and hence bonding of the entire composite is suggested.

Key Words: Al-10 percent Si alloy; electron probe microanalyzer; fiber composites; matrix-whisker bonding; Ni coated sapphire whiskers; optical metallography; sapphire whiskers.

Howlett, G. L., **Variation of absorptance-curve shape changes in pigment concentration,** *J. Res. NBS* **72A** (*Phys. and Chem.*), *No. 4, (July–Aug. 1968).*
A complete quantitative analysis is presented of changes in the shape of the spectral absorptance curve of any Beer's-law pigment solution (or other Bouger's-law material) as concentration of the pigment, or thickness of the solution layer, is varied. The relative abortance curve, normalized to unit maximum, is taken as defining the shape of the absolute absorptance curve, and the index of shape change is taken to be the difference between the normalized curves. All concentration changes from infinite decrease to infinite increase are covered, with some extreme cases requiring limit methods. Formulas and graphs are given for determining as a function of concentration change and peak absolute absorptance of the original curve, where along the curve the shape change is greatest, and how large the maximum change is. Implications for color vision theory are discussed and it is shown that the assumption of low peak absorptances (< 10%) for the visual photo-pigments accounts for the constancy of the color-matching functions for moderate luminances, but not, in itself, for the breakdown of matches at high luminances; while the assumption of high peak absorptances (≈ 80%), although it contradicts recent microspectrophotometric measurements, seems to account for both phenomena.

Key Words: Absorptance; adaptation; Beer's law; chromatic adaptation; color vision; concentration; cones; high luminance; metameric matches; pigment; photopigment; vision.

Roberts, G. N., Hamer, W. J., **A galvanic cell with a low emf-temperature coefficient,** *J. Res. NBS* **72A** (*Phys. and Chem.*), *No. 4, (July–Aug. 1968).*
This paper presents data on a modified cadmium sulfate saturated standard cell in which a tertiary amalgam containing 11.2 percent bismuth and 8.4 percent cadmium is used as anode and the double salt, $CdSO_4 \cdot Na_2SO_4 \cdot 2H_2O$ is added to the usual $CdSO_4$ electrolyte in an amount more than sufficient to saturate the solution with the double salt. Crystals of $CdSO_4 \cdot Na_2SO_4 \cdot 2H_2O$ are placed over the surface of both electrodes. The emf of the cell, as a function of temperature, is given by

$$E(\text{in volts}) = 1.018243 + 3.0956 \times 10^{-5}t - 8.559 \times 10^{-7}t^2 + 1.3534 \times 10^{-8}t^3$$

with the standard deviation for the reproducibility of the experimental data being 3.78 μV. At 25 °C the cell has an emf-temperature coefficient of +13.5 μV/°C while the conventional saturated cadmium sulfate cell has a dE/dT of −49.4 μV/°C. Data on the emf-temperature hysteresis of the cell on cooling and on heating are also given in graphical form. Data on the changes in Gibbs energy, enthalpy, entropy, and heat capacity for the cell reaction are given for the temperature range of 5 to 40 °C.

Key Words: Double salt; galvanic cell with low temperature coefficient; galvanic cells; standard cells.

Napolitano, A., Macedo, P. B., **Spectrum of relaxation times in GeO_2 glass,** *J. Res. NBS* **72A** (*Phys. and Chem.*), *No. 4, (July–Aug. 1968).*

Index-of-refraction versus time isotherms have been established for germania glass. Using the crossover technique with air-quenched samples and applying the two relaxation time modes previously reported for borosilicate glass, it was found that the width of the spectrum of relaxation times for germania glass was temperature dependent. Upon analyzing this in terms of a distribution of activation energies, the results showed that, similarly to B_2O_3, activation energies smaller than the activation energy present in the Arrhenius region appear at low temperatures.

Extensive viscosity measurements by the fiber elongation method were made from 10^{11} to 6×10^{14} poises. From this data a lower and better known value of the activation energy ($E_\eta = 72.3$ kcal/mol) in the annealing range was obtained.

Key Words: Activation energy; annealing; germania glass; index of refraction; thermal expansion; relaxation times; two relaxation models; viscosity.

Hamer, W. J., **Resumé of values of the Faraday,** *J. Res. NBS* **72A** (*Phys. and Chem.*), *No. 4, (July–Aug. 1968).*

A resumé is given of the determinations of the value of the Faraday. Values obtained by silver deposition, iodide oxidation, oxalate oxidation, the omegatron and silver dissolution, are reviewed. All values are converted to the unified ^{12}C international scale of atomic weights using the international atomic weights of 1967. Values of the Faraday are given in terms of both the NBS (legal) and absolute units of electrical measure. In the latter the new value for the acceleration of gravity is used in computing the absolute value of electric current. On this basis and using the atomic weight of silver determined by Shields, Craig, and Dibeler, and converting to the ^{12}C scale the value of faraday is $96{,}486.9\pm1.6$ absolute coulombs per gram-equivalent which differs by only 1 ppm from the value recommended by the National Academy of Sciences–National Research Council. If the atomic weight of silver recommended in 1967 by the International Atomic Weight Commission is used the faraday on the new gravity value is $96{,}486.5\pm1.6$ absolute coulombs per gram-equivalent which differs by 5 ppm from that recommended by the National Academy of Sciences–National Research Council.

Key Words: Coulometers; Faraday; inclusions in silver coulometers; values of Faraday.

Aissen, M., **Means and the minimization of errors,** *J. Res. NBS* **72B** (*Math. Sci.*), *No. 1, 1–4, (Jan.–Mar. 1968).*

Let $0<a<b$. How should a number p be chosen so that the maximum "relative error" obtained, by replacing a number x varying in the closed interval $[a, b]$, by p, is a minimum? For a large number of "relative errors," p must be chosen as the geometric mean of a and b.

Key Words: Arithmetic mean; geometric mean; means; harmonic mean; relative error.

Hogben, D., **The distribution of the sample correlation coefficient with one variable fixed,** *J. Res. NBS* **72B** (*Math. Sci.*), *No. 1, 33–35 (Jan.–Mar. 1968).*

For the usual straight-line model, in which the independent variable takes on a fixed, known set of values, it is shown that the sample correlation coefficient is distributed as Q with $(n-2)$ degrees of freedom and noncentrality $\theta=(\beta/\sigma)\sqrt{\Sigma(x_i-\bar{x})^2}$. The Q variate has been defined and studied elsewhere by Hogben et al. It is noted that the square of the correlation coefficient is distributed as a noncentral beta variable.

Key Words: Analysis of variance; calibration; correlation coefficient; degree of freedom; distribution; fixed variable; noncentral beta variable; noncentrality.

Myers, V. W., **Solutions of the time-dependent Klein-Gordon and Dirac equations for a uniform electric field,** *J. Res. NBS* **72B** (*Math. Sci.*), *No. 1, 37–42 (Jan.–Mar. 1968).*

The time-dependent Klein-Gordon and Dirac equations are solved for the motion of a charged particle in a classical uniform electrostatic field of infinite extent. The elementary solutions have a position dependents of the form $e^{ik\cdot r}$ with the component of K in the field direction varying linearly with time.

Key Words: Dirac and Klein-Gordon equations; time-dependent solutions; uniform electric field.

Alt, F. L., Kirsch, R. A., **Citation searching and bibliographic coupling with remote on-line computer access,** *J. Res. NBS* **72B** (*Math. Sci.*), *No. 1, 61–78 (Jan.–Mar. 1968).*

Experiments were performed on a remote, multiple access computer to retrieve bibliographic items based on citation data. The citations were from some 25,000 physics papers. Estimates were made of the relevance of bibliographies derived from such citations. Some extrapolations are made to future systems with remote multiple access capability.

Key Words: Bibliographies; citations; computer; information retrieval; remote consoles; timesharing.

Jarvis, S., Jr., **On the diffusion of an ion sheet in Poiseuille flow,** *J. Res. NBS* **72B** (*Math. Sci.*), *No. 2, (Apr.–June 1968).*

A nonuniform sheet of ions generated at time $t=0$ diffuses in a cylindrical ion diffusion tube containing a nonreacting neutral species flowing with parabolic velocity distribution. Calculation of the on-axis ion density at a point z downstream as a function of time t is reduced to a single numerical integration for each (z, t) involving some functions which have been computed once for all. An example is given showing the effect of the velocity distribution compared with a uniform flow with the same flow rate. The results appear to be corroborated by experiment.

Key Words: Diffusion; ion flow tubes.

Blaine, R. L., Arni, H., and DeFore, M. R., **Interrelations between cement and concrete properties. Part 3, compressive strengths of Portland cement test mortars and steam-cured mortars,** *Bldg. Sci. Series 8 (Apr. 1968), 55 cents.*

The relationships between cement characteristics and compressive strength of 1:2.75 (cement to graded Ottawa sand) mortars of standard of consistency at ages of 24 hours to 10 years, and made with 199 cements of different types, were studied by fitting multivariable regression equations with the aid of a digital computer. The dominant variables associated with the differences of compressive strength, strength gain, and strength ratios were different at the various test ages, and after different curing conditions. The additional use of certain trace elements with commonly determined independent variables resulted in a significantly better fit between the equations and the observed data. Interactions between the fineness values and other independent variables were noted. Certain parallelisms and differences were noted with respect to variables associated with compressive strength differences at various ages and the heat of hydration of the cements at these ages.

Key Words: Chemical composition; fineness; heat of hydration; strength gain of Portland cements; trace elements.

Furukawa, G. T., Saba, W. G., and Reilly, M. L., **Critical analysis of the heat-capacity data of the literature and evaluation of thermodynamic properties of copper, silver, and gold from 0 to 300 °K,** *Natl. St. Ref. Data Series 18 (Apr. 1968), 40 cents.*

The literature sources of heat-capacity data on copper, silver, and gold between 0 and 300 °K have been compiled and the data critically analyzed. Tables of heat capacity (C_p), enthalpy ($H-H_0^\circ$), entropy (S°), Gibbs energy ($G-H_0^\circ$), enthalpy function $\left(\frac{H-H_0^\circ}{T}\right)$, and Gibbs energy function $\left(\frac{G-H_0^\circ}{T}\right)$ have been obtained from the analyses. The literature values of the heat capacity, the electronic coefficient of heat capacity (γ), and 0 °K limiting Debye characteristic temperature ($\theta_p(0)$) are compared with the selected values. The sources of the data are tabulated chronologically along with the temperature range of measurements, purity of sample, and the pertinent experimental procedures used. A bibliography of the references is listed. A brief appraisal of low-temperature calorimetry is given.

Key Words: Calorimetry; copper; Debye theta (θ); electronic coefficient of heat capacity; enthalpy; entropy; Gibbs energy; gold; heat capacity; silver; temperature scales; thermodynamic properties.

Ho, C. Y., Powell, R. W., and Liley, P. E., **Thermal conductivity of selected materials, Part 2,** *Natl. Std. Ref. Data Series 16 (Feb. 1968), $2.00.*

The work presented in this report comprises the critical evaluation, analysis, and synthesis of the available thermal conductivity data and the generation of recommended values for twelve metallic elements, mainly for the solid state, for a range of graphites, and for three fluids in the gaseous state. These are cadmium, chromium, lead, magnesium, molybdenum, nickel, niobium, tantalum, tin, titanium, zinc, zirconium, Acheson graphite, ATJ graphite, pyrolytic graphite, 875S graphite, 890S graphite, acetone, ammonia, and methane. For each of the materials recommended values are given over a wide range of temperature.

Key Words: Critical evaluation; gases; graphites; metallic elements; metals; recommended values; thermal conductivity; standard reference data.

Lee, R. W., and Worral, R. W., Ed., **Electronic composition in printing.** *Proceedings of a Symposium held at the National Bureau of Standards June 15–16, 1967, Spec. Publ. 295 (Feb. 1968), 70 cents.* (This series was formerly known as the Miscellaneous Publication Series.)

A Symposium on Electronic Composition in Printing was held at the Gaithersburg Laboratories of the National Bureau of Standards June 15 and 16, 1967. Sponsored by the NBS Center for Computer Sciences and Technology, the symposium was a state-of-the-art review of a rapidly advancing field of computer application with great potentialities for increased efficiency and savings in the Federal Government.

Twenty-nine papers were presented and are published in this Proceedings. They include a diverse group by industry representatives reporting recent technological advancements in the field. Several papers define government policy and describe the new Linotron system of photocomposition at the Government Printing Office; another series is devoted to nongovernment applications and research; and a final group details specific applications within several Government agencies.

Key Words: Character generation; composition language; computer technology; computerized text processing; electronic composition; electronic computer; electronic printing; GRACE; Linotron; MACRO coding; MEDLARS; microfilm; photocomposition; Photon; programming; text editing.

Petersen, P. H., and Watstein, D., **Shrinkage and creep in prestressed concrete,** *Bldg. Sci. Series 13 (Mar. 22, 1968), 15 cents.*

The loss of prestress resulting from creep and shrinkage in concrete was investigated for concrete specimens made with Type I portland cement and with Type III portland cement. The primary variables in this study were:

1. Relative humidity at which the concrete was maintained while under observation.
2. Age of the concrete at the time it was prestressed.
3. Ratio of prestress to strength; variation of this parameter required that the ratio of reinforcement be a variable.
4. Mass ratio factor defined as the ratio of the cross-section area of concrete specimen to its surface area per unit length.

Forty-nine sets of specimens were fabricated and tested; each set consisted of a prestressed specimen and an otherwise identical companion specimen without reinforcement.

The length changes with time were observed at intervals up to an age of 500 days. These observations were made for concretes subjected to different levels of prestress, and for concretes prestressed at different ages. Length changes in nonreinforced companion specimens were also obtained. Thus this study is concerned with elastic deformation occurring at time of stress transfer, shrinkage or swelling, and creep.

Key Words: Creep; relaxation; prestressed concrete; shrinkage; loss of prestress; variable prestress.

Radebaugh, R., **Thermodynamic properties of He^3-He^4 solutions with applications to the He^3-He^4 dilution refrigerator,** *Tech. Note 362 (Dec. 29, 1967), 70 cents.*

The thermodynamic properties of liquid He^3-He^4 solutions between 0 and 1.5 °K are calculated by using the weakly interacting Fermi-Dirac gas model for He^3 in He^4. Certain experimental data below about 0.4 °K are used to evaluate some of the parameters in the model. The properties of both He^3 in He^4 and the total solution are calculated for concentrations of He^3 up to 30 percent. All experimental data agree very well with the calculated results, although little data exist below 0.4 °K. The calculated properties are used to analyze the behavior of the He^3-He^4 dilution refrigerator in both the continuous and single-cycle processes. The maximum heat absorption below about 0.04 °K is found to be 82 T^2 joules per mole of He^3 circulated. The effect of an imperfect heat exchanger and He^4 circulation on the refrigeration capacity is discussed. An analysis of two new types of single-cycle processes is also given.

Key Words: Cryogenics; dilution refrigerator; enthalpy; entropy; Fermi-Dirac gas; helium-3; helium-4; liquid; mixtures; osmotic pressure; quantum fluid; specific heat; thermodynamic properties.

Roberts, A. G., **Organic coatings. Properties, selection, and use,** *Bldg. Sci. Series 7 (Feb. 1968), $2.50.*

This publication was prepared to fill the need for a comprehensive, unifying treatise in the field of organic coatings. Besides presenting practical information on the properties, selection, and use of organic coatings (and certain inorganic coatings), it provides basic principles in a number of important areas such as polymer structure, coatings formulation, pigment function, use of thinners, coating system compatibility, and theory of corrosion. Each chapter deals with a major area of the coatings field, including types of coatings, properties of synthetic resins, selection of coating systems, storage and safety, application methods, and surface preparation and pretreatment. There is also a consolidating chapter with illustrative examples of solutions to typical coatings problems. Interrelationships among the various areas of information are indicated through appropriate cross-referencing in the text. Specific references to Federal, Military, and other specifications are given where pertinent, and an entire chapter is devoted to a quick guide and summary of Federal specifications for organic coating materials. Finally, a selected bibliography and a comprehensive index are provided. While written primarily to meet the informational needs of the engineer, architect, maintenance superintendent, and responsible coatings procurement officer, the treatise is sufficiently broad in scope to serve as a general manual, a concise text, or a convenient reference source in the field of organic coatings.

Key Words: Application; coatings; coating systems; corrosion-inhibiting; Federal specifications; fire-retardant; lacquer; latex; multicolor; organic coatings; paint; pigments; polymers; properties; resins; selection; substrates; surface preparation; varnish; water-thinned.

Robbins, D., Ed., **Disclosures on: Autoeditor—a semi-automatic copy-editing apparatus,** *Tech. Note 440 (Apr. 1968), 40 cents.*

This note is a disclosure on a semi-automatic apparatus for incorporating editorial revisions in narrative text using punched paper tape combined with mark-sensing techniques. Pencil marks placed on the original draft by the editor are sensed and arranged to automatically capitalize the first letter of a word, to capitalize an entire word, or stop the apparatus at the point where a change is to be made. Addition of text is entered manually with an electric typewriter; deletion of text is accomplished by activating a "mark skip" key which advances the tape without typing until the next control mark is sensed.

Key Words: Narrative text editing; editorial mark sensing; automatic capitalization; automatic stop for revision; manual additions; automatic deletions; punched paper tape typewriter.

Shelton, C. F., **Spectral emission properties of NBS standard phosphor samples under photo-excitation,** *Tech. Note 417 (Mar. 1968), 25 cents.*

The photo-excitation spectral emission properties of 10 of the 14 NBS standard phosphor samples have been determined. Pressed tablets of the phosphors were excited by radiation from a mercury arc lamp, passing through a narrow band-pass filter to obtain either 2537Å or 3650Å excitation. The measurement system is described,

correction of the data is discussed, and the spectral emission data are presented. Relative quantum efficiencies were calculated. The results are compared with measurements reported by two other laboratories.

Key Words: Phosphors; photo-excitation; photoluminescence; spectral emission; spectral radiometry; standard phosphor samples.

Standard reference materials: catalog and price list of standard materials issued by the National Bureau of Standards, *Misc. Publ. 260, 1968 Edition (Jan. 31, 1968), 45 cents. (Supersedes NBS Misc. Publ. 260, 1967 Edition.)*
This catalog describes the various Standard Reference Materials issued by the National Bureau of Standards. These materials are used to calibrate measurement systems and provide scientific information that can be referred to a common base. A schedule of prices and quantities is included for each material, as well as directions for ordering. Listed are the types and compositions of those chemical standards that are presently available. Announcements of new standard reference materials are made in the Federal Register, in scientific and trade journals, and in the Technical News Bulletin of the National Bureau of Standards. Changes affecting the current status of the various standards will be indicated by an insert sheet available quarterly from the Bureau.

Key Words: Analysis; catalog; certificate; characterization; composition; price list; property of material; purity of material; standard reference materials; standards.

Wegstein, J. H., **A computer oriented single-fingerprint identification system,** *Tech. Note 443 (Mar. 1968), 25 cents.*
A procedure is described for computing a set of numerical descriptors that identify a single fingerprint. The procedure starts with the X and Y coordinates and the individual directions of the minutiae (ridge endings and bifurcations) of a fingerprint impression. Sets of descriptors are computed corresponding to groups or constellations of these minutiae. Descriptors corresponding to various fingerprint impressions are stored on magnetic tape. A fragment of a fingerprint impression such as occurs in a latent fingerprint may also be used.
A second computer program reads the descriptors corresponding to two different fingerprint impressions from magnetic tape. A score is computed that indicates how well the two impressions match. Preliminary experimental results suggest that this procedure might be suitable as a basis for a single-fingerprint classification system.

Key Words: Classification; computer; descriptor; file; fingerprint; identification; pattern-recognition.

Landgrebe, A. R., McSharry, W. O., and Cefola, M., **The Radiometric titration of trace amounts of zinc,** *Intern. J. Appl. Radiation Isotopes* **19,** *1, 23–26 (1968).*
A method of radiometric titration for the determination of trace amounts of metals has been developed. The EDTA complex of the metal to be determined is formed, and the excess, uncomplexed metal ions are removed by means of a cationic exchanger. A titration curve is then constructed by plotting the activity of the liquid phase, versus the amount of EDTA added. Both the batch and column method were tried in this laboratory, and it is our opinion that the batch method is easier from a manipulative point of view. A new method of determining the end point was developed. If both the resin and solution are counted, this is a simple way of determining the half equivalent point. Methods are underway to maximize the sensitivity for zinc by chelating radiometric titration.

Key Words: Radiometric; titrations; zinc; EDTA; batch; column; cationic exchanger.

Landgrebe, A. R., Rodriguez-Pasques, R. H., and Schima, F. J., **The rapid radiochemical separation of radioactive praseodymium from radioactive cerium,** *Intern. J. Appl. Radiation Isotopes* **19,** *No. 2, 147–149 (1968).*
A method of rapid radiochemical separation was developed to separate the cerium and praseodymium radioactivities produced after a praseodymium target was irradiated at the NBS Linac. The praseodymium metal is dissolved in nitric acid and the solution is divided into at least two portions. One fraction is used to precipitate cerium (IV) iodate, giving an aqueous phase free of cerium radioactivity. A second fraction is extracted with hydrogen di-(2 ethylhexyl) orthophosphoric acid (HDEHP). The organic phase is free from any praseodymium radioactivities.

Key Words: Rapid separation; praseodymium; cerium; radioactive; linac; solvent extraction; precipitation.

Pella, P. A., Landgrebe, A. R., DeVoe, J. R., and Purdy, W. C., **Differential controlled-potential coulometry utilizing substoichiometric radioisotope dilution,** *Anal. Chem.* **39,** *1781–1785 (Dec. 1967).*
A controlled-potential coulometric procedure is described which permits the utilization of the principle of substoichiometric radioisotope dilution. This technique employs two identical cells connected in series. Under prescribed conditions, the same amount of the element to be analyzed is deposited in each cell. The procedure involves the addition of a known amount of the element to the control cell, which is held at a constant potential, and an unknown amount to the sample cell. An equal, known amount of a radioisotope of that element is then added to each cell. The difference in the amount is determined by measuring the radioactivity remaining in each of the cells after a finite electrolysis time. This method was applied to the determination of cadmium in an NBS Standard Reference Material, zinc spelter, with a result of 0.0928% with a standard deviation of the mean of 0.0005%.

Key Words: Coulometry; radioactive tracers; trace analysis; electrolysis; substoichiometric; radioisotope dilution; cadmium; zinc spelter.

Taylor, L. S., **Responsibilities of the physician in his use of radiation,** *Rev. Mex. Radiol.* **XVIII,** *No. 69, 22–31 (Jan.–Feb. 1964).*
After comparing various sources of radiation exposure to which the public is subjected, suggestions are given with regard to the responsibility of the medical profession in the protection of patients during medical procedures.
Attention is directed to the substantial differences in practice between the radiologist and the general practitioner. Practically all of the conditions under which the general practitioner has to operate militate against maximizing the protection of the patient as well as the staff.
Public concern over radiation hazards in medical procedures has reached such proportions that better doctor-patient relationships in the administration of radiation are clearly called for.

Key Words: Radiation exposure; radiation hazards.

Barnes, J. A., Allan, D. W., **An approach to the prediction of coordinated universal time,** *Frequency* **5,** *No. 6, 15–20 (Nov.–Dec. 1967).*
By computing the root mean square of the third differences of the fluctuations of Universal Time for various sample times, a spectral classification of the fluctuations is made. For periods from 0.02 years to 20 years, the data indicates a power spectral density for the fluctuations given by $|\omega|^{-\alpha}$ where α lies in the range $3 \leq \alpha \leq 5$. Based on the spectral classification, some simple and practical methods of predicting frequency offsets for coordinated Universal Time are compared to theoretically optimum (linear) prediction. Three methods are considered and are applied to past UT 2 data for comparison. A conclusion from the paper is that the frequency offset for the coordinated time scales may be predicted such that no resets of epoch are required for roughly 60% of the years for which the prediction is made.

Key Words: Coordinated universal time; prediction; offset frequency; rotation of the earth.

Jensen, M. W., **Milk meters, farm milk tank testing, and plastic containers for milk,** *Proc. 31st Annual Meeting International Association of Milk Control Agencies, Biloxi, Mississippi, Oct. 23–25, 1967, pp. 26–31 (1968).*
The role of the National Bureau of Standards in weights and measures administration was discussed, as were current technical developments in mechanical metering of milk, gauging and testing of farm milk tanks, and acceptance for measuring and packaging purposes of plastic containers for milk.

Key Words: Milk meters; farm milk tanks; plastic milk containers and milk handling.

Mielenz, K. D., Nefflen, K. F., Rowley, W. R. C., Wilson, D. C., and Engelhard, E., **Reproducibility of helium-neon laser wavelengths at 633 nm,** *Appl. Opt.* **7,** *No. 2, 289–293 (Feb. 1968).*
Measurements on helium-neon lasers stabilized on the Lamb dip, performed at NBS, NPL, and PTB, have shown that the wavelengths of such lasers are reproducible within approximately 1 part in 10^7. Beyond this limit, different lasers were found to emit different wavelengths. In addition, the wavelength of a given laser may vary during the life of its discharge tube. Pressure shifts appear to be a major cause of such variations.

Key Words: Frequency-stabilized; helium-neon; krypton 86 lamp; Lamb dip; laser; wavelength.

Allan, D. W., Fey, L., Machlan, H. E., and Barnes, J. A., **An ultra-precise time synchronization system designed by computer simulation,** *Frequency* **6,** *No. 1, 11–14 (Jan. 1968).*
Any two independent time scales will exhibit time departure due to two main causes, i.e., systematic differences in the frequency standards and inherent random noise processes. For time synchronization, some theoretical considerations indicate the plausibility of a third-order feedback system which will automatically remove the systematic difficulties of typical frequency standards used in time scale work. Because of the random nature of the second difficulty, the whole system is simulated with a computer to determine the systems feasibility and operating parameters. Two basic assumptions are that time comparisons for synchronization would be intermittent and that the model for the frequency standard is represented by a systematic linear frequency drift with a random flicker noise spectrum $\left(\frac{1}{|\omega|}\right)$ of the frequency fluctuations.
On the basis of the computer results an electromechanical system was designed and built. When the input to the system is the frequency from a high quality quartz crystal oscillator, the output frequency has no frequency drift. If synchronization is performed every 12 hours, the rms time error predicted by the system at the time of the next synchronization is 70 nanoseconds, which is near optimum.

Key Words: Time scales; time synchronization; computer simulation; flicker noise; optimum prediction; frequency drift; third order feedback system.

Christ, B. W., and Giles, P. M., **Metallurgical uses of the Fe^{57} Mössbauer effect in metallic iron and plain carbon steels,** *Book, Advances in Mössbauer Methodology* **3,** *37–65 (Plenum Press, Inc., New York, N.Y., Jan. 1967).*
Literature describing the Fe^{57} Mössbauer effect in metallic iron, steels and ferrous compounds occurring in steels is reviewed and compared with new, computer-analyzed data obtained in 298 °K measurements on metallic iron and carbon steels. Characteristics of Mössbauer patterns are sensitive to carbon content and thermomechanical history. Relative to standard sodium nitroprusside, the average effective magnetic field (EMF) for three grades of recrystallized iron is 339 ± 3 kilo-oersteds.
Patterns reveal several superimposed hyperfine interactions between 0.02 and 1 w/o C. The most intense magnetic hyperfine pattern (MHP) is attributable to iron atoms remote from interstitials. The EMF of this pattern increases with increasing C in solution, e.g., 355 ± 3 kilo-oersteds at 1 w/o C. In quenched 0.3, 0.7 and 1 w/o C alloys, irregularities in peak shape arise from sets of iron atoms with various C near-neighbor configurations. A weak, resolvable MHP exhibiting a small quadrupole effect and an EMF 20% smaller than that of the intense pattern originates at iron atoms with one carbon nearest neighbor.
Phases identifiable by their patterns include ferrite, martensite, austenite, cementite, and ϵ-carbide. Dislocations produce no detectable effect. Application of Mössbauer spectroscopy to the study of martensite tempering and quantitative analysis for retained austenite is discussed.

Key Words: Fe^{57} iron; carbon steels; tempering; retained austenite hyperfine.

deWit, R., **Thermodynamic force on a dislocation,** *J. Appl. Phys.* **39,** *No. 1, 137–141 (Jan. 1968).*
The thermodynamic force on a dislocation is defined as the negative gradient of the Gibbs free energy of the crystal with respect to dislocation motion. This is shown to lead to a consistent force expression which contains two terms: the Peach-Koehler force due to the stress and the Bardeen-Herring force due to the vacancy concentration. The precise definition of these two terms is arbitrary, though their sum is unique. Various forms of the force expression are derived in terms of different reference vacancy concentrations, including the original forms of Weertman and Lothe and Hirth.

Key Words: Concentration; crystal; defect; dislocation; energy; equilibrium; force; hydrostatic; pressure; vacancy.

Hafner, N., Simpson, J. A., and Kuyatt, C. E., **Comparison of the spherical deflector and the cylindrical mirror analyzers,** *Rev. Sci. Instr.* **39,** *No. 1, 33–35 (Jan. 1968).*
The calculated performance of the cylindrical mirror deflection energy analyzer for charged particles is compared with that of the spherical analyzer. It is shown that through terms in α^3 the cylindrical device is significantly superior.

Key Words: Cylindrical mirror; electron energy analyzer; electron optics; spherical deflector.

Kamper, R. A., **Millidegree noise thermometry,** *Proc. Symp. Physics of Superconducting Devices, University of Virginia, Apr. 28–29, 1967, pp. M–1–M–5 (Office of Naval Research, Wash., D.C., 1968).*
Assuming that the linewidth of the A. C. Josephson radiation is caused entirely by thermal fluctuations in the bias voltage, we show that it can be used with quite simple instrumentation to measure absolute temperatures down to one millidegree or lower.

Key Words: Millidegree; noise; thermometry; Josephson effect; linewidth; superconductivity.

Pfeiffer, E. R., and Schooley, J. F., **Effect of stress on the superconductive transition temperature of strontium titanate,** *Phys. Rev. Letters* **19,** *No. 14, 783–785 (Oct. 2, 1967).*
The superconductive transition temperatures T_c of single crystal specimens of reduced strontium titanate have been measured as functions of hydrostatic and uniaxial compressional stresses up to 1.5 kbar. The prominent features of the experimental results are a large non-linear hydrostatic pressure effect and an anisotropic uniaxial stress effect. The relative decrease of transition temperature with pressure $d \ln T_c/d p$ is about an order of magnitude larger than that seen in metallic superconductors.

Key Words: Anisotropic uniaxial stress effect; hydrostatic pressure; reduced strontium titanate; single crystal; stresses; superconductive transition temperatures; uniaxial stresses.

Swartzendruber, L. J., and Bennett, L. H., **The effect of Fe on the corrosion rate of copper rich Cu-Ni alloys,** *Scripta Metallurgica* **2,** *93–98 (1968).*
The occurrence of a minimum in the reduction of the corrosion rate in hot sea water upon the addition of small quantities of Fe to copper rich Cu-Ni alloys is studied in relation to the Mössbauer spectra of ^{57}Fe in these alloys. It is proposed that as long as Fe remains in solid solution it reduces the corrosion rate due to the formation of local magnetic moments, but when Fe rich precipitates are formed the corrosion rate increases.

Key Words: Corrosion; iron; copper, nickel; Mössbauer effect; magnetic moment; *d*-electron.

Yakowitz, H., and Heinrich, K. F. J., **Quantitative electron probe microanalysis: Absorption correction uncertainty,** *Mikrochim. Acta* **1,** *182–200 (1968).*
The accuracy of the x-ray absorption correction for quantitative microprobe analysis is affected by errors in the input parameters (mass attenuation coefficients, x-ray emergence angle, and operating voltage), as well as by inaccuracies in the proposed absorption correction models. If the mass attenuation coefficient is known within 5%, then to keep the error of this correction below 1%, the absorption function, $f(\chi)$, must be equal to or higher than 0.8. Experimental conditions leading to small absorption corrections are discussed, and the advantages of high x-ray emergence angles

319-617 O - 68 - 3

are demonstrated. As an illustration, the analysis (theoretical and experimental) of aluminum-magnesium alloys is discussed.

Key Words: Absorption of x-rays; Al-Mg analysis; electron microprobe; errors in microanalysis; quantitative microanalysis; microprobe absorption correction comparisons; microprobe experimental conditions.

Bates, R. G., and Covington, A. K., **Behavior of the glass electrode and other pH-responsive electrodes in biological media,** *Ann. N.Y. Acad. Sci.* **148,** *67–80 (Feb. 1, 1968).*
The theory and experimental techniques underlying the use of hydrogen-ion-responsive electrodes in biological systems are reviewed. Particular attention is given to the development of special forms of electrodes for bio-medical purposes and to applications reported during the past 15 years.

Key Words: Electrodes; bioelectrodes, *p*H measurement; biological systems; glass electrode; antimony electrode; quinhydrone electrode; membrane electrodes.

Currie, L. A., **Limits for qualitative detection and quantitative determination, application to radiochemistry,** *Anal. Chem.* **40,** No. 3, 586–593 (*Mar. 1968*).
The occurrence in the literature of numerous, inconsistent and limited definitions of a "detection limit" has led to a re-examination of the questions of signal detection and signal extraction in analytical chemistry and nuclear chemistry. Three limiting levels have been defined: L_C—the net signal level (instrument response) above which an *observed* signal may be reliably recognized as "detected"; L_D—the "true" net signal level which may be *a-priori* expected to lead to detection; L_Q—the level at which the measurement precision will be satisfactory for quantitative determination. Exact defining equations as well as series of working formulae are presented both for the general analytical case and for radioactivity. The latter, assumed to be governed by the Poisson distribution, is treated in such a manner that accurate limits may be derived for both short- and long-lived radionuclides either in the presence or absence of interference. The principles are illustrated by simple examples of spectrophotometry and radioactivity, and by a more complicated example of activation analysis in which a choice must be made between alternative nuclear reactions.

Key Words: Detection limit; determination limit; decision level; analytical chemistry; activation analysis: interference; radioactivity; Poisson distribution; hypothesis testing.

Haller, W., **Correlation between chromatographic and diffusional behaviour of substances in beds of pore controlled glass. Contribution to the mechanism of steric chromatography,** *J. Chromatog.* **32,** *676–684 (1968).*
Chromatography and diffusion experiments were performed with columns and suspensions of grains of pore-controlled glass of 620 Å pore diameter. The elution positions of tobacco mosaic virus and of benzyl alcohol coincide with the actual void volume and the total fluid volume of the column. A spherical virus (MS2) of 260 Å diameter eluted at a normalized elution volume of $k_e = 0.44$, and its peak position shifted only very slightly over a wide range of elution rates.
The diffusional uptake of virus (MS2) by the porous glass grains from a well stirred suspension indicated that the total pore volume of the glass was accessible to the virus. It took approximately 30 seconds for one half of the ultimate amount of virus to penetrate the glass. In the light of these results it is very unlikely that a volume exclusion mechanism determines the elution position of the virus. Since porous glass columns of uniform and controlled pore size display elution spectra similar to those of gel columns, it is also unlikely that volume exclusion governs the elution spectrum in steric chromatography on gels.

Key Words: Chromatography; diffusion; gel chromatography; gel filtration; gel-permeation chromatography; glass chromatography; GPC; pore-controlled glass; restricted diffusion; steric-exclusion chromatography.

Hetzer, H. B., Robinson, R. A., and Bates, R. G., **Conventional pa_H values for buffer solutions of piperazine phosphate from 0° to 50 °C,** *Anal. Chem.* **40,** *634–636 (Mar. 1968).*
Values of pa_H ($= -\log a_{H^+}$) have been determined for solutions of piperazine phosphate (molality 0.02 and 0.05 mol kg^{-1}) from 0 to 50 °C by means of emf measurements of cells without liquid junction.

Key Words: Piperazine phosphate; buffer solutions; *p*H.

Ito, J., **A new yttrium magnesium silicate garnet, $Y_6Mg_3Si_5O_{24}$ and its rare earth and nickel analogues,** *Mater. Res. Bull.* **2,** *1093–1098 (1967).*
A new magnesium yttrium silicate garnet and its rare-earth analogues with 4 and 6 coordinated magnesium and nickel ions have been synthesized hydrothermally. Its solid solubility with yttrium aluminum garnet was investigated.

Key Words: Hydrothermal synthesis; rare-earth garnet; crystal chemistry; x-ray powder analysis.

May, L., Spijkerman, J. J., **Mössbauer spectroscopy,** *Chemistry* **40,** *14–17 (Dec. 1967).*
A review of Mössbauer Spectroscopy is presented for the high senior and college freshmen chemistry students. The fundamental concepts of nuclear resonance fluorescence are described in particular for its application to Chemistry. Specific examples are given of how Mössbauer Spectroscopy solved analytical and structural problems. A list of selected references are included for further study by the readers.

Key Words: Review; Mössbauer spectroscopy; chemistry.

Rasberry, S. D., Caul, H. J., and Yezer, A., **X-ray fluorescence analysis of silver dental alloys with correction for a line interference,** *Spectrochim. Acta* **23B,** *345–351 (Mar. 1968).*
An x-ray fluorescence spectrometric method has been developed for the rapid analysis of granular silver dental amalgam alloys having the nominal composition, in percent, of silver 69, tin 26, copper 4, and zinc 1. Several methods of specimen preparation were investigated; a method employing briquettes pressed at 1400 kg/cm² without binder was the most satisfactory. Analytical curves relating intensities of K_α lines to concentration of silver, copper, and zinc were linear but no calibration curve could be obtained for the tin K_α line due to line interference from the silver K_β emission. To correct for this interference, the ratio of intensities (Sn K_α + Ag K_β)/Ag K_α was plotted versus the ratio of concentrations Sn/Ag, producing a linear analytical curve. Observed typical coefficients of variation for the method were Ag 0.4 percent, Sn 0.8 percent, Cu 3 percent, and Zn 0.6 percent.

Key Words: Analysis; line interference correction; silver dental alloys; specimen preparation; spectrometry; x-ray fluorescence.

Spijkerman, J. J., **The Mössbauer chemical shift in tin chemistry,** *Advan. Chem. Ser.* **68,** *105–112* (1968).
The Mössbauer spectra of a large number of organic and inorganic tin compounds have been published. From these spectra, the oxidation state of tin in most compounds can be determined.
To interpret the Mössbauer spectra properly, the relationship between the chemical shift and the electron density at the Sn nucleus must be established. This requires that the magnitude and sign of $\Delta R/R$ (a factor that relates the change in the effective charge radius of the tin nucleus on passing from the excited to the ground state) must be known; in most instances, this factor can be determined from nuclear shell model calculation, but, for tin, it must be evaluated experimentally. The discussion includes the results of the various experiments that were designed to obtain this factor so that the chemical shift observed for tin compounds could be interpreted correctly.

Key Words: Mössbauer spectroscopy; chemical shift; tin chemistry.

Astin, A. V., **A time for action in international standardization,** *Mater. Res. Std.* **8,** *No. 5, 18–24 (May 1968).*
Technology and economics find a common challenge in the field of international standardization. How well or poorly America faces this challenge will have a great influence on the stature of the United States in the world markets. Since the resources for standards used in U.S. trade are in the private sector, it behooves private industry and groups such as ASTM in the private sector to fulfill the urgent need for sound standards.

Key Words: Standards; evaluation; consumers; purchasing.

Blandford, J. M., **A progress report on the NBS–ARF apparel materials evaluation project,** *First Annual Conf. Apparel Research Foundation, Nov. 29–Dec. 1, 1967, Washington, D.C. (Apparel Research Foundation, Washington, D.C. 20036 1967).*
A project on the evaluation of apparel materials, to be conducted in collaboration with the Apparel Research Foundation (ARF), was initiated in the Materials Evaluation Division of the Institute for Applied Technology (IAT) in July 1967. Its objective is to aid the small manufacturers of apparel in evaluating the essential properties of materials purchased and products fabricated. This report summarizes a survey made by visits with experts in representative apparel companies and supplier firms of the operations and problems which relate to quality control and testing; current evaluation and testing procedures; value to the industry of the project; and development of the project.

Key Words: Apparel materials; quality control; test methods.

Marzetta, L. A., **Incorrect usage of exact closed-loop voltage gain formula in operation amplifiers,** *Analog Dialogue Letter* **2,** *No. 1, 6 (Mar. 1968).*
Much of the literature currently available on operational amplifiers has been found to contain an incorrectly applied gain formula. The publications in question offer an expression for calculating exact closed-loop voltage gain in amplifiers. In their neglect of the phasor nature of one of the factors, the formula can lead to serious errors when applied to operational type amplifiers.

Key Words: Closed-loop gain; operational amplifiers; voltage gain.

Bowman, R. R., **Remarks on the paper "Field strength above 1 GHz: Measurement procedures for standard antennas,** *Proc. IEEE* **56,** *No. 2, 216 (Feb. 1968).*
Some comments concerning error analysis and the measurement of standard gain horns are made in reply to a correspondence item by E. V. Jull.

Key Words: Electromagnetic horns; gain measurements; error analysis; gain corrections.

Jespersen, J. L., Kamas, G., and Morgan, A. H., **A proposed ranging system with application to VLF timing,** *IEEE Trans. Instr. Meas.* **IM–16,** *No. 4, 282–285 (Dec. 1967).*
In general, it is not possible to determine the range between a radio transmitting and receiving site by making only passive observations at the receiving site. However, if the medium is dispersive, signals transmitted simultaneously from the same site, at different carrier frequencies, will not arrive simultaneously at some distant point. Thus, the difference in arrival time is related to the observer's distance from the transmitter. This effect is considered in conjunction with the VLF two-frequency timing system.

Key Words: VLF; range; time; dispersion.

Hanley, H. J. M., and Childs, G. E., **Discrepancies between viscosity data for simple gases,** *Science* **159,** *No. 3819, 1114–1117 (Mar. 8, 1968).*
It has been known for some time that Kestin and his co-workers have reported dilute gas viscosity coefficients which differ from the usually accepted values. Recent work supplements Kestin's results. We show that there is no evidence for not accepting this different data. We feel that the whole subject of dilute gas viscosity measurements above room temperature should be reexamined both from the experimenter's and correlater's viewpoint. There is evidence that published tables may be incorrect by as much as 10 percent above about 600 °K.

Key Words: Dilute gas; high temperature viscosity; discrepancies; argon; potential function; correlation.

Beckett, C. W., **Status of properties research in the kilodegree range,** *Book, The Characterization of High-Temperature Vapors, Ed. J. L. Margrave, ch. 1, pp. 3–15 (John Wiley & Sons, Inc., New York, N.Y., 1967).*
This paper is an informal discussion of the status of thermodynamic and other properties at high temperatures in relation to current technical needs. It contains comment on a few noteworthy achievements, some unexplored areas, and on the lag between basic research on properties and well-known technical needs. It is to be included in the transactions of an ACS symposium on high temperature chemistry at the request of the publisher.

Key Words: High temperature chemistry; high temperatures; kilodegree range; thermodynamic properties; vapors.

Bozman, W. R., **The application of computers in printing scientific manuscripts,** *Book, New Techniques in Office Operation, ch. 13, pp. 120–124 (The Business Press, Elmhurst, Ill., Mar. 1968).*
A description is given of the use of computers to help prepare a file of information on 30,000 organic and inorganic crystals. Some of the problems of input keyboarding, and data corrections are discussed, as well as cross-checking the data for internal consistency and preparation of the final output magnetic tape for operation of a phototypesetting machine.

Key Words: Data processing, phototypesetting; photocomposing, computer typesetting.

Campbell, P. G., and Wright, J. R., **Asphalt hardening by gaseous oxidants: the relationship between softening point and chemical change as measured by infrared spectroscopy,** *J. Mater.* **2,** *No. 3, 581–596 (Sept. 1967).*
The use of oxidized asphalts has been increasing steadily and much work had been reported on the process of blowing asphalt fluxes to produce a coating grade asphalt. Previous work was reviewed in which asphalt fluxes were treated with various oxidants (oxygen, ozone, air, nitrogen oxides) at relatively mild temperatures and the complex changes taking place during the hardening process were studies by infrared spectroscopy. This work was extended to include other gaseous mixtures (sulfur dioxide, sulfur dioxide-air, nitrogen dioxide-air).
The study of the effects of the gaseous oxidants on the softening points of the asphalt fluxes with time of blowing indicated that, in every case, the rate of softening point increase was greater than that obtained when air alone was used to harden the flux. Infrared spectral analysis, in which changes in functionality are detected, was found to be a convenient method to follow the asphalt hardening process.

Key Words: Asphalt flux; carbonyl absorbance; coating-grade asphalt; infrared analysis; nitrogen oxides; oxidation; softening point; sulfur dioxide.

Catanzaro, E. J., **Absolute isotopic abundance ratios of three common lead reference samples,** *Earth and Planetary Sci. Letters,* **3,** *No. 4, 343–346 (1968).*
The absolute isotopic abundance ratios have been determined for three common lead reference samples, using solid-sample mass spectrometry. Samples of known isotopic composition, prepared from nearly pure separated ^{206}Pb and ^{208}Pb isotopes, were used to calibrate the mass spectrometers. The resulting absolute values are as follows. GS 4: $^{204}Pb/^{206}Pb = 0.061888 \pm 0.000065$, $^{207}Pb/^{206}Pb = 0.95342 \pm 0.00036$, $^{208}Pb/^{206}Pb = 2.2181 \pm 0.0010$; NBS 200: $^{204}Pb/^{206}Pb = 0.068353 \pm 0.000072$, $^{207}Pb/^{206}Pb = 1.00538 \pm 0.00038$, $^{208}Pb/^{206}Pb = 2.3675 \pm 0.0011$; C.I.T. Pb Std.: $^{204}Pb/^{206}Pb = 0.060151 \pm 0.000063$, $^{207}Pb/^{206}Pb = 0.93081 \pm 0.00035$, $^{208}Pb/^{206}Pb = 2.1835 \pm 0.0010$. The indicated uncertainties are overall limits of error based on 95 percent confidence limits for the mean and allowances for effects of known sources of possible systematic error.

Key Words: Lead; isotopic abundances; absolute ratios; reference samples.

Clark, J. E., and Harrison, C. W., **Accelerated weathering of polymers: radiation,** *Appl. Polymer Symp.* **4,** *97–110 (1967).*
The objective of this work was to study the radiation characteristics in three artificial weathering devices and to do a preliminary survey of the effects of high-intensity irradiation on plastics.
An absolute radiometer was used to measure radiation characteristics in the zenon arc and sunshine carbon and enclosed carbon arc Weather-Ometers. The irradiance from the xenon arc was stable over one hour, but the irradiance from the carbon arcs fluctuated. Irradiance received in one hour at the sample drum

for sunshine and enclosed carbon arcs ranged from 315 to 1020 watts/m² and 297 to 679 W/m², respectively, while the xenon arc showed a relatively constant irradiance of 910 W/m². All three devices had a maximum irradiance near the center of the sample drum with intensities at top and bottom being 15–40 percent less. Seven plastic films were exposed to a xenon arc over a 200-fold intensity range by decreasing the arc-to-sample distance.
At up to 6.1 times earth-level sunlight, no significant changes resulted within 100 hours. At 81 times earth-level sunlight, white-pigmented film decomposed within 30 hours and clear films showed changes in ultraviolet and infrared spectra within 69 hours. At 379 times earth-level sunlight, five clear plastics decomposed within 12 hours or less.

Key Words: Carbon arc; degradation; irradiance; photodegradation; plastics; polymers; radiation; radiometry; sun; weathering; xenon arc.

Covington, A. K., Paabo, M., Robinson, R. A., and Bates, R. G., **Use of the glass electrode in deuterium oxide and the relation between the standardized pD(pa_D) scale and the operational pH in heavy water,** *Anal. Chem.* **40,** *No. 4, 700–706 (Apr. 1968).*
Commerical glass electrodes have been compared both directly and indirectly with the deuterium gas electrode at 25 °C in buffered solutions of *p*D from 1 to 13. It is confirmed that the glass electrode functions as well in heavy water as in ordinary water. The relation between the operational *p*H of a buffer solution in heavy water (obtained with a glass electrode standardized in an ordinary light buffer solution) and its *p*D or pa_D value obtained from measurements on cells without liquid junction has been examined and correction factors determined for both glass and gas electrodes. The operational *p*H of buffer solutions in heavy water at 25 °C, measured with the glass electrode, can be converted into a *p*D value by adding 0.41 (molar scale) or 0.45 (molal scale) for $2 < pD < 9$.

Key Words: Glass electrode; deuterium oxide; heavy water; deuterium electrode; acidity; *p*D measurement.

Hughes, E. E., **A simple technique for the absolute determination of atmospheric oxygen,** *Environ. Sci. Technol.* **2,** *No. 3, 201–203 (Mar. 1968).*
A method is presented for the absolute determination of oxygen at concentrations near atmospheric. The oxygen in a sample is determined gravimetrically after reaction with either white phosphorus or a sodium-potassium alloy. The method requires little time and simple laboratory equipment and is capable of yielding values for oxygen concentrations having an overall uncertainty of ±0.1 mole percent.

Key Words: Oxygen analysis; gas analysis; atmospheric composition.

Maienthal, E. J., and Taylor, J. K., **Polarographic methods in determination of trace inorganics in water,** *Book, Trace Inorganics In Water, ch. 10, Advances in Chemistry Series* **73,** *172–182 (American Chemical Society, Wash., D.C., Apr. 1968).*
Polarography is a particularly suitable method for the determination of trace inorganic material in water. Owing to the selectivity of electrode processes, interferences and hence prior chemical separations are minimized. Often several elements may be determined concurrently in the same supporting electrolyte. Anodic stripping and linear sweep voltammetry give an increased sensitivity which permits determinations in the ppb range to be made. Polarographic methodology is reviewed. A survey of the literature concerned with determination of trace inorganic material in water is given. Procedures used in this laboratory for the determination of such elements as aluminum, arsenic, cadmium, copper, indium, iodine, iron, lead, tellurium, and zinc are discussed. The matrices include laboratory distilled water, river water, and reactor cooling water. In addition a comparative technique is described whereby precisions of better than 1 percent can be obtained at the 0.1 ppm level.

Key Words: Trace analysis; water analysis; polarographic analysis.

Maki, A. G., **Assignment of some DCN and HCN laser lines,** *Appl. Phys. Letters* **12,** *No. 4, 122–124 (Feb. 15, 1968).*
The far infrared laser lines in DCN are explained as being due to transitions involving the 22^20 and $09^{1c}0$ levels which are mixed by a Coriolis resonance at J = 21. The HCN laser lines near 130 microns are explained by a Coriolis resonance which affects the 12^20, 12^20, and 05^10 levels. New laser transitions are predicted for these systems.

Key Words: DCN; emission; far infrared; HCN; lasers; spectra.

Mies, F. H., **Quantum oscillations in the shape of pressure-broadened atomic lines,** *J. Chem. Phys.* **48,** *No. 1, 482–494 (Jan. 1, 1968).*
Oscillatory or bandlike structure is predicted to occur in the wings of pressure broadened atomic lines when the interaction potential between the emitting atom M* and the perturbing atom A is deeply attractive compared to kT and the interaction in the final state is repulsive. The oscillations in intensity arise from quantum effects and are associated with the nodal structure of the continuum wavefunction which describes the dissociated state of the diatomic molecule (A + M*). The number of maxima in the line shape is a measure of the number of bound states which can be supported in the potential while the amplitude and resolution of the oscillations depends on the long range behavior of the potential. The bandlike structure, which may extend over thousands of cm^{-1} on the long wavelength side of the atomic emission line, is resolvable as long as $kT <$ approx. 1/10 the vibrational quantum $\hbar\omega_e$ of the AM* molecule. This is a generalization of similar bandlike structure which has been calculated *and observed* to occur in the collision induced radiation of helium metastable atoms and which is merely a special case of pressure broadening involving forbidden lines. Specific calculations are presented for the broadening of the hydrogen Lyman-α line by H(1*s*), and the visible absorption spectra of the H(1*s*), and the visible absorption spectra of H(1*s*) in the presence of free protons.
The quantum theory of line shape which is employed here was first developed by Jablonski but then neglected due to difficulties involved in evaluating essentially the bandstrength for continuum-continuum transitions of diatomic molecules. Jablonski introduced the W.K.B. and other approximations into his theory which reduced it to the classical statistical theory. These approximations are compared to exact quantum mechanical calculations. The W.K.B. approximation is shown to be quite valid in the special case of attractive-repulsive transitions, but Jablonski then improperly averaged over these very quantum oscillations of interest here. This structure offers a unique and extremely sensitive method of studying interaction potentials involving excited states of atoms.

Key Words: Pressure broadening; atomic lines; broadening; quantum mechanics; interaction potential; emission absorption; wavefunctions; W.K.B.; diatomic molecules; continuum-continuum transitions; band strengths.

Woelfel, J. B., and Paffenbarger, G. C., **Evaluation of complete dentures lined with resilient silicone rubber,** *J. Am. Dent. Assoc.* **76,** *582–590 (Mar. 1968).*
Twenty four complete dentures, which had been in use for at least seven years, were lined with a soft resilient silicone rubber. The dentures did not warp or change dimensions significantly during or after the lining. The liner was tasteless, odorless, was well tolerated by the tissues, did not bond well to the periphery of the hard denture base, could not be easily removed for the relief of inflamed mucosa, nor were the stability and retention of the dentures improved over that expected from rebasing or relining a denture with a hard resin. On half of the lined dentures colonies of Candida albicans developed on the silicone rubber. Many of the colonies could not be brushed or scraped off and attacked the lining. The liner is not a cure all for denture problems as has been reported in the literature and its routine use is not recommended, but it has some limited applications in special cases.

Key Words: Dentures; resilient reliners; silicone rubber; retention; stability, Candida albicans; dimensional changes in dentures; oral tissues.

Armstrong, R. W., NBS **dynamic seat belt tester,** *Proc. 10th Stapp Car Crash Conf., 6571st Aeromedical Research Laboratory, Alamogordo, N. Mex., Nov. 8–9, 1966, pp. 38–45 (Society of Automotive Engineers, New York, N.Y., 1966).*

The NBS Dynamic Seat Belt Tester provides relatively inexpensive laboratory equipment capable of simulating an automobile crash. The machine is economical to operate with reproducible output. The sled of the test machine carries a seat and belted dummy or other equipment and is given an acceleration simulating the deceleration experienced by the passenger compartment of an automobile in a 30 mile per hour crash. The acceleration is produced by a rotating flywheel through a tow tape attached to the sled. The ratio of the combined momentum of the flywheel and the sled to that of the dummy is about that of an automobile to a passenger. The test machine has an overall length of 35 feet and is adequately powered by a 10 horsepower motor.

Key Words: Acceleration; anthropomorphic dummy; automobile crash simulator dynamic tests; flywheel; seat belts.

Astin, A. V., **Welcoming remarks** (*Proc. Fifth Transducer Workshop, National Bureau of Standards, Gaithersburg, Md., Oct. 3–4, 1967), Telemetry Working Group Document 112–68, 3–4 (Secretariat, Range Commanders Council, White Sands Missile Range, New Mexico, 1968*).
Welcoming remarks addressed to attendees of the Fifth Transducer Workshop (Oct. 3–4, 1967, National Bureau of Standards, Gaithersburg, Md.) describe NBS' responsibilities as a scientific and technical service agency. NBS activities are generally in two major program areas—physical measurement system and transfer of technology. Mentioned as being instrumental in carrying out these responsibilities are such Bureau efforts as the data program, materials research program, assistance to standards-writing groups, and a number of specialized information services.
Further remarks call attention to the new NBS facilities, particularly those available for conference activities.

Key Words: NBS; Transducer Workshop.

Bloss, R. L., **The measurement of strain** (*Proc. 22nd Annual ISA Conf., Sept. 11–14, 1967, Chicago, Ill.) ISA Preprint No. P1–1–PHYMMID–67 (1967*).
This paper presents a brief overview of the field of strain measurement, including some discussion of philosophy, history and current "state of the art" of the field. There is some discussion of benefits that have resulted from the technical advances in the field of strain measurement, and a few predictions of future developments.

Key Words: Measurement; strain; strain gage; extensometer; historical; state of the art.

Foster, B. E., **Attenuation of x-rays and gamma rays in concrete,** *Mater. Res. Std.* **8,** *No. 3, 19–24 (Mar. 1968*).
Concrete is widely used as a shielding material against X-ray and gamma-ray sources. The purpose of the paper is to furnish a brief elementary background for the concrete technologist on the physics of X-ray shielding. A brief description is given of the characteristics of X-ray and gamma rays. This is followed by a short discussion of attenuation by the photoelectric, pair-production, and Compton effect mechanisms, as a function of X-ray or gamma-ray energy, and barrier material. Performances of various shielding materials in various energy ranges are compared, and the problems in shield design brought about by the scattering processes are discussed.

Key Words: X-ray attenuation; gamma-ray attenuation; concrete shields.

Hilten, J. S., **The National Bureau of Standards inter-agency transducer project—a progress report** (*Proc. Fifth Transducer Workshop, National Bureau of Standards, Gaithersburg, Md., October 3–4, 1967), Telemetry Working Group Document 112–68, 17–36 (Secretariat, Range Commanders Council, White Sands Missile Range, New Mexico, 1968*).
This paper describes some of the techniques and apparatus used for the evaluation of pressure and acceleration transducers. Both static and dynamic tests are covered. Included are earth's field static calibrator, dual centrifuge, earth's field dynamic calibrator, shock tube, quick opening valve pressure calibrators, thermal transient test, temperature storage and cycling test, and life-cycling test.

Key Words: Transducer; calibrator; pressure; acceleration; life-cycling; thermal transient; shock tube; dual centrifuge; dynamic; Inter-Agency Transducer Project.

Kushner, L. M., **The role of the Institute for Applied Technology** (*Proc. Fifth Transducer Workshop, National Bureau of Standards, Gaithersburh, Md., Oct. 3–4, 1967), Telemetry Working Group Document 112–68, 5–10 (Secretariat, Range Commanders Council, White Sands Missile Range, New Mexico, 1968*).
Welcoming address describing the major programs of the Institute for Applied Technology.

Key Words: Transfer of technology; technological measurements.

Motz, J. W., and Sparrow, J. H., **A simple device for the energy and current measurement of an accelerator electron beam,** *Record of the IEEE 9th Ann. Symp. Electron, Ion, and Laser Beam Technology, Berkeley, Calif., May 9–11, 1967, pp. 34–41 (San Francisco Press Inc., San Francisco, Calif., May 1967*).
A simple apparatus has been developed which permits the simultaneous measurement of the electron energy and current of an accelerator electron beam. This measurement is accomplished with negligible interference of the beam during the continuous operation of the accelerator and applies to electron energies greater than approximately 50 keV. The apparatus consists of a thin aluminum foil which intercepts the beam with a negligible energy loss (less than one kilovolt), and two cylindrical aluminum electrodes which are positioned respectively on the incident and exit sides of the foil with axes normal to the foil surface and coincident with the beam direction. With a suitable distribution of electric potentials in this system, the incident electrode current, I_i is inversely proportional to the square of the electron velocity and the exit electrode current, I_e, is inversely proportional to the square of the product of the electron velocity and momentum. Therefore, when an electron beam passes through this system, the electron energy can be determined from the current ratio, I_i/I_e, and the incident electron current can be determined from the current, I_i, as shown in previous measurements with secondary emission monitors. The energy dependences described above for each electrode has been confirmed over a wide range of electron velocities by measurements carried out with a constant potential electron accelerator in the energy region from 50 to 500 keV.

Key Words: Electron beam; energy current; secondary electron; Møller scattering; Mott scattering; thin foils.

Stern, J., **Activities of the Basic Instrumentation Section** (*Proc. Fifth Transducer Workshop, National Bureau of Standards, Gaithersburg, Md., Oct. 3–4, 1967), Telemetry Working Group Document 112–68, 13–15 (Secretariat, Range Commanders Council, White Sands Missile Range, New Mexico, 1968*).
The activities of the Basic Instrumentation Section are described. Major emphasis in the work of the Section is placed on the fundamentals of instrumentation, among them transducer problems in many areas including measurement of high temperatures. In addition, considerable effort is devoted to the development of information services for the field of instrumentation and the necessary methodology for this.

Key Words: Instrumentation; transducer; Information Services; high temperatures.

Berendt, R. D., Winzer, G. E., and Burroughs, C. B., **A guide to airborne, impact, and structure-borne noise-control in multifamily dwellings, FT/TS–24** (*U.S. Dept. Housing and Urban Development, Supt. Doc's., Government Printing Office, Wash., D.C., Jan. 1968, $2.50*).
The guide analyzes the basic causes of the airborne, impact, and structure-borne noise problems in multifamily dwellings and recommends corrective measures, building structures and construction techniques to alleviate and control such problems.
Airborne and impact sound insulation criteria for three grades of multifamily dwellings are presented and recommended for use by the FHA in its Minimum Property Standards. Sound insulation data, fire ratings, descriptions and architectural illustrations are presented for 137 wall constructions and 111 ceiling-floor structures. The guide is illustrated with 345 detailed architectural drawings which show the proper construction and installation of wall and floor assemblies, building equipment, appliances, heating, airconditioning, plumbing

and electrical systems, services or utilities required for adequate sound insulation, noise control and privacy in multifamily dwellings. In addition, the guide summarizes the sound insulation criteria of various foreign countries and contains three appendices which discuss fire ratings, the relationship between laboratory and field measurements of sound insulation and common noise sources. Highly technical and mathematical discussions were purposely avoided in the writing of this guide, so that it could be widely used and readily understood by architects, builders, craftsmen, laymen and others engaged in the design and construction of multifamily residences.

Key Words: Airborne; multifamily; noise control; structure-borne noise control.

Bowman, H. A., Gallagher, W., and Schoonover, M. R., **The development of a working density standard** (*Proc. 20th Annual ISA Conf., Oct. 4–7, 1965, Los Angeles, Calif.*) *ISA Preprint No. 14.8–4–65 (1965).*
Inasmuch as density is the ratio between two well standardized quantities, any working standard of density must be consistent with them. The establishment of fixed reference points on the density scale presents several unique problems which demand techniques and apparatus of interest to instrumentation scientists. NBS has gone far down the road toward a working standard. Progress to date and goals believed achievable at the present state of the art will be discussed.

Key Words: Density; density standard; volume; volumetric measurement; hydrostatic weighing.

Bullis, W. M., and Coleman, J. A., **Characterization of germanium and silicon for nuclear radiation detectors,** *Book, Nucleonics in Aerospace, Ed. P. Polishuk, pp. 166–175 (Plenum Press Inc., New York, N.Y., 1968).*
Semiconductor detectors have been extensively used for about eight years. Uncontrolled variations in the quality of germanium and silicon intended for this application have occurred during this period for reasons which, even now, are not well understood. Crystals are presently selected on the basis of room temperature resistivity, photoconductive decay lifetime and etch pit density. Use of these parameters does not always enable one to discriminate between material suitable for detector fabrication and material which is not. This paper describes a research program now in progress at the National Bureau of Standards which has the objective of identifying those parameters which will be the most useful in specifying detector-grade material. Because of the immediacy of the problem, study of results of this program should also be applicable in the characterization of detector-grade silicon.

Key Words: Carrier; drift mobility; carrier trapping; charge collection efficiency; energy resolution; gamma ray detectors; hall mobility; infrared absorption; lithium drift mobility; lithium precipitation; oxygen, photoconductive decay lifetime; reverse recovery time.

Bur, A. J., and Roberts, D. E., **High polymeric materials,** *Digest of Literature on Dielectrics* **28,** *231–260 (1964).*
The literature on polymer dielectrics published in 1964 is reviewed. The following subjects are covered: theory; relaxation phenomena; dipole moments; semiconducting polymers; biopolymers; effects of radiation; and technology. This paper contains 229 references.

Key Words: Dielectrics; electrical insulation; polymeric materials; polymer dielectrics.

Canfield, L. R., Johnson, R. G., Codling, K., and Madden, R. P., **Comparison of an ionization chamber and a thermopile as absolute detectors in the extreme ultraviolet,** *Appl. Opt.* **6,** *No. 11, 1886–1888 (Nov. 1967).*
A comparison has been made between a calibrated thermopile and an argon ionization chamber as absolute detectors of radiant flux of wavelengths 584 and 735 Å. Corrections were applied to the data to account for the absorption due to gases in the monochromator, the energy carried away from the thermopile by photoejected electrons, non-uniformity of response across the surface of the thermopile and uneven illumination of the thermopile by the flux from the monochromator. The two detectors were found to agree within the 3% estimated probable error in the measurements.

Key Words: Absolute radiometry; detectors; extreme ultraviolet ionization chamber; monochromator; thermopile.

Cassidy, E. C., **Time-resolved studies of spectra produced by electrically exploded wires,** *Naturwissenschaften* **55,** *No. 3, 125–128 (1968).*
Time-resolved spectroscopic studies of electrically exploded wires are described. The spectral distribution of the radiation emitted by aluminum and titanium wires exploded in various controlled atmospheres are given. Atomic and molecular species produced by the explosion are identified. The effects of environment, pressure, and electrical energy input on the explosion spectrum are discussed, and conditions which were found to be conductive to the production of several selected spectral features by the exploding wire method are indicated. This paper summarizes the results of spectroscopic exploding wire studies at the U.S. National Bureau of Standards over the past few years.

Key Words: Exploding wire; time-resolved spectroscopy; electrical discharge; molecular spectra; atomic spectra; AlO.

Deslattes, R. D., **X-ray monochromators and resonators from single crystals,** *Appl. Phys. Letters* **12,** *No. 4, 133–135 (Feb. 15, 1968).*
Single crystal specimens shaped so as to permit successive X-ray diffraction by two non-parallel atomic planes are fixed wavelength monochromators. It is shown that certain plane pairs in Si and Ge pass wavelengths sufficiently close to strong characteristic lines to allow production of intense highly monochromatic beams. For interplanar angles of $2\pi/n$, resonators and retroreflectors may be obtained.

Key Words: Monochromators; single crystals; X-ray resonators.

Goldman, D. T., **Suggested procedures for utilizing MUFT resonance parameters to include Doppler broadening,** *Nucl. Sci. Engr.* **31,** *No. 2, 346–349 (Feb. 1968).*
Keeping within the MUFT framework a method is proposed for including the effect of Doppler (temperature) broadening of resonances on the calculation of resonance integrals. This method is seen to be simple in its application. Some attempt has been made to determine its range of validity especially in comparison with the technique presently in use in MUFT. Finally an additional proposal is made to replace the Narrow Resonance Infinite Mass approximation presently in use in MUFT with the Narrow Resonance approximation for all nuclei.

Key Words: Neutron; resonances; Doppler broadening; slowing down.

Tauke, J., Litovitz, T. A., and Macedo, P. B., **Viscous relaxation and non-Arrhenius behavior in B_2O_3,** *J. Am. Ceramic Soc.* **51,** *No. 3, 158–163 (Mar. 1968).*
Ultrasonic shear and longitudinal relaxation measurements were made in B_2O_3 over a large temperature range (650°–1000 °C). From this data both the shear and volume relaxation time spectra were determined. Both spectra had the same temperature dependence, although the volume spectrum was always broader than the shear. The shear relaxation process can be represented by a single relaxation time above 800 °C in the region where the shear viscosity is Arrhenius. Both processes exhibit an increasingly broad distribution of relaxation times in the non-Arrhenius region. The temperature dependence of the shear spectrum was analyzed in terms of a distribution of activation energies. A surprising conclusion of this study is that activation energies smaller than the activation energy present in the Arrhenius region appear at low temperatures.

Key Words: Viscous relaxation; ultrasonic relaxation; B_2O_3; shear spectra of relaxation times.

Other NBS Publications

J. Res. NBS 72A (Phys. and Chem.), No. 3 (May–June 1968) $1.00.

Peiser, H. S., Wachtman, J. B., Jr., Jump rates for point defects in special positions held by a trapping center of noncubic symmetry.

Robinson, R. A., Covington, A. K., The thermodynamics of the ternary system: water-potassium chloride-calcium chloride at 25 °C.
Levin, I. W., Abramowitz, S., Force field for SiF_4.
Pope, C. I., Blemish formation in processed microfilm. (See above abstract.)
Catanzaro, E. J., Murphy, T. J., Shields, W. R., Garner, E. L., Absolute isotopic abundance ratios of common, equal-atom, and radiogenic lead isotopic standards. (See above abstract.)
Yakowitz, H., Jenkins, W. D., Hahn, H., Role of nickel in Al-10 percent Si composites containing nickel-coated sapphire whiskers. (See above abstract.)

J. Res. NBS 72A (Phys. and Chem.), No. 4 (July–Aug. 1968) $1.00.

Krauss, M., Walker, J. A., Dibeler, V. H., Mass spectrometric study of photionization. X. Hydrogen chloride and methyl halides.
Iglesias, L., The fourth and fifth spectra of vanadium (V IV and V V).
Howett, G. L., Variation of absorptance-curve shape with changes in pigment concentration. (See above abstract.)
Fatiadi, A. J., Periodic acid, a novel oxidant of polycyclic aromatic hydrocarbons.
Roberts, G. N., Hamer, W. J., A galvanic cell with a low emf-temperature coefficient. (See above abstract.)
Ito, J., Synthesis of cerite.
Klein, M., Smith, F., Tables of collision integrals for the $(m, 6)$ potential function for 10 values of m.
Napolitano, A., Macedo, P. B., Spectrum of relaxation times in GeO_2 glass. (See above abstract.)
Hamer, W. J., Resumé of values of the Faraday. (See above abstract.)

J. Res. NBS 72B (Math. Sci.), No. 1 (Jan.–Mar. 1968), 75 cents.

Aissen, M., Means and the minimization of errors. (See above abstract.)
Shisha, O., On Taylor's theorem.
Thompson, R. C., Principal submatrices III: Linear inequalities.
Osgood, C. F., The diophantine equation $P(x, y)=(xy+d)z$.
Gray, H. L., Atchison, T. A., A note on the G-transformation.
Hogben, D., The distribution of the sample correlation coefficient with one variable fixed. (See above abstract.)
Myers, V. W., Solutions of the time-dependent Klein-Gordon and Dirac equations for a uniform electric field. (See above abstract.)
McLynn, J. M., Goldman, A. J., Meyers, P. R., Watkins, R. H., Analysis of a market split model.
Alt, F. L., Kirsch, R. A., Citation searching and bibliographic coupling with remote on-line computer access. (See above abstract.)
Maximon, L. C., Simple analytic expressions for the total Born approximation cross section for pair production in a coulomb field.

J. Res. NBS 72B (Math. Sci.), No. 2 (Apr.–June 1968), 75 cents.

Goldberg, K., Goldman, A. J., Newman, M., The probability of an equilibrium point.
Hearon, J. Z., Evans, J. W., Differentiable generalized inverses.
Hearon, J. Z., Evans, J. W., On spaces and maps of generalized inverses.
Thompson, R. C., Principal submatrices V: Some results concerning principal submatrices of arbitrary matrices.
Sopka, J. J., Mathematical basis for the plasma kinetic equations (BBGKY).
Jarvis, S., Jr., On the diffusion of an ion sheet in Poiseuille flow. (See above abstract.)
Hobbs, A. M., Grossman, J. W., A class of thickness-minimal graphs.

Corliss, C. H., and Tech, J. L., Oscillator strengths and transition probabilities for 3288 lines of Fe I, Mono. 108 (Mar. 1968), 45 cents.
Glennon, B. M., and Wiese, W. L., Bibliography on atomic transition probabilities, May 1966 through December 1967, Misc. Publ. 278 Supplement (Apr. 1968), 30 cents.
Hanley, H. J. M., and Klein, M., On the selection of the intermolecular potential function: application of statistical mechanical theory to experiment, Tech. Note 360 (Nov. 20, 1967), 50 cents.
Koeser, R. L., Editor, Report of the 52nd National Conference on Weights and Measures 1967, Spec. Publ. 297 (May 1968), $1.25. (This series was formerly known as the Miscellaneous Publication Series.)
Shimanouchi, T., Tables of molecular vibrational frequencies, Part 3, Natl. Std. Reference Data Series 17 (Mar. 1968), 30 cents.
Safety rules for the installation and maintenance of electric supply and communication lines, Handb. 81, Supplement 2 (Mar. 1968), 5 cents.
Arenhovel, H., and Hayward, E., Scattering of plane-polarized photons by the giant resonances of nuclei, Phys. Rev. **165,** No. 4, 1170–1174 (Jan. 20, 1968).
Ausloos, P., and Lias, S. G., Gas-phase photolysis of hydrocarbons in the photoionization region, Rad. Res. Rev. **1,** No. 1, 75–107 (Mar. 1967).
Ausloos, P., and Lias, S. G., Gas-phase radiolysis of hydrocarbons, Book, Actions Chimique et Biologiques des Radiations, Ed. M. Haissinsky, 10, 1 (Masson and Company, Paris, France, 1967).
Ausloos, P., and Lias, S. G., Photoionization of cycloalkanes in the gas phase. A study of charge transfer-processes, Book, The Chemistry of Ionization and Excitation, Ed. G. Johnson and G. Schales, pp. 77–89 (Taylor and Francis, Ltd., London, England, 1967).
Ausloos, P., Scala, A. A., and Lias, S. G., Ion-molecule reactions in the condensed-phase radiolysis of hydrocarbon mixtures. II. Cyclopentane and cyclohexane, J. Am. Chem. Soc. **89,** 3677–3683 (1967).
Brady, G., McIntyre, D., Myers, M. E., Jr., and Wims, A. M., Critical scattering of perfluoroheptane-isooctane system (Proc. Conf. Small-angle X-ray Scattering, Syracuse Univ., Syracuse, N.Y., June 1965), Book, Small-Angle X-ray Scattering, Ed. H. Brumberger, pp. 425–448 (Gordon and Breach, Science Publ. Inc., New York, N.Y., 1967).
Bennett, L. H., Swartzendruber, Watson, R. E., Hyperfine fields and electronic structure of CsCl-type ternary alloys of the first transition series, Phys. Rev. **165,** No. 2, 500–505 (Jan. 10, 1968).
Berger, M. J., Energy deposition in water by photons from point isotropic sources, J. Nucl. Med. Suppl. **1,** 15–25 (Feb. 1968).
Braun, W., and Lenzi, M., Resonance fluorescence method for kinetics of atomic reactions. Reactions of atomic hydrogen with olefins, Disc. Far. Soc. **44,** 252–261 (1967).
Bridges, J. M., and Wiese, W. L., Comparison of the Stark widths of the Balmer lines H_β and H_α, Proc. Seventh Intern. Conf. Phenomena in Ionized Gases, Ed. B. Perovic and D. Tosic, III, No. 165, 165–167 (Gradevinska Knjiga Publ. Co., Beograd, Yugoslavia, 1966).
Brown, R. L., and Dittmann, S., Vibrational relaxation and quenching in the yellow nitrogen afterglow, Chem. Commun. **21,** 1144–1146 (Nov. 8, 1967).
Brown, W. E., A mechanism for growth of apotitic crystals (Proc. Intern. Symp. Composition, Properties and Fundamental Structure of Tooth Enamel, London, England, Apr. 1964), Book, Tooth Enamel, pp. 11–14 (John Wright & Sons, Ltd., Bristol, England, 1965).
Butterfield, M. A., Care and preservation of the new media-equipment needs, Proc. A Pioneer Presentation of a National Symposium on the Impact of Automation on Documentation, Denver, Colo., Apr. 27–29, 1967, pp. 60–64 (1968).
Coleman, J. A., Germanium for gamma-ray detectors. A review of current problems, Book, Lithium-Drifted Germanium Detectors, STI/Publ./132, pp. 37–41 (International Atomic Energy Agency, Vienna, Austria, 1966).
Coleman, J. A., Love, D. P., Trainor, J. H., and Williams, D. J., Low-energy proton damage effects in silicon surface-barrier detectors, IEEE Trans. Nucl. Sci. **NS-15,** No. 1, 482–490 (Feb. 1968).
Cook, R. L., and Kirchhoff, W. H., Further investigations on the microwave spectrum of NSF; evaluation of the molecular force field, centrifugal distortion constants, and the dipole moment, J. Chem. Phys. **47,** No. 11, 4521–4527 (Dec. 1, 1967).
Cuthill, J. R., McAlister, A. J., Williams, M. L., Watson, Phys. Rev. **164,** No. 3, 1006–1007 (Dec. 15, 1967).
Damburg, R. J., and Geltman, S., Excitation of $n=2$ states in hydrogen by electron impact, Phys. Rev. Letters **20,** No. 10, 485–487 (Mar. 4, 1968).
Deslattes, R. D., Photoionization of the M shell of xenon, Phys. Rev. Letters **20,** No. 10, 483–484 (Mar. 4, 1968).

Dibeler, V. H., and Liston, S. K., Mass-spectrometric study of photoionization. VIII. Dicyanogen and the cyanogen halides, J. Chem. Phys. **47,** No. 11, 4548–4555 (Dec. 1, 1967).

Domsitz, M. G., Transducer activities at NBS (Proc. Fifth Transducer Workshop, National Bureau of Standards, Gaithersburg, Md., Oct. 3–4, 1967), Telemetry Working Group Document 112–68, 11–12 (Secretariat, Range Commanders Council, White Sands Missile Range, New Mexico, 1968).

Eberhard, J. P., Systems and design—an extrapolation to 2000 A.D., Mater. Res. Std. **8,** No. 5, 12–17 (May 1968).

Fatiadi, A. J., Stable radicals obtained by treatment of azulene with periodic acid and other oxidants, Chem. Commun. **8,** 456–458 (Apr. 24, 1968).

Hall, J. L., and Siegel, M. W., Angular dependence of the laser photodetachment of the negative ions of carbon, oxygen, and hydrogen, J. Chem. Phys. **48,** No. 2, 943–945 (Jan. 15, 1968).

Hamer, W. J., A Joule centennial, J. Chem. Educ. **45,** No. 2, 123–125 (Feb. 1968).

Holt, H. K., Observation of the effect of frequency correlations on a cascade transition, Phys. Rev. Letters **20,** No. 9, 410–412 (Feb. 26, 1968).

Hummer, D. G., Non-coherent scattering—III. The effect of continuous absorption on the formation of spectral lines, Monthly Notices Roy. Astron. Soc. **138,** No. 1, 73–108 (1968).

Johannesen, R. B., Brinckman, F. E., and Coyle, T. D., Nuclear magnetic resonance studies of inorganic fluorides. V. Fluorosilanes, J. Phys. Chem. **72,** 660–667 (1968).

Kasuya, T., Lafferty, W. J., and Lide, D. R., Jr., Microwave spectrum, structure, boron quadrupole coupling constants, and dipole moment of difluoroborane, J. Chem. Phys. **48,** No. 1, 1–4 (Jan. 1, 1968).

Klein, R., and Scheer, M. D., Mechanism of O(^{3}P) addition to condensed films. II. Propene, 1-butene, and their mixtures, J. Phys. Chem. **72,** No. 2, 616–622 (Feb. 1968).

Krause, R. F., Jr., and Douglas, T. B., The vapor pressure, vapor dimerization, and heat of sublimation of aluminum fluoride, using the entrainment method, J. Phys. Chem. **72,** No. 2, 475–481 (Feb. 1968).

Lafferty, W. J., Direct *l*-type doubling transitions in some axially symmetric molecules, J. Mol. Spectry. **25,** No. 8, 359–364 (Mar. 1968).

LeLevier, R. E., and Branscomb, L. M., Ion chemistry governing mesospheric electron concentrations, J. Geophys. Res., Space Physics **73,** No. 1, 27–41 (Jan. 1, 1968).

Lias, S. G., and Ausloo, P., Gas-phase photolysis and radiolysis of isobutane, J. Chem. Phys. **48,** No. 1, 392–400 (Jan. 1, 1968).

McKinley, J. D., Effects of the reaction with bromide on nickel surface morphology, Surface Sci. **10,** No. 2, 287–290 (May 1968).

Manson, S. T., and Cooper, J. W., Photo-ionization in the soft x-ray range: *Z* dependence in a central-potential model, Phys. Rev. **165,** No. 1, 126–138 (Jan. 5, 1968).

Marantz, S., and Armstrong, G. T., Heats of combustion of trans-stilbene and trans-2,2′,4,4′,6,6′-hexanitrostilbene (HNS), J. Chem. Eng. Data **13,** No. 1, 118–121 (Jan. 1968).

Marshak, H., Langsford, A., Wong, C. Y., and Tamura, T., Total neutron cross section of oriented ^{165}Ho from 2 to 135 MeV, Phys. Rev. Letters **20,** No. 11, 554–558 (Mar. 11, 1968).

Maximon, L. C., and Tzara, C., Influence of the radiative background on muon and electron scattering from nuclei, Physics Letters **26B,** No. 4, 201–203 (Jan. 22, 1968).

Mies, F. H., Quantum oscillations in the shape of pressure-broadened atomic lines, J. Chem. Phys. **48,** No. 1, 482–494 (Jan. 1, 1968).

Miller, K. J., and Krauss, M., Born inelastic differential cross sections in H_2, J. Chem. Phys. **47,** No. 10, 3754–3762 (Nov. 15, 1967).

Milligan, D. E., and Jacox, M. E., Matrix-isolation study of the infrared and ultraviolet spectra of the free radical NCO, J. Chem. Phys. **47,** No. 12, 5157–5168 (Dec. 15, 1967).

Milligan, D. E., and Jacox, M. E., Infrared and ultraviolet spectroscopic study of the products of the vacuum-ultraviolet photolysis of methane in Ar and N_2 matrices. The infrared spectrum of the free radical CH_3, J. Chem. Phys. **47,** No. 12, 5146–5156 (Dec. 15, 1967).

Moore, C. E., Carl C. Kiess, Necrology, J. Opt. Soc. An. **58,** No. 2, 292–293 (Feb. 1968).

O'Connell, J. S., and Prats, F., Photodisintegration of the trinucleon system in a separable potential model, Physics Letters **26B,** No. 4, 197–200 (Jan. 22, 1968).

Okabe, H., and Lenzi, M., Photodissociation of NH_3 in the vacuum ultraviolet, J. Chem. Phys. **47,** No. 12, 5241–5246 (Dec. 15, 1967).

Rebbert, R. E., and Ausloos, P., Photolysis of methyl iodide in matrices of organic compounds at 20° and 77° K. Reactions of hot methyl radicals, J. Chem. Phys. **48,** No. 1 306–311 (Jan. 1, 1968).

Scala, A. A., and Ausloos, P., Condensed-phase photolysis and radiolysis of 2-methylbutane, J Chem. Phys. **47,** No. 12, 5129–5139 (Dec. 15, 1967).

Schima, F. J., and Hutchinson, J. M. R., Energy of the isomeric transition in ^{109}Ag, Nucl. Phys. **A102,** 667–672 (1967).

Schofer, R. E., and Levin, B. M., The urban transportation planning process, Socio-Econ. Plan. Sci. **1,** 185–197 (Pergamon Press Ltd., London, England, 1967).

Simpson, J. A., Special sources of monoenergetic electrons, Book, Methods of Experimental Physics, Volume **4,** Atomic and Electron Physics, Chapter, Sources of Atomic Particles, Section 1.1.7, pp. 124–135 (Academic Press Inc., New York, N.Y., 1967).

Swanson, N., Characteristic energy-loss spectra and $-\mathrm{Im}(1/\epsilon)$ for amorphous and polycrystalline Al_2O_3, Phys. Rev. **165,** No. 3, 1067–1070 (Jan. 15, 1968).

Vriens, L., Simpson, J. A., and Mielczarek, S. R., Tests of born approximations: differential and total 2^3S, 2^1P, and 2^1S cross sections for excitation of He by 100- to 400-eV electrons, Phys. Rev. **165,** No. 1, 7–15 (Jan. 5, 1968).

van Reuth, E. C., and Waterstrat, R. M., Atomic ordering in binary A15-type phases, Acta Cryst. **B24,** Part 2, 186–196 (Feb. 1968).

Weiss, A. W., Theoretical electron affinities for some of the alkali and alkaline-earth elements, Phys. Rev. **166,** No. 1, 70–74 (Feb. 5, 1968).

Weiss, A. W., Theoretical multiplet strengths for Mg I, Al II, and and Si III, J. Chem. Phys. **47,** No. 9, 3573–3578 (Nov. 1, 1967).

Wells, J. S., Matarrese, L. M., and Sukle, D. J., Electron spin resonance in single crystals of anhydrous copper sulfate, J. Chem. Phys. **47,** No. 7, 2259–2262 (Oct. 1, 1967).

Whittaker, J. K., Instability and decoupling in nuclear electronics, Nucl. Instr. Methods **57,** No. 1, 156 (Dec. 1967).

**Publications for which a price is indicated are available by purchase from the Superintendent of Documents, U.S. Government Printing Office, Washington, D.C. 20402 (foreign postage, one-fourth additional). The NBS nonperiodical series are also available from the Clearinghouse for Federal Scientific and Technical Information, Springfield, Va. 22151. Reprints from outside journals and the NBS Journal of Research may often be obtained directly from the authors.*

JOURNAL OF RESEARCH of the National Bureau of Standards—C. Engineering and Instrumentation
Vol. 72C, No. 4, October–December 1968

INDEX TO VOLUME 72C

January to December 1968

A

Absolute gravity ... 1
Acceleration ... 1
Acceleration due to gravity at the National Bureau of Standards ... 1
Adams, J. W., Jarvis, S., Jr., Calculation of substitution error in barretters ... 127
Adiabatic saturation ... 33
Adiabatic saturation psychrometer ... 33
Admittance meter ... 81
Admittance meter technique to measure the complex permeability at VHF ... 81
Allred, C. M., Rasmussen, A. L., An admittance meter technique to measure the complex permeability at VHF ... 81
Aluminum ...
Amalgam ... 203, 215
Analysis and design of an oscilloscope deflection system with a calculable transfer function ... 117
Analysis of *n*-degree elliptical elastic rings of nonuniform cross section ... 139
Analytical studies of probe conduction errors in ground temperature measurements ... 243
Application to coaxial chokes to a-c bridge circuits ... 161
Attenuation calibration ... 81

B

Barretter ... 127
Bassali's theory ... 21
Bolometer ... 127
Bolometric voltage and current (Bolovac) standard for high and microwave frequencies ... 61
Bridge ... 161

C

Calculation of substitution error in barretters ... 127
Calibration ... 49
Capacitance ... 161
Carbon dioxide ... 27
Chromatographic detector ... 187
Coaxial cable ... 161
Controlled small reflections ... 197
Creep ... 167, 203, 215
Creep activation energy ... 215
Creep rupture properties of Ti-8Al-1Mo-IV alloy ... 167
Creitz, E. C., Gas density balance design considerations ... 187
Curved bar analysis ... 139, 249

D

Davenport, R. M., Dickson, G., Oglesby, P. L., The steady-state creep of dental amalgam ... 215
—, *Oglesby, P. L., Dickson, G., Rodriguez, M. L., Sweeney, W. T.*, Viscoelastic behavior of dental amalgam ... 203
Deflection ... 21
Deflection of thin circular elastic plates under symmetrically distributed loading ... 21
Deflector ... 117
Dickson, G., Oglesby, P. L., Davenport, R. M., The steady-state creep of dental amalgam ... 215
—, —, *Rodriguez, M. L., Davenport, R. M., Sweeney, W. T.*, Viscoelastic behavior of dental amalgam ... 203
Density detector ... 187
Dental ... 203
Dental amalgam ... 215
Discrete variables ... 249
Drift space ... 117
Dynamic method for determining the vapor pressure of carbon dioxide at 0 °C ... 27

E

Earth temperature ... 243
Edwards, J. L., Johnson, D. P., A dynamic method for determining the vapor pressure of carbon dioxide at 0 °C ... 27
Elastic ... 249
Elasticity ... 21, 139
Engineering design ... 167
Experiments ... 231

F

Fixed point ... 27
Flexure ... 21
Force transducer ... 139, 249
Free-fall ... 1

G

g ... 1
Gas density ... 187
Gas density balance design considerations ... 187
Gas detector ... 187
Gas mixtures ... 33
Gravity ... 1
Greenspan, L., Wexler, A., An adiabatic saturation psychrometer ... 33
Ground loop ... 161

H

Hettche, L. R, Theoretical and experimental study on longitudinal impact of tapered rods ... 231
High temperature ... 167
Homan, D. N., Application of coaxial chokes to a-c bridge circuits ... 161
Humidity ... 33
Hygrometer ... 33
Hypsometer ... 27

I

Inductive voltage divider ... 49
Inductance ... 161
Injection method for self-calibration of inductive voltage dividers ... 49
In-phase deviation ... 49

J

Page

Jarvis, S., Jr., Adams, J. W., Calculation of substitution error in barretters..... 127
Jenkins, W. D., Willard, W. A., Creep rupture properties of Ti-8Al-1Mo-LV alloy..... 167
Johnson, D. P., Edwards, J. L., A dynamic method for determining the vapor pressure of carbon dioxide at 0 °C..... 27

K

Kaplan, J. L., Mitchell, R. A., Nonlinear constrained optimization by a nonrandom complex method..... 249
Kirstein, A. F., Woolley, R. M., Deflection of thin circular elastic plates under symmetrically distributed loading..... 21

L

Lewin, L., Standard mismatch—The production of controlled small reflections in waveguides..... 197
Longitudinal impact..... 231
Lossy magnetic materials..... 81

M

Magnetic core..... 161
Magnetic measurement methods..... 81
Measurement voltages..... 61
Measurements..... 49
Microwave power measurements..... 127
Microwave voltages..... 61
Minimum weight..... 249
Mismatch..... 197
Mitchell, R. A., Analysis of *n*-degree elliptical elastic rings of nonuniform cross section..... 139
—, *Kaplan, J. L.*, Nonlinear constrained optimization by a nonrandom complex method..... 249
Mixing ratio..... 33
Moist gas..... 33

N

n-Degree elliptical ring..... 139, 249
Nonlinear constrained optimization by a nonrandom complex method..... 249
Nonlinear programming..... 139, 249
Nonrandom complex method..... 249
Numerical solution..... 231

O

Oglesby, R. L., Dickson, G., Davenport, R. M., The steady-state creep of dental amalgam..... 215
—, —, *Rodriguez, M. L., Davenport, R. M., Sweeney, W. T.*, Viscoelastic behavior of dental amalgam..... 203
One-dimensional..... 231
Optimization..... 139, 249
Oscilloscope..... 117

P

Peavy, B. A., Analytical studies of probe conduction errors in ground temperature measurements..... 243
Permeability..... 81
Phase changes..... 167
Plastic-weave propgation..... 231
Point supports..... 21
Potsdam..... 1
Pressure standard..... 27
Probe conduction errors..... 243
Proving ring..... 139
Psychrometer..... 33
Psychrometric factor..... 33
Purification..... 27

Q

Page

Quadrature..... 49

R

Rasmussen, A. L., Allred, C. M., An admittance meter technique to measure the complex permeability at VHF..... 81
Rate-independent theory..... 231
Ratio calibration..... 49
Reflector posts..... 197
RF magnetic materials..... 81
Rib-stiffened plate..... 249
Rodriguez, M. L., Oglesby, P. L., Dickson, G., Davenport, R. M., Sweeney, W. T., Viscoelastic behavior of dental amalgam..... 203
Rupture..... 167

S

Saturation..... 33
Selby, M. C., Bolometric voltage and current (Bolovac) standards for high and microwave frequencies..... 61
Silver amalgam..... 215
Steady periodic heat flow..... 243
Steady-state creep..... 203
Steady-state creep of dental amalgam..... 215
Stonebraker, D. M., Analysis and design of an oscilloscope deflection system with a calculable transfer function..... 117
Stray magnetic field..... 161
Stress-strain..... 203
Strip-line standard..... 117
Structural analysis..... 249
Structural design..... 139
Substitution error..... 127
Sweeney, W. T., Oglesby, P. L., Dickson, G., Rodriguez, M. L., Davenport, R. M., Viscoelastic behavior of dental amalgam... 203
Symmetrically distributed load..... 21
Sze, W. C., An injection method for self-calibration of inductive voltage dividers..... 49

T

Tapered rods..... 231
Tate, D. R., Acceleration due to gravity at the National Bureau of Standards..... 1
Theoretical and experimental study on longitudinal impact of tapered rods..... 231
Theory..... 139
Thermodynamic wet-bulb temperature..... 33
Thin plates..... 21
Titanium alloy..... 167
Transfer function..... 117
Transformer..... 49
Transient creep..... 203
Transmission-line voltages..... 61
Two-stage voltage transformer..... 49

V

Vapor content..... 33
Vapor pressure..... 27
VHF bridge..... 81
VHF magnetic materials..... 81
Viscoelastic..... 203
Voltage divider..... 49
Voltage measurements..... 61
Voltage ratio..... 49

W

Waveguide..... 197
Wet-bulb..... 33
Wexler, A., Greenspan, L., An adiabatic saturation psychrometer..... 33
Willard, W. A., Jenkins, W. D., Creep rupture properties of Ti-8Al-1Mo-IV alloy..... 167
Woolley, R. M., Kirstein, A. F., Deflection of thin circular elastic plates under symmetrically distributed loading..... 21

U.S. GOVERNMENT PRINTING OFFICE : 1968 O—319-617

UNIVERSITY MICROFILMS INC
SERIALS SECTION
300 NORTH ZEEB ROAD
ANN ARBOR MICHIGAN 48106

UNIT
GOVERNMENT
DIVISION OF
WASHINGTON, D.C. 20402

OFFICIAL BUSINESS

POSTAGE AND FEES PAID
U.S. GOVERNMENT PRINTING OFFICE

JOURNAL OF RESEARCH of the National Bureau of Standards Vol. 72C, No. 4 October–December 1968
C. Engineering and Instrumentation

Contents

	Page
Theoretical and experimental study on longitudinal impact of tapered rods. L. R. Hettche.	231
Analytical studies of probe conduction errors in ground temperature measurements. B. A. Peavy.	243
Nonlinear constrained optimization by a nonrandom complex method. R. A. Mitchell and K. L. Kaplan.	249
Publications of the National Bureau of Standards.	259
Index to volume 72C, January to December 1968.	271

Library of Congress Catalog Card Number: 62–3900

For sale by the Superintendent of Documents, U.S. Government Printing Office, Washington, D.C. 20402. Price 75¢ (single copy). Subscription price: $2.75 a year; 75¢ additional for foreign mailing.
UNITED STATES GOVERNMENT PRINTING OFFICE, WASHINGTON : 1968